

University of Windsor

Scholarship at UWindor

Electronic Theses and Dissertations

Theses, Dissertations, and Major Papers

7-15-2019

Source Apportionment of Ambient Mercury at Flin Flon, Manitoba

Morounfolu Adeyeye
University of Windsor

Follow this and additional works at: <https://scholar.uwindsor.ca/etd>

Recommended Citation

Adeyeye, Morounfolu, "Source Apportionment of Ambient Mercury at Flin Flon, Manitoba" (2019).
Electronic Theses and Dissertations. 7774.
<https://scholar.uwindsor.ca/etd/7774>

This online database contains the full-text of PhD dissertations and Masters' theses of University of Windsor students from 1954 forward. These documents are made available for personal study and research purposes only, in accordance with the Canadian Copyright Act and the Creative Commons license—CC BY-NC-ND (Attribution, Non-Commercial, No Derivative Works). Under this license, works must always be attributed to the copyright holder (original author), cannot be used for any commercial purposes, and may not be altered. Any other use would require the permission of the copyright holder. Students may inquire about withdrawing their dissertation and/or thesis from this database. For additional inquiries, please contact the repository administrator via email (scholarship@uwindsor.ca) or by telephone at 519-253-3000ext. 3208.

Source Apportionment of Ambient Mercury at Flin Flon, Manitoba

by

Morounfolu Adeyeye

A Thesis
Submitted to the Faculty of Graduate Studies
through the Department of **Civil and Environmental Engineering**
in Partial Fulfilment of the Requirements for the
Degree of **Master of Applied Science** at the
University of Windsor

Windsor, Ontario, Canada

© 2019 Morounfolu Adeyeye

Source apportionment of ambient mercury at Flin Flon, Manitoba

by

Morounfolu Adeyeye

APPROVED BY:

T. Bolisetti
Department of Civil and Environmental Engineering

P. Henshaw
Department of Civil and Environmental Engineering

X. Xu, Advisor
Department of Civil and Environmental Engineering

July 15, 2019

DECLARATION OF ORIGINALITY

I hereby certify that I am the sole author of this thesis and that no part of this thesis has been published or submitted for publication.

I certify that, to the best of my knowledge, my thesis does not infringe upon anyone's copyright nor violate any proprietary rights and that any ideas, techniques, quotations, or any other material from the work of other people included in my thesis, published or otherwise, are fully acknowledged in accordance with the standard referencing practise. Furthermore, to the extent that I have included copyrighted material that surpasses the bounds of fair dealing within the meaning of the Canada Copyright Act, I certify that I have obtained a written permission from the copyright owner(s) to include such material(s) in my thesis and have included copies of such copyright clearances to my appendix.

I declare that this is a true copy of my thesis, including any final revisions, as approved by my thesis committee and the Graduate Studies office, and that this thesis has not been submitted for a higher degree to any other University or Institution.

ABSTRACT

The sources and processes, including re-emission of gaseous elemental mercury, affecting speciated atmospheric mercury (Hg) at Flin Flon, Manitoba were identified and quantified using the positive matrix factorisation (PMF) model and principal component analysis (PCA). The input data contain the concentrations of gaseous elemental mercury (GEM), gaseous oxidized mercury (GOM), particulate-bound mercury (PBM), PM_{2.5} and its components (elements and ions), sulphur dioxide (SO₂) as well as temperature, precipitation, relative humidity and wind speed. Eighty-one daily samples and twenty chemical species concentrations as well as meteorological parameters, measured from July 2010 to May 2011, were analysed.

PMF identified six factors, namely secondary aerosol and re-emission, industrial, crustal/soil dust, road salt/biomass burning, Hg oxidation and coal combustion. Among the factors, secondary aerosol and re-emission, road salt/biomass burning and bromine source profiles contained one or two Hg forms. The bromine source and, secondary aerosol and re-emission were the dominant GEM contributing factors with average contributions of 48% and 43%, respectively. PMF most closely predicted the observed daily concentrations of PBM then GOM and PBM.

PCA of the same concentration data set extracted six principal components. These were largely consistent with the PMF factors. A component identified as long-range transport of Hg with loadings on GEM and GOM only was identified by PCA. With inclusion of meteorological data in the input, the long-range transport of Hg was divided into re-emission and a new component, dispersion of GEM. Overall, PCA identified three Hg-associated components, including re-emission of GEM. The long-range transport of Hg predominantly contributed to GEM in PCA of dataset. The dispersion component's contribution to GEM was dominant when meteorological data was included in the input. PCA most closely predicted PBM then GOM and GEM, regardless of whether or not meteorological data was included.

DEDICATION

To the Almighty God, my parents, my siblings and my wife.

ACKNOWLEDGEMENTS

I am thankful to everyone who contributed to my success in writing this thesis. My deep appreciation goes to my supervisor, Dr Iris Xu, for her supervision and support during my study in University of Windsor. My appreciation goes to the Department Head, Dr Paul Henshaw and my committee members, for their constructive comments and suggestions on my thesis.

I appreciate Tianchu Zhang for his assistance during the data processing stage of this work. I am thankful to Environment and Climate Change Canada for providing the data and funding assistance to undertake this project. I acknowledge the United States Environmental Protection Agency (USEPA) for the PMF5.0 model used in the study.

I deeply thank my parents Mr & Mr S.A. Adeyeye, my siblings and their families for their prayers, love and support throughout my master's degree program in the University of Windsor. I also want to thank my amiable, loving and caring wife, Olayemi for standing by me all through my study in the university. Thank you all and God bless.

TABLE OF CONTENTS

DECLARATION OF ORIGINALITY	iii
ABSTRACT	iv
DEDICATION	v
ACKNOWLEDGEMENTS	vi
LIST OF TABLES	x
LIST OF FIGURES	xi
CHAPTER 1 INTRODUCTION	1
1.1 Background	1
1.2 Objectives	6
CHAPTER 2 LITERATURE REVIEW	8
2.1 Mercury in the Environment	8
2.1.1 Chemistry of atmospheric Hg	8
2.1.2 Mercury cycle	9
2.2 Fate, Transformation and Transport of Atmospheric Hg	11
2.2.1 Emissions	11
2.2.2 Transformation and transport	11
2.2.3 Deposition	12
2.2.4 Re-emission	13
2.3 Health Impacts from Exposure to Hg	14
2.4 Source Apportionment Methods	15
2.4.1 Source apportionment by PMF model	16
2.4.2 Source apportionment by PCA	20
2.4.3 Treatment of missing data	25
2.5 Past studies of source apportionment of speciated atmospheric Hg	26
2.6 Inter-comparison of receptor models	28
CHAPTER 3 METHODOLOGY	30
3.1 Study Area	30
3.2 Monitoring data	32
3.2.1 Speciated Hg	32
3.2.2 PM _{2.5} speciation	33
3.2.3 Sulphur Dioxide (SO ₂)	34
3.3.4 Meteorological data	35
3.3 Emission Data	35
3.4 Data screening	36
3.4.1 Below detection limit	38
3.4.2 Linear correlation test	39
3.4.3 Outliers	40
3.5 Data Processing	40
3.6 Treatment of missing data	42
3.7 Choice of receptor models	43
3.8 PMF Model setup and performance evaluation	44
3.9 PCA setup and performance evaluation	47
3.10 Estimation of PCA components contributions	49

CHAPTER 4 RESULTS AND DISCUSSION.....	51
4.1 PMF Results	51
4.1.1 Estimation of number of factors.....	51
4.1.2 Comparison of 5, 6 and 7-factors profiles	52
4.1.3 Comparison of 5, 6 and 7 factors' distribution of scaled residual	54
4.1.4 Comparison of 5, 6 and 7 factors regression statistics	56
4.1.5 Interpretation of PMF factors	57
4.1.6 Seasonal and overall source contributions	63
4.1.7 Performance of PMF using pred/obs scatter plot	66
4.1.8 Performance of PMF using pred/obs time series plot	68
4.2 PCA Results.....	70
4.2.1 Suitability of data set.....	70
4.2.2 Selection of component to retain in PCA of dataset	71
4.2.3 PCA results from concentration dataset	72
4.2.4 PCA factor contributions to ambient Hg derived from data set	76
4.2.5 Statistical relationships between Hg and meteorological factors	77
4.2.6 Performance of PCA of concentration dataset on speciated Hg	80
4.2.7 Including meteorological parameters	81
4.2.8 Factor contributions in PCA including meteorological data.....	83
4.2.9 Factor contributions time series in PCA including of meteorological parameters	84
4.2.10 Performance assessment of PCA	87
4.3 Comparison of PMF model and PCA results	88
CHAPTER 5 CONCLUSIONS AND RECOMMENDATIONS.....	90
5.1 Conclusions	90
5.2 Recommendations	91
REFERENCES	93
APPENDICES.....	108
Appendix A: Elsevier licence	108
Appendix B: Point sources of Hg and other air pollutants	109
B1: Point sources of Hg and other air pollutants in Manitoba in 2010	109
B2: Point sources of Hg and other air pollutants in Manitoba in 2011	112
B3: Point sources of Hg and other air pollutants in Saskatchewan in 2010	115
B4: Point sources of Hg and other air pollutants in Saskatchewan in 2011	118
Appendix C: List of output from principal component analysis (PCA).....	120
C: List of PCA outputs categorized as 'used' and 'unused'	120
Appendix D: Correlation between variables	121
D1: Correlation between variables in the input data set before imputation	121
D2: Correlation between variables in the input data set after imputation	122
Appendix E: Calculated values of Q and IM&IS from scaled residuals	123
E1: Table of Q values	123
E2: Table of IM and IS values	123
Appendix F: Time series plots of air pollutants from July 2010 – May 2011	124
F1: Time series plot of GEM from July 2010 – May 2011	124
F2: Time series plot of GOM from July 2010 – May 2011.....	124

<i>F3: Time series plot of GEM with date from July 2010 – May 2011</i>	124
<i>F4: Time series plot of PM_{2.5} mass from July 2010 – May 2011</i>	125
<i>F5: Time series plot of Al mass from July 2010 – May 2011</i>	125
<i>F6: Time series plot of Si mass from July 2010 – May 2011</i>	125
<i>F7: Time series plot of K mass from July 2010 – May 2011</i>	126
<i>F8: Time series plot of Fe mass from July 2010 – May 2011</i>	126
<i>F9: Time series plot of Zn mass from July 2010 – May 2011</i>	126
<i>F10: Time series plot of SO₂ mass from July 2010 – May 2011</i>	127
<i>F11: Time series plot of SO₄²⁻ mass from July 2010 – May 2011</i>	127
<i>F12: Time series plot of NO₃⁻ mass from July 2010 – May 2011</i>	127
<i>F13: Time series plot of Ca²⁺ mass from July 2010 – May 2011</i>	128
<i>F14: Time series plot of Cl⁻ mass from July 2010 – May 2011</i>	128
<i>F15: Time series plot of Na⁺ mass from July 2010 – May 2011</i>	128
<i>F16: Time series plot of NH₄⁺ mass from July 2010 – May 2011</i>	129
<i>F17: Time series plot of Mg²⁺ mass from July 2010 – May 2011</i>	129
<i>F18: Time series plot of K⁺ mass from July 2010 – May 2011</i>	129
<i>F19: Time series plot of Oxalate mass from July 2010 – May 2011</i>	130
<i>F20: Time series plot of Br mass from July 2010 – May 2011</i>	130
Appendix G: PMF Outputs	131
<i>G1: Base run summary table for 5-factors</i>	131
<i>G2: Factor profiles for 5-factor solution (% of species sum)</i>	131
<i>G3: Regression diagnostics for 5-factors</i>	132
<i>G4: Base run summary for 6-factor solution</i>	132
<i>G5: Factor profiles for 6-factor solution (% of species sum)</i>	133
<i>G6: Regression diagnostics for 6-factors</i>	133
<i>G7: Base run summary for 7-factor solution</i>	134
<i>G8: Factor profiles for 7-factor solution (% of species sum)</i>	134
<i>G9: Regression diagnostics for 7-factors</i>	135
Appendix H: PCA Outputs	136
<i>H1: Varimax rotated factor loadings with data set (5 factors)</i>	136
<i>H2: Varimax rotated factor loadings with data set (6 factors)</i>	137
<i>H3: Varimax rotated factor loadings with meteorological factors (6 factors)</i>	138
<i>H4: Varimax rotated factor loadings with meteorological factors (7 factors)</i>	139
VITA AUCTORIS	140

LIST OF TABLES

Table 1.1: Physical and chemical properties of Hg	3
Table 3.1: PM _{2.5} speciation and analytical instruments.....	34
Table 3.2: Monitoring data counts and the percentage of data below detection limit (BDL) from July 2010 to May 2011	37
Table 3.3: PM _{2.5} components data with $\leq 20\%$ BDL and $>20\%$ BDL	38
Table 3.4: Detailed input-output requirements of CMB, PCA and PMF	44
Table 3.5: PMF model handling of missing data and sample size	45
Table 3.6: PCA handling of missing data and sample size	48
Table 4.1: Profile of five factors (% of species sum) with major variables $>25\%$ in bold, blanks $<15\%$)	53
Table 4.2: Profile of six factors (% of species sum) with major variables $>25\%$ in bold, blanks $<15\%$)	53
Table 4.3: Profile of seven factors (% of species sum) with major variables $>25\%$ in bold, blanks $<15\%$)	55
Table 4.4: Scaled residuals of PMF solutions	56
Table 4.5: Regression diagnostics of PMF solution	57
Table 4.6: Estimated annual source contributions to speciated Hg (rank in bracket)	66
Table 4.7: Ratios of PMF predicted to observed Hg concentrations	70
Table 4.8: KMO and Bartlett's Test	71
Table 4.9: Varimax rotated factor loadings of PCA with data set (major variables >0.25 in bold, blanks $\leq \text{abs } 0.25$	73
Table 4.10: Contributions of PCA factors derived from data set (N=81).....	76
Table 4.11: PCA factor contributions derived from data set rescaled after removing negative contribution estimates	77
Table 4.12: Varimax rotated factor loadings of PCA including meteorological parameters (major variables >0.25 in bold, blanks ≤ 0.25)	82
Table 4.13: Contributions of PCA factors with inclusion of meteorological data (N=81) ..	83
Table 4.14: PCA factor contributions to Hg rescaled after removing negative contribution estimate (N = 81)	84
Table 4.14: PCA factor contributions to Hg rescaled after removing negative contribution estimates (N = 81).....	84
Table 4.15: Factor comparison in PMF and PCA.....	89

LIST OF FIGURES

Figure 2.1: Mercury cycling in the environmental media	10
Figure 2.2: Types of receptor models in order of the knowledge required about the source prior to modelling	15
Figure 2.3: Example of scree plot for PCA Eigenvalue (variance) on y-axis	22
Figure 3.1: Location of Hg, SO ₂ and PM _{2.5} sampling site, HBM&S facility with emission >20kg/yr. based on NPRI, meteorological stations for hourly temperature, RH, WS and daily precipitation	30
Figure 3.2: Scatter plots of (a) SO ₄ ²⁻ (IC) and sulphur (XRF) (b) Ca ⁺ and Ca and (c) K ⁺ and K from July 2010 to May 2011	42
Figure 4.1: Plot of Q _{robust} and Q _{true} against the number of factors	52
Figure 4.2: Plot of IM and IS against the number of factors	52
Figure 4.3: Time series relations of PMF factor contributions to GEM with temperature...59	59
Figure 4.4: Time series relations of PMF factor contributions to GOM with temperature ..60	60
Figure 4.5: Time series relations of PMF factor contributions to PBM with temperature ..61	61
Figure 4.6: Average seasonal contributions of PMF resolved factors to GEM	64
Figure 4.7: Average seasonal contributions of PMF resolved factors to GOM	64
Figure 4.8: Average seasonal contributions of PMF resolved factors to PBM	64
Figure 4.9: Pred/Obs concentrations scatter plot for GEM in PMF model	66
Figure 4.10: Pred/Obs concentrations scatter plot for GOM in PMF model	66
Figure 4.11: Pred/Obs concentration scatter plot for PBM in PMF model	66
Figure 4.12: Pred/Obs concentration time series for GEM concentrations	68
Figure 4.13: Pred/Obs concentration time series for GOM concentrations	68
Figure 4.14: Pred/Obs concentration time series for PBM concentrations	68
Figure 4.15: Time series of source contributions to GEM with temperatureWS	76
Figure 4.16: Time series of source contributions to GOM with temperature and WS	77
Figure 4.17: Time series of source contributions to PBM with temperature ad WS	77
Figure 4.18: Pred/Obs GEM concentrations time series for components from PCA of dataset	78
Figure 4.19: Pred/Obs GOM concentrations time series for components from PCA of dataset	78
Figure 4.20 Pred/Obs PBM concentrations time series for components from PCA of dataset	79
Figure 4.21: Time series GEM contribution patterns of PCA factors with meteorological parameters	83
Figure 4.22: Time series GOM contribution patterns of PCA factors with meteorological parameters	84
Figure 4.23: Time series PBM contribution patterns of PCA factors with meteorological parameters	85
Figure 4.24: Time series of predicted/observed GEM, GOM and PBM daily concentrations in PCA.....	86

CHAPTER 1

INTRODUCTION

1.1 Background

Mercury (Hg) is a metal with atomic number 80. Among other metals, it is an important one because it is the only metal ever known to be in liquid state under standard temperature and pressure (USEPA, 2007). Hg can slowly evaporate regardless of any change in the environmental conditions. Hg is typically found in the form of its ore cinnabar (mercury sulphite), which is commonly referred to as quicksilver because of its mobility. Because of the uniqueness and other properties of Hg including high specific gravity and constant volume of expansion, its economic significance in diverse areas of human activities including manufacturing, metallurgy, medicine and dentistry vastly increased during the industrial revolution. Due to the persistence, toxic and bioaccumulative nature of Hg, its presence in the environment has attracted global interest. Atmospheric Hg is bidirectional. Once Hg is emitted, it deposits in terrestrial and aquatic environment. Deposition in aquatic environment leads to build-up in aquatic food chain (Schroeder and Munthe, 1998). Consequently, it enters the human body via either inhalation or injection. Direct contact with Hg or inhalation into the body system can cause a series of complicated health conditions including respiratory system disorder and kidney malfunctions. The indirect impacts of atmospheric Hg are of greater concern. They through consumption of contaminated fish, wildlife, and plants that are contaminated with Hg (Meili et al., 2003, Wright et al., 2016). The consumption of Hg contaminated plants and animal species poses risks to the neurological, immune and reproductive systems (Rice et al., 2014). Indirect impacts of atmospheric Hg on wildlife include reduced reproduction, behavioural changes and changes in egg incubation times (Penglase et al., 2014). When Hg combines with trace elements such as gold, silver, zinc and cadmium, it forms alloys, otherwise known as amalgams. The most common of such

amalgams in use is dental amalgam. Globally, atmospheric Hg pollution caused by emissions from numerous point and non-point sources remains a major problem of concern for public health and wildlife. In the atmosphere, Hg goes through a series of complex chemistry and progresses via direct or indirect routes into human body and the ecosystem. The major health issues caused by exposure to atmospheric Hg have motivated the interest of different national and international environmental organizations, such as the United Nations (UN), Environment and Climate Change Canada (ECCC), United States Environmental Protection Agency (USEPA) and several other agencies of governments (UNEP, 2013), to set up control measures aimed at reducing the impacts.

Numerous sources of atmospheric Hg, including natural and anthropogenic (human activity-induced) sources, exist. Another important source of atmospheric Hg is re-emission of Hg previously deposited from natural and anthropogenic sources on land, water or vegetation surfaces (Pirrone et al., 2010). The most important natural sources of atmospheric Hg include volcanoes, forest fires, volatilisation from oceans and water surfaces, and weathering of the earth surfaces (Gustin et al., 2000; Hedgecock et al., 2006). Large proportion of atmospheric Hg contributed by natural sources exists in gaseous phase and volatilization of Hg from ocean surfaces contributes about 70% of the total Hg emissions from natural sources (Gaffney and Marley, 2014). Re-emission of previously deposited Hg mostly affects ambient concentrations in the local environment. The re-emission of Hg previously deposited on land, water and vegetation surfaces are enhanced by biomass burning, land use type, exchange of gaseous Hg at the air-water/topsoil, soil/snow ice pack interfaces, and the prevailing meteorological conditions (Gustin et al., 2000; Pirrone et al., 2001). Anthropogenic sources of atmospheric Hg are numerous and predominantly occur via industrial processes such as fossil fuel (coal) combustion, metal smelting, artisanal and small scale gold mining, and chloro-alkali production (Pacyna et al., 2006, Veiga et al., 2006). The extent of Hg

pollution from anthropogenic sources largely depends on the magnitude of the emissions (Pirrone et al., 2010). When Hg is emitted, its behaviour in the atmosphere is mostly affected by its physical and chemical properties. Some selected properties of Hg are listed in Table 1.1.

Table 1.1: Physical and chemical properties of Hg (Schroeder and Munthe, 1998)

Property	Measure
Physical state at 0°C, 1atm	Liquid
Boiling point (°C)	357
Melting point (°C)	-39
Specific gravity at 20°C	13.55
Solubility in water at 20°C (g/l)	49.4×10^{-6} for Hg; 66 for HgCl ₂
Electrical resistivity at 50°C (Ω m)	9.84×10^{-7} for Hg
Vapour pressure at 1 atm (Pa)	0.180 for Hg; 8.99×10^{-3} for HgCl ₂

Atmospheric Hg is practically measured in three forms, which are operationally defined as gaseous elemental mercury (GEM or Hg⁰), gaseous oxidized mercury (GOM or Hg²⁺), and particulate bound mercury (PBM or Hg_p) (Pandey et al., 2011). All the three Hg forms together are known as total atmospheric Hg. When GEM and GOM are added together, the total is known as total gaseous Hg, whereas GOM and PBM, added together constitute reactive Hg. Inter-conversion between these three Hg forms occurs via oxidation-reduction and adsorption reactions depending on the prevailing atmospheric conditions (Pacyna et al., 2006). For instance, GOM can be produced by homogenous and heterogeneous chemical reactions of GEM with atmospheric oxidants such as O₃, Br/BrO or OH (Subir et al., 2011). There seems to be far-reaching agreement on which particular oxidant is most important under certain atmospheric conditions. Previous studies have shown the high tendencies of O₃ to oxidize GEM in most cases.

Emissions from anthropogenic sources, primarily combustion processes, contain all three forms of Hg in different proportions. Among the three Hg forms, GEM is the predominant form in ambient air (Gustin, 2011). Under standard atmospheric conditions, >95% of the total atmospheric Hg is GEM (Poissant et al., 2005). It has a northern

hemispherical background concentration of $\sim 1.7 \text{ ng/m}^3$ (Slemr et al., 2003). Atmospheric processes such as photochemical reactions rapidly transform GEM to GOM thereby increasing the GOM available for wet or dry deposition in the local environment (Poissant, 1997). GOM and PBM are of low magnitude in the atmosphere approximately, less than 5% (Pacyna and Pacyna, 2002) and the uncertainties of their measurements are high. However, during special atmospheric reactions such as oxidation by ozone, GOM can be produced by rapid oxidation of GEM leading to elevated GOM concentrations (Lindberg et al., 2002). The impacts of natural sources and processes on atmospheric Hg concentrations may vary according to the geographical location and time. This depends on a number of factors including prevailing meteorological conditions, magnitude of exchange processes between soil and water surfaces, and the atmosphere, re-emission of Hg previously deposited on topsoil and vegetation from natural and anthropogenic sources, and the frequency of the occurrence of forest fires (Pirrone et al., 2010). Re-emission of previously deposited Hg can also influence the ambient GEM concentration levels particularly in areas that have previously been under the impacts of active industrial operations for many years.

The reactivity, solubility and toxicity of each Hg form are different. The most stable form of Hg in the ambient air is GEM. It is inert and highly volatile. GEM has a residence time of 0.5 to 2 years (Schroeder and Munthe, 1998; Corbit et al., 2011). This allows it to undergo long-range transport over thousands of kilometres, making it evenly distributed globally, hence its universal description as a 'global pollutant' (UNEP, 2008). Long-range transport of Hg in the atmosphere is a major pathway via which Hg contaminates pristine ecosystem in remote locations (Fu et al., 2010). The concentration of GEM in ambient air is about 100-1000 times the concentrations of GOM and PBM. GOM and PBM are more reactive, highly soluble in water and less volatile than GEM. All the three Hg forms undergo dry and wet deposition but GOM and PBM are more quickly wet deposited than GEM. GOM

can remain in the air for hours to weeks (Schroeder and Munthe, 1998) whereas the removal of PBM from the atmosphere may depend on the size and diameter of the particles (Poissant et al., 2005). The short atmospheric residence times of GOM and PBM allows an increase in the rate of deposition locally with elevated levels near the ground around the source (Eckley et al., 2013). The vertical dispersion of GOM and PBM in the lower part of the atmosphere is constrained to the areas of their releases because of rapid scavenging via wet and dry deposition mechanisms (Lindberg et al., 2007).

Flin Flon Manitoba's Hudson Bay Mining and Smelting (HBM&S) complex has been a major copper and zinc mining, smelting and processing hub. Incidentally, Hg, among other metals, was a major constituent of the ore extracted and processed. Throughout its years of operation (~80 years), it was the largest atmospheric Hg point source in Canada, contributing as much as 6% of North America's anthropogenic Hg releases (USEPA NEI, 2007). Mercury concentrations in Canada are higher in the eastern part than in the west due to the legacy of high emissions to the south (Depew et al., 2013). The amount of Hg released into the ambient air before the 1990s remained uncertain because no information was provided in the Canada's National Pollutant Release Inventory (NPRI). However, between 1999 and 2009, the total average release rate of Hg from the stack was 1093 ± 261 kg/yr. (Environment Canada NPRI, 2018). The plant permanently closed on July 1st, 2010 due to its age and changes in environmental regulations. Prior to the closure of the plant, the concentrations of Hg in Flin Flon was high due to large emission of Hg from HBM&S and caused severe damage to residents of the area. After the plant's closure, some light industrial operations continued at the site. Despite a reduction in Hg emissions due to the plant closure, the atmospheric concentrations of Hg in the local environment remained above the background concentrations at other remote Canadian monitoring sites. The two nearest rural background monitoring sites include Experimental Lake Area, Ontario with average GEM of 1.25 ± 0.16 ng/m³ and Bratt's

Lake, Saskatchewan with average TGM of $1.24 \pm 0.18 \text{ ng/m}^3$ (Eckley et al., 2013). Flin Flon is remote ($>450 \text{ km}$) from significant industrial and urban centres.

This study recognizes and examines the elevated Hg concentrations measured at the Flin Flon sampling site immediately after the closure of the plant. However, the plant site remains a site of concern and further investigation into the re-emission sources and processes, influencing the atmospheric Hg concentrations, is needed given the consequent legacy of contamination of the local soil from long-term deposition of Hg and other air pollutants. . In previous studies of source apportionment of speciated atmospheric Hg, identification and quantification of major point sources of atmospheric Hg has been the common focus neglecting the significant influence of re-emission of distributed long-term Hg from contaminated soil. The input concentration dataset were analysed with two frequently used multivariate receptor models: Positive Matrix Factorization (PMF) model and Principal Component Analysis (PCA), in order to identify and quantify the sources and processes affecting the atmospheric concentration of Hg in Flin Flon.

1.2 Objectives

The objectives of this study are as follows:

- To identify and quantify the sources and processes, including re-emission of gaseous elemental Hg, contributing to the ambient Hg at Flin Flon from July 2010 to May 2011;
- To compare the results obtained from PMF and PCA techniques;
- To assess the performances of PMF and PCA in reproducing the concentrations of speciated atmospheric Hg;
- To evaluate the effects of including meteorological parameters on PCA extracted components.

This study will contribute to knowledge by:

- Providing information on re-emission affecting ambient levels of Hg at Flin Flon, Manitoba but are not listed in the National Pollutant Release Inventory (NPRI)
- The relationship between the meteorological conditions and changes in ambient Hg concentrations
- Knowing the limitations of each modeling technique, performance and what other pollutants needed to be measured at the site for inclusion in future studies in order to improve the modeling results.

CHAPTER 2

LITERATURE REVIEW

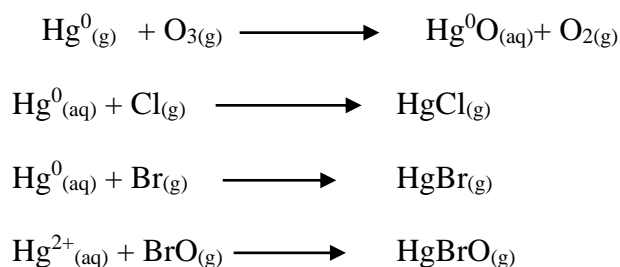
2.1 Mercury in the Environment

2.1.1 Chemistry of atmospheric Hg

Atmospheric Hg can continuously undergo physical and chemical transformations from one form to another before eventually being deposited back to ground level surfaces. Hg exists in three oxidation states denoted as Hg^0 , Hg^+ and Hg^{2+} (Lin and Pehkonen, 1999; Petrucci et al., 2007). The chemical properties of Hg and its behaviour in the atmosphere are strongly dependent on its oxidation state (Otten et al., 2011). For instance, Hg^0 is principally the dominant form in the gaseous phase and has long residence time but Hg^+ is unstable at room temperature (Schroeder and Munthe, 1998). Conversely, Hg^{2+} either tends to be present in atmospheric water in dissolved form or absorbed on atmospheric particles in droplets (Ross and Vermette, 1995).

The atmosphere is an important media, not for transporting Hg only but also a transient reservoir where various Hg transformations affect its transport characteristics and depletion rate. Oxidation of Hg^0 is the most important process of Hg depletion from the atmosphere (Gworek et al., 2017; Schroeder and Munthe, 1998). Because Hg^0 is dominant in the ambient air, its depletion and gas-to-particle conversion are often preceded by oxidation reaction (Sommar et al., 2001). Hg^0 has numerous oxidation pathways in the atmosphere and can occur either in the gas or in aqueous phases. Gas-phase reactions with oxidants like O_3 , NO_3 , OH and H_2O_2 are not well understood because there are substantial uncertainties regarding the reaction rates with these oxidants (Han et al., 2004; Ariya et al., 2015). The main oxidation reaction with Hg^0 is with O_3 (Gworek et al., 2017). Oxidation reactions of Hg^0 in the aqueous phase is more important than gaseous phase oxidation due to its higher rate of reaction in water (Han et al., 2004). Previous laboratory study (Hall, 1995) found that Hg^0 reaction with

O₃ is the most likely reaction in the gas phase but the reaction constant is still very small. In the Arctic, sub-Arctic and Antarctica, oxidation of Hg is mediated by sunlight and bromine atoms derived from atmospheric reactive halogens with marine sea salt in surface snow/icepack or aerosols (Balabanov and Peterson, 2003; Ariya et al., 1998). The halogens can react directly with Hg⁰ or via further reaction with O₃ from halogen oxide radicals (BrO·/ClO·) which undergo reaction with Hg⁰ and convert it to Hg²⁺. The primary halogen atoms (Br/Cl) and molecular halogens (Br₂/Cl₂) have also been found to oxidize Hg⁰ to HgBr₂ and HgCl₂, respectively (Pal and Ariya, 2004; Horowitz et al., 2017). Some possible reactions of Hg⁰ with a variety of other oxidants have been investigated using their thermodynamic dataset, and these suggested that O₃ and Cl₂ are important oxidants of Hg⁰ (Ariya et al., 2002) while SO₂ and NO inhibit reduction of Hg²⁺ to Hg⁰ (Zhao et al., 2006). Oxidation of Hg⁰ with free radicals (HO₂·, HO· and NO₃·) is also an important pathway of Hg⁰ depletion particularly during daytime in the atmosphere (Lin and Pehkonen, 1999). The following equations illustrate different reactions of Hg⁰ with O₃ and few other oxidants (Gworek et al., 2017; Petrucci et al., 2007):



(aq) = aqueous

(g) = gas phase molecule

2.1.2 Mercury cycle

Once Hg is emitted into the environment from natural and anthropogenic sources, it undergoes constant cycling and recycling via a biogeochemical cycle. There are a number of steps involved in Hg cycling in the environment. In Figure 1.1, Hg is initially emitted from

natural and anthropogenic sources, and from re-emission sources. Based on Hg speciation, elemental Hg can last for a considerable period in the atmosphere and is eventually dispersed during turbulent conditions. The elemental vapour then undergoes oxidation in the presence of sunlight to form inorganic Hg, which combines with water vapour; undergo deposition back to the earth's surface as rain or snow. The Hg-rich rainwater is deposited in soil surface and water bodies. In soil, the deposited Hg accumulates and reduces to elemental form via some photo-induced reactions or action of bacteria (Lindberg et al., 2007) until physical events such as biomass burning and/or forest fires mobilize it and eventually it gets re-emitted back to the atmosphere and is again conveyed during air mass movement until it gets deposited far away.

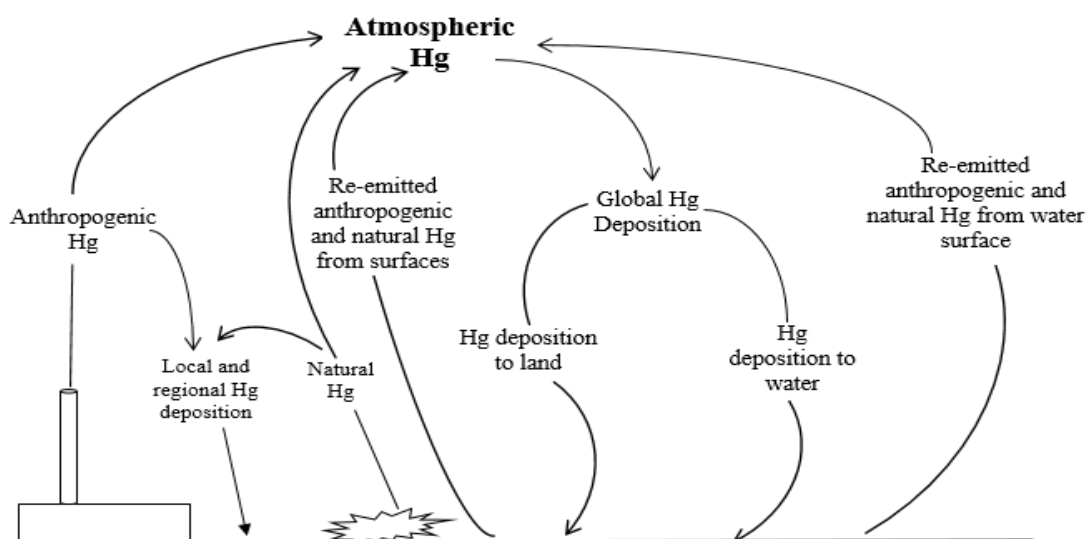


Figure 2.1: Mercury cycling in the environmental media (adapted from Tewalt et al., 2001)

In surface water, inorganic Hg can be converted into insoluble Hg sulphide (HgS) which is further acted upon by microorganisms that process sulphate into the most toxic Hg compound, called as methylmercury (CH_3Hg). These microorganisms are either consumed by the organisms next higher up in the food web or the microorganisms potentially release CH_3Hg from their body into the water where it is adsorbed on plankton, which is also consumed by organisms higher up the food chain. This pattern continues with small fish being progressively consumed by bigger and bigger fish until humans or other animals high up in

the food web eventually consume the fish. Alternatively, both Hg^0 and CH_3Hg in soil and water surface can vaporize and be re-emitted back into the atmosphere and cycles in the environment.

2.2 Fate, Transformation and Transport of Atmospheric Hg

2.2.1 Emissions

Atmospheric Hg is from natural and anthropogenic origins. The emissions from natural processes are primarily in elemental form (Schroeder and Munthe, 1998). It is imperative to know that Hg emissions could result from two natural components: Hg present as part of pre-industrial equilibrium and Hg mobilized by physical processes from geological deposits and added to atmospheric load. Anthropogenic Hg releases are however, dominated by industrial and combustion processes that release Hg into the atmosphere (Pacyna et al., 2006). Gaseous Hg emissions include both Hg^0 and Hg^{2+} , while the emission of Hg-rich particles compose primarily of oxidized compounds due to the relatively high vapour pressure of Hg^0 . Hg^0 and Hg^{2+} absorbed or bound to particles increase the Hg_p content in the atmosphere. The speciation of Hg in emission plumes is often dependent on the type of processes and the fuel used (e.g. coal, oil, municipal waste) and operating temperature. Anthropogenic activities on sites that are no longer operational still continue to emit significant amount of Hg into the atmosphere from historically contaminated soil.

2.2.2 Transformation and transport

As previously stated, Hg^0 stays longer in the atmosphere than Hg^{2+} and Hg_p and thus is evenly distributed in the troposphere. Hg^{2+} and Hg_p may be deposited relatively quickly by wet scavenging and dry deposition processes, hence the short residence time. Longer residence times are also possible to occur. The residence time of Hg_p in the atmosphere may sometimes approach that of Hg^0 (Porcella et al., 1996). The transformation of Hg^0 to Hg^{2+} and Hg_p in cloud water demonstrates a likely mechanism by which Hg^0 ambient air can be deposited into

the soil and water. This deposition can often occur far away from the releasing source. Hg^0 uptake in cloud water could be slow (Gallup, 2018) because it is insoluble. Hg^{2+} is expected to deposit at a faster rate instantly after release than Hg_p with an assumption that most of the particles are less than one microgram in diameter. The large variation in atmospheric residence time between Hg^0 and other Hg forms leads to very much larger scales of transport and deposition of Hg^0 . Generally, emission of Hg^0 from anthropogenic sources, its fluxes from contaminated soils and water bodies and natural emissions all contribute to a global atmospheric load. Atmospheric circulation of Hg on a global scale can take Hg^0 from their point of release and transport them anywhere on the globe before transformation and deposition occur. Hg^{2+} and Hg_p are likely to deposit to the earth's surface before they thoroughly mix with the atmosphere.

2.2.3 Deposition

Deposition of Hg is simply the removal of Hg dispersed in the atmosphere via wet and dry deposition mechanisms. Once in the atmosphere, Hg^{2+} and Hg_p are often subjected to faster removal than Hg^0 (Shannon and Voldner, 1994). Both Hg^{2+} and Hg_p are primarily subject to dry deposition (i.e. deposition in the absence of precipitation) at significant rates when and where their measureable concentrations exist. The deposition velocity of Hg_p is dependent on the state of the atmosphere and particle size (Zhang et al., 2012; Wright et al., 2016). Hg^{2+} and Hg_p can also be subjected to wet deposition through scavenging by precipitation. Overall, Hg^{2+} undergoes more rapid and effective removal by both dry and wet deposition processes than Hg_p (Shannon and Voldner, 1994) due to the high reactivity and water solubility of Hg^{2+} . Contrarily, Hg^0 may not be susceptible to any major direct deposition to the soil because it has high vapour pressure and lower water solubility. Although, Hg^0 could be formed in soil and water due to the chemical reduction of Hg^{2+} , this Hg^0 is expected to

volatilize into the ambient atmosphere. The reduction of Hg^{2+} to Hg^0 in aqueous systems could reduce the amount of Hg^{2+} available for methylation.

There is a potential for deposition of Hg^0 through plant-leaf uptake. It has been reported that forest canopies could accumulate Hg^0 via gas exchange at the surface of leaves followed by Hg assimilation in the leaf interior during the daylight hours. This process causes downward flux of Hg^0 from the atmosphere thereby leading to high deposition velocity of Hg^0 . At lower ambient concentrations, the forests appear to act as a source of Hg^0 to the atmosphere, with measured Hg flux in the upward direction. This may be explained by the volatilization of Hg^0 from the soil.

2.2.4 Re-emission

The re-emission of Hg from topsoil and water surfaces into the atmosphere predominantly results from the formation of Hg^0 in the soil and natural waters. In this process, Hg emitted from anthropogenic sources is deposited to the soil mainly as Hg^{2+} , which is subsequently reduced to Hg^0 by some bacteria and re-emitted back into the atmosphere. The soil Hg content, in most cases, controls Hg^0 evasion under comparable weather conditions including high solar radiation and temperature (Lin et al., 2010). According to Mason et al. (1995), re-emission processes account for ~30% of the total Hg flux from soil to the atmosphere. Eckley et al. (2015) reported an elevated soil Hg^0 efflux after a closure of a huge base-metal smelter in Canada. A recent study by Zhu et al. (2018) in China also indicated that Hg^0 concentration in soils near a closed smelter was found to be up to two orders of magnitude higher than the local background soil concentration. This increase was linked to the cumulative deposition of industrial plant Hg emissions. Mason et al. (1995) further estimated that total Hg re-emissions has increased by a factor of 4.5 since pre-industrial use and has increased the concentrations in the atmospheric and oceanic reservoirs by a factor 3. This scenario was attributed to increased local deposition. The affinity of Hg species for soil

mainly results in soil acting as a large reservoir for anthropogenic-related deposited Hg. Thus, even if emissions from anthropogenic sources were to cease totally, the efflux of Hg from soil into the atmosphere might be expected to remain elevated for many years afterwards. Nevertheless, re-emission of Hg previously deposited on soil from natural and anthropogenic sources will continue to have significant effects on the atmospheric concentrations of Hg.

2.3 Health Impacts from Exposure to Hg

All known Hg compounds are toxic (Bernhoft, 2012) and have devastating impacts on human health regardless of the amount. The impact of atmospheric Hg can be direct or indirect depending on the exposure route. Although, the background Hg concentrations in ambient air is about 1.7 ng/m³ (Ebinghaus et al., 2003), this is not perceived as high enough to cause direct human health problems. Once Hg²⁺ is deposited into soil and water, it is converted by some active microorganisms under acidic and anaerobic conditions to the more toxic form known as methylmercury. Methylmercury (CH₃Hg) enters human body predominantly through consumption of fish and shellfish leading to escalated health problems such as the case of Minamata disease in Japan in 1956. Exposure to CH₃Hg is of more concern than Hg⁰ because the body absorbs approximately 95% of the CH₃Hg ingested through the gastrointestinal tract, lung and skin (Al-Zubaidi and Rabee, 2017) compared to 50-100% absorption of elemental Hg vapour inhaled via the lungs. Exposure to Hg during pregnancy is of most concern, because it inhibits the development of an unborn baby's brain (Lando and Lo, 2014). CH₃Hg can cross the placenta and readily pass through the blood-brain, with higher levels of CH₃Hg reported in fetal than in maternal circulation (Kim and Zoh, 2012). Infants and young children with developing body organs are highly vulnerable to damages from exposure to CH₃Hg because it causes learning disabilities in children. Studies have also shown that exposure to small increase in Hg concentration adversely affect the heart and

circulatory system. Mercury inhaled can also cause neurological and behavioural disorders causing memory loss, irritability and social withdrawal (Ratcliffe et al., 1996).

2.4 Source Apportionment Methods

Investigations into the sources and processes affecting air pollutant concentrations at a receptor are performed using multivariate receptor models. Receptor models are used to explore the variance in a concentrations dataset, in order to identify and quantify air pollutant sources, including speciated Hg. It has also aided in examining the influence of emission, transport, transformation and deposition processes involving speciated Hg concentrations at receptor locations (Cheng et al., 2015). Numerous receptor model applications require varying degrees of knowledge about the sources. In Figure 2.2, the level of knowledge required by various types of receptor models are shown.

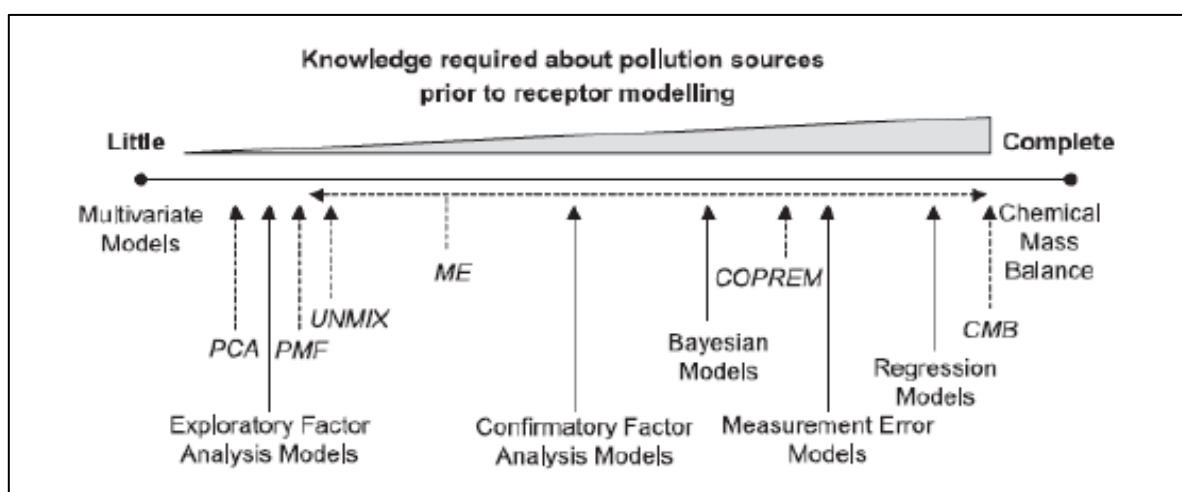


Figure 2.2: Types of receptor models in order of the knowledge required about the source prior to modelling (Reprinted from Source apportionment of particulate matter in Europe: A review of methods and results by Viana, M., Kuhlbusch, T., Querol, X., Alastuey, A., Harrison, R., Hopke, P., ...Hitzenberger, R. (2008), *Journal of Aerosol Science*,39(10), p. 829. Copyright 2008 by Elsevier)

Among these multivariate models, the most frequently used ones in concentration data analysis include Chemical Mass Balance (CMB) model (Heaton et al., 1992; Watson et al., 2001), Principal Component Analysis (PCA) (Lynam and Keeler, 2006; Temme et al., 2007) and Positive Matrix Factorization (PMF) (Keeler et al., 2006; Brown et al., 2007).

Mathematically, the concentration of an air pollutant measured at a receptor location is expressed as the sum of the products of the pollutant compositions and contributions from sources. The CMB model had been used in previous studies to determine the contributions of sources to particulate matter and volatile organic compounds in ambient air and pollutants in soil. An assumption in the CMB model is that all significant sources of air pollutants have been identified and their emissions fully quantified (Chow and Watson, 2002). However, this assumption is physically invalid in Hg apportionment studies because there may be sources potentially affecting the ambient concentrations, which had not been physically identified and reported in the emission inventory. For this singular reason, CMB is rarely used for source apportionment of speciated atmospheric Hg. PMF and PCA have mostly been used in apportionment of particulate matter (Viana et al., 2008). An important advantage of PMF and PCA over CMB is that the knowledge about the sources and their profiles is not an initial requirement to apply both methods. They only require the input of ambient Hg data with or without meteorological data (Hopke, 2016).

2.4.1 Source apportionment by PMF model

The PMF model is a multivariate statistical model developed in the mid-1990s (Paatero and Taper, 1994). It has been applied to numerous ambient concentration data obtained from different locations including urban, semi-urban and rural locations (Viana et al., 2008). PMF has also been applied in apportioning speciated atmospheric Hg in the ambient atmosphere at Kejimikujik National Park, Nova Scotia (Liao, 2016; Xu et al., 2017) as well as Hg in precipitation (Keeler et al., 2006) to the respective potential sources. One important feature of PMF is the input of uncertainties data, which allows individual variable data point to be weighted in order to resolve the factorization problem (Paatero and Taper, 1994). The use of uncertainties in the PMF model makes it a non-data-sensitive method where non-representative data including missing values, below detection limit (BDL) values and outliers

could be managed by the model thereby reducing their influence on the results (Paatero and Taper, 1994). Additionally, the PMF model algorithm constraints the source profiles and contributions to be non-negative allowing more physically realistic solutions to be obtained (Reff et al., 2007). The PMF algorithm begins from the fundamental mass balance formula shown in Equation 2.1 (USEPA, 2014):

$$X_{ij} = \sum_{k=1}^p g_{ik} f_{kj} + e_{ij} \quad 2.1$$

where,

X_{ij} is the concentration of j^{th} chemical species measured in the i^{th} sample

g_{ik} is the contribution from source k to the i^{th} sample

f_{kj} is the mass fraction of the j^{th} species from the source k

e_{ij} is the residual (the difference between input values and predicted values)

p is the number of resolved factor representing the sources

It follows that PMF model decomposes an input concentration data into source profiles and source contributions. Before running the model, no prior information about the sources is needed. The model solves equation (2.1) through a weighted least squared algorithm and computes the factor profiles and factor contributions by minimizing the objective function Q , given as:

$$Q = \sum_{i=1}^n \sum_{j=1}^m \left[\frac{X_{ij} - \sum_{k=1}^p g_{ik} f_{kj}}{\sigma_{ij}} \right]^2 \quad 2.2$$

where,

σ_{ij} is the uncertainty associated with each concentration measurement.

The weighting of each data point using individual uncertainty estimates optimizes the information inherent in the data. Any problematic data point could therefore, be suitably weighted in this way. Furthermore, all the elements in the factor mass fractions and factor contributions are constrained to be non-negative in order to make the solution physically realistic (Paatero and Tapper, 1994).

In the input file for this work, rows are the dates of measurements (i.e. sampling dates) while each chemical species has a column. The PMF model does not run if there is missing data in the input file. Missing data require treatment outside the model before PMF can run. According to the PMF5.0 user guide, uncertainties are calculated using two methods. The first is observation-based uncertainties, which reflect sampling and measurement errors. The second method is equation-based uncertainty calculated using concentrations, error fractions and method detection limit. The user specifies the error fraction based on the measurement and knowledge of the species calculated. Uncertainty equations (Equations 2.3a&b) based on method detection limits (MDL) are given below:

$$\text{Uncertainty} = (5/6) * \text{MDL} \quad 2.3a$$

for concentration \leq MDL

$$\text{Uncertainty} = \sqrt{(\text{Error fraction} \times \text{Concentration})^2 + (0.5 \times \text{MDL})^2} \quad (2.3b)$$

for concentration > MDL

Specific variables known as markers are used to identify the sources and these are expected to be present in the input data. These markers are categorized as ‘good’, ‘bad’ or ‘weak’ (USEPA, 2014). The model uses markers categorized as good, weak ones are automatically down-weighted and the bad ones are excluded from the analysis. In PMF models, specific source markers in the input should not be categorized as bad. For instance, SO₂ is a source marker for coal combustion. Categorizing SO₂ as ‘bad’ in the input file will make coal combustion identification to be difficult. This categorization also applies to identifying other sources such as biomass burning and road salt sources using their respective source markers: K⁺, Mg, Na and Cl. In cases when information in the data set is insufficient for categorising the chemical species, the signal-to-noise (S/N) ratio is used. The S/N ratio shows whether the variability in the concentration data is real or within the noise of the data (USEPA, 2014). The variables with S/N ratio <0.5 should be set as ‘bad’ and variables with S/N ratio between 0.5 and 1.0 is set as ‘weak’. Total variable could be specified by the user to

help in the post-processing of the results such as the percentage of the total mass in each of the factors. The total variable is an artificial variable, which is the total mass of the same species type. For instance, if the input data are mainly PM_{2.5} and its components, PM_{2.5} mass is calculated and chosen as the total variable (USEPA, 2014). Because total variable could have a significant impact on the result, it is required to be categorized as ‘weak’ variable. The concentration time series and concentration scatter plot are other tools that can help to analyse input data before running the PMF model. The concentration time series helps to examine if there are measurements that deviate from trends in the data. The samples with unusual data are then excluded from the data set. The concentration scatter plot indicates the correlation between two user-specified variables. A correlation between two variables is an indication that they are associated with the same source (USEPA, 2014). The user specifies three parameters including number of runs, number of factors and seed number. The number of runs recommended by USEPA is 20 because this allows the stability of the result to be evaluated (USEPA, 2014). The start of iteration is the seed number. PMF accept either a random start or fixed point. For the determination of the number of factors, several methods could be used to select a range of factors. The maximum individual column mean (IM) and individual maximum standard deviation (IS) of the scaled residual matrix are evaluated to determine the factor range (Lee et al., 1999). When the number of factors attains a critical value, IM and IS will experience a drastic drop. The change in Q values can also provide helpful information on deciding the number of factors (Viana et al., 2008). Different number of factors in the range determined by IM, IS and change in Q-value are required to be conducted and the interpretability of the results is checked. The final solution is a compromise of the trend of lines of these three parameters (Ceasari et al., 2016).

The factor profiles, source contributions and the residuals (difference between the measured and modeled concentrations) are the PMF outputs. There are three kinds of output

profiles (1) concentrations of each variable in each factor, (2) percentage of a variable's total mass for each variable in each factor and (3) the percentage of total mass within the factor for each variable in each factor. To calculate the predicted concentrations of the species of interest from the k^{th} source, each species concentrations from the k^{th} source are multiplied by the source contributions. The sum of the products is added up. Adding the concentrations from all factors yields the overall model-predicted concentration of the variable of interest, which is equivalent to the X_{ij} value in Equation 2.1. Sources with high percentage contributions indicate that the sources contribute majorly to the receptor concentration. The performance indices in the PMF model are Q-values, scaled residuals and regression statistics. Other indices include the predicted/observed scatter plot and time series plots.

PMF factor profiles for Hg source apportionment are interpreted using major variables e.g. speciated atmospheric Hg with co-pollutants including $\text{PM}_{2.5}$ mass, elements and ions on $\text{PM}_{2.5}$, and gaseous compounds measured concurrently at the same site with pre-selected cut off point on PMF factor profiles. Because speciated atmospheric Hg are emitted in different proportions by a variety of sources, it may be difficult to specifically identify a source using Hg species alone. The ease of source profile interpretation arises when characteristic air pollutants for potential sources are combined with speciated atmospheric Hg. For instance, the coal combustion source has been identified with the a profile containing GEM, GOM, PBM, $\text{PM}_{2.5}$ and SO_2 because $\text{PM}_{2.5}$ and SO_2 are markers for coal combustion (Lynam and Keeler, 2006). Similarly, a profile with GEM and K^+ was identified as biomass burning in another study because K^+ is a marker for biomass burning (Tao et al., 2017).

2.4.2 Source apportionment by PCA

Principal component analysis (PCA) is a multivariate data reduction method. It is practically used for reducing a large set of concentration data containing inter-correlated variables to a smaller set of uncorrelated components/factors. In the PCA method, the major

goal is to reduce the dimensionality of a complex data set, with little loss in the information contained in it. PCA is among the most common data analysis methods used in air quality studies (Pires et al., 2008 Chang et al., 2009) as well as soil and sediment data analysis (Bhuiyan et al., 2010). The original variables in the data set are projected into a new reference frame, which minimizes the variance in the data set. The factors derived after the reduction are called the *principal components* (PCs) and are extracted in decreasing order of significance in terms of explaining the maximum variance in the data. The first PC explains as much of the variance in the data set as possible and each succeeding PC explains as much of the information in the remaining variability as possible (Jolliffe, 2002). The PCs consist of some of the original variables from the data set, which are specific source markers. The new uncorrelated variables in the PCs represent a particular linear combination of the original variables (Davis, 2002).

The input of PCA includes chemical species concentration and/or meteorological measurement. The PCA method is data-sensitive and requires that the input data be pre-treated before using PCA in order to obtain a more suitable data set for its application (Reimann et al., 2002). A data set having variables with different numerical ranges could result in incorrect PCs because the variables with the largest variance in the data will have major influence on results (Reimann et al, 2002). In addition, outliers are needed to be removed prior to applying PCA on data sets. If outliers contain essential information, they can bias the results (Reimann et al., 2002). Normalization makes both large and small concentration data points have the same influence. The normalization formula is given as:

$$X_{ik} = \frac{C_{ik} - C_i}{\sigma_i} \quad (2.4)$$

where:

X_{ik} is the standardized value of the i^{th} species in the sample k

C_{ik} is the concentration of species i in sample k

C_i is the average concentration for the i^{th} species over all observations

σ_i is the standard deviation of species concentration over all samples.

The analysis using the following statistical tests assess the suitability of a data set for PCA: The first statistical test is the Kaiser-Meyer-Olkin (KMO) measure of sampling adequacy. According to Tabachnick and Fidell (2001), a KMO value >0.6 indicates good factor analysis. The second statistical test is Bartlett's Test of Sphericity. The input data set with significant level of Bartlett's Test of Sphericity is $p < 0.05$. Three primary methods are used to determine the number of factors to retain in PCA. The first method is based on the use of a scree plot. The scree plot is a line graph showing the eigenvalues (representing the variance) on the vertical axis and the respective number of PCs on the horizontal axis (Figure 2.2). When the scree plot is carefully examined, the curve tends to drop sharply for the first PCs until it reaches a point commonly referred to as an "elbow". The number of principal components to select is provided by the PC number at the elbow point or just above. The second important method is known as Kaiser's criterion. It requires only the PCs having an eigenvalue (variance) >1 to be retained. The last method of selecting the number of PCs to retain is based on the cumulative variance. Since the first few PCs are thought to account for a large percentage of the total variance, only the PCs, which represent 70-80% of the cumulative percentage of the variance, are selected.

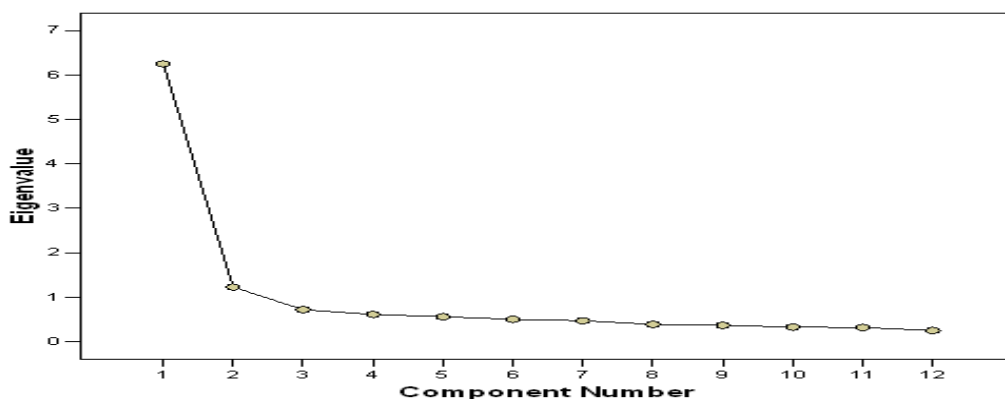


Figure 2.3: Example of scree plot for PCA. Eigenvalue (variance) on y-axis

After the initial extraction of the PCs, rotations are usually applied after fixing the number of PCs in order to obtain a clearer pattern of factor loadings so that the PCs can be interpreted as realistic sources. Typical types of rotations employed include varimax, quartimax and equamax (Joliffe, 2002). Among these three rotations, varimax rotation is often used to find a rotation that maximizes the variance of the first principal component extracted. Thus, a rotation must be defined and usually the choice of varimax method is the default criteria in statistical packages. Other rotation methods could also be used but may produce different results.

There are many outputs of PCA with the commonly used ones in bold form in Table B. The majorly used outputs contain the percent variance of the data explained by each of the rotated components and a table illustrating the component/factor loadings. The loadings are the correlation coefficients between the variables in the data set and the components/factors. The factor loadings are used to characterise the sources. User cut-off values are considered major loadings. The factor loadings can be positive or negative. High loadings between a variable and a PC show that the variable is associated with the direction of the maximum amount of variation in the data set (Joliffe, 2002). The interpretation of the components is based on assessing variables with large component loadings (Cheng et al., 2013). More than one variable can be loaded on a PC, explaining its origin (pollution source or chemical process). The closer to unity the loading on a PC is, the stronger the correlation with that component. The major limitation of PCA is that it provides negative scores, which might not always have direct physical interpretation (Tauler et al., 2004). PCA of a dataset does not require specific statistical software. Any basic statistical packages such as IBM SPSS® can be used. Each component is assigned to sources and processes by comparing with variables with the same sign in the results of other studies. When source markers are lacking in PCA input, the interpretation of factors may be subjective (Viana et al., 2008). The contribution of PCA

identified sources are estimated using the Absolute Principal Component Scores (APCS). As the component, scores are in normalised form with mean of zero and standard deviation equal to 1, the true zero value for each factor score is calculated by introducing an artificial sample with all species concentrations as zero. The APCS for each component can then be estimated by subtracting the component scores of the artificial sample from the component scores of each one of the true samples. Regression of the concentration data for Hg species on these APCS gives the estimates of the coefficients which convert the APCS into the source contribution to each sample. The source contribution can now be computed by using the multiple linear regression procedure according to the relationship below:

$$C_i = (b_0)_i + \sum APCS_p * b_{pi}$$

where,

C_i is the arithmetic mean concentration of species i

$(b_0)_i$ is the constant term of multiple linear regression for pollutant i

b_{pi} is the coefficient of multiple regression of the source p for pollutant i

$APCS_p$ is the scaled value of rotated factor p for the considered sample

$APCS_p * b_{pi}$ is the contribution of source p to C_i in a sample

p is the source from 1, 2, 3, ..., n

To illustrate a PCA output, an extract from the work of Liao (2016) is used. According to Liao (2016), the variables with loadings >0.25 were considered as the major variables of the PCs. The naming of PCs was done using the major variables. PC1 was named combustion/industrial emission because it is characterised with high positive loading of variables including O_3 , SO_2 , Ca^{2+} , HNO_3 , K^+ , NH_4^+ , NO_3^- and SO_4^{2-} . Because of the positive signs on the loadings, it means they either increase together or decrease together. HNO_3 , NO_3^- and SO_4^{2-} in this component were associated with transport of combustion/industrial emissions. Their precursors (SO_2 and NO_x) may be oxidised during transport. The high positive loading of NH_4^+ indicates release of ammonia from local or regional agricultural activities, which could react with HNO_3 or H_2SO_4 to form NH_4^+ . Moderate loading on O_3

indicates transport of combustion emission because its precursors (NO_x and VOC) are rich in combustion emissions. The positive loading on PBM indicates coal combustion. PCA has been applied several times in source apportionment of gaseous and particulate matter pollutants (Song et al., 2006; Chang et al., 2009; Deng et al., 2018), ambient trace metals (Huang et al., 2013) and speciated atmospheric Hg (Cheng et al., 2009; Huang et al., 2010).

2.4.3 Treatment of missing data

Ambient concentrations data from continuous measurements are not often devoid of missing data. In environmental quality monitoring, missing data frequently occur due to equipment failure, routine maintenance and human errors (Noor et al., 2015). In source apportionment studies, e.g. apportionment of speciated atmospheric Hg, treatment of missing data is an essential step because some receptor models do not accept missing values (Liao, 2016). Therefore, it is imperative to handle missing data before performing source apportionment analysis to prevent inaccurate results. Two important methods of dealing with missing data in receptor modeling include exclusion (listwise deletion and pairwise deletion) and imputation. Listwise deletion removes all cases or samples with one or more missing data. Particularly, if the missing data is limited to a small number of measurements, it may be ideal to remove them from analysis without distorting the information in the data. However, if there are many missing data for one variable, listwise deletion causes a large reduction in data set and may bias the results because it favours variables with high concentrations (Huang et al., 2010). However, pairwise deletion removes the information when needed in the analysis and thus uses the entire available data. The advantage of this technique is that it increases the power of the data analysis. However, the disadvantage of pairwise deletion is that it reduces the number of variables in dataset thereby ending up with few data in which information in the data might have been distorted, making result interpretation difficult (Noor et al., 2015). The imputation method involves replacing missing data with predicted value based on

available measurements. The measures of central tendency of the measurements are commonly used in imputation. This method is important because it does not consider the time series characteristics between variables. Mean imputation is the most common technique used in previous Hg source apportionment studies (Liao, 2016; Michael et al, 2016) but it has a disadvantage of reducing the variance in the dataset and could also be affected by outliers in the dataset (Noor et al., 2015). If a data set consists of many missing values, exclusion of such missing data may reduce the variance and subsequently affect further analysis. However, PCA calculations do not require inclusion of all variables at a time. Thus, all treatment explained above could be accepted by PCA. When PMF and PCA results are to be compared, the same treatment of missing values is required.

2.5 Past studies of source apportionment of speciated atmospheric Hg

Quite a number of individual-site source apportionment studies of ambient speciated Hg using PMF model and PCA have been published. A review of past studies on source apportionment of speciated Hg is available in Cheng et al. (2015). Hg source profiles generated in these studies and sources identified as potential Hg sources contain one or combination of Hg forms and other air pollutants including gaseous pollutants (O₃, SO₂, CO, NO_x) and particulate matter components (elements and ions). Additionally, atmospheric processes that affect ambient Hg concentrations have also been identified using meteorological parameters such as temperature, relative humidity, wind speed and solar radiation, which are associated with Hg factors (Huang et al., 2010; Eckley et al., 2015; Liao, 2016). The PMF profiles used for interpreting Hg sources in many studies were similar, majorly linking ambient Hg with local or regional sources using major air pollutant variables as source markers.

In North America, source profiles have been derived with PMF model at receptor locations including Toronto (Cheng et al., 2009) and Kejimikujik National Park (Cheng et al., 2013;

Liao, 2016) in Canada; Detroit, Michigan (Lynam and Keeler, 2006) and Mississippi (Ren et al., 2014) in USA; Xiamen (Xu et al., 2015) and Mt Changbai (Liu et al., 2019) in China. These and similar Hg apportionment studies at different locations identified sources that mostly represented Hg sources including combustion (e.g. coal combustion, biomass burning, mobile source, and incineration of wastes) and industrial (iron and zinc smelting). Most of the sources identified showed profiles representing Hg sources with combination of Hg forms and specific source markers such as SO₂ for coal combustion, Al, Fe, Si, Zn, K for crustal/soil dust and SO₄²⁻, NO₃⁻ and NH₄⁺ as regional source. The consideration and use of source markers in source apportionment of atmospheric Hg has provided interpretable profiles for identifying specific Hg sources influencing receptor sites. For instance, the PMF model factor profile containing GOM, PM, HNO₃, NH₄⁺ and SO₄²⁻ as the major variables of the factor was identified as combustion emission in Liao (2016). Another factor identified to be photochemistry and re-emission of Hg has a profile with major variables comprising of GEM, GOM, PBM, PM, O₃, Ca²⁺ and K⁺. Atmospheric processes including photochemistry, wet deposition, gas-phase oxidation and condensation on particles, during winter, also play important role in the variation in ambient Hg concentration (Cheng et al., 2013; Liao, 2016). Previous studies have also revealed consistent diurnal and seasonal patterns in ambient Hg concentrations with GEM correlating significantly with temperature in winter and GOM with O₃ in summer (Duan et al., 2017). Re-emission of gaseous phase Hg has also been identified at sites previously under the influence of heavy industrial operations particularly in Canada (Eckley et al., 2015) and China (Zhu et al., 2018).

Principal component analysis of a seven-month ambient data containing Hg and other gases showed that GEM, PBM and SO₂ correlated strongly with a component suggesting that coal combustion was an important source of GEM and PBM (Duan et al., 2017). They also found out that gas-to-particle partitioning might also be another source of PBM because this

component was had loadings on GOM and PBM with few other air pollutants. Conversion of GEM to GOM in the presence of sunlight is an important reaction in atmospheric Hg research. Selin and Jacob (2008) suggested that a substantial contribution to speciated atmospheric Hg was due to photochemical conversion of GEM emitted from distance sources. Li et al (2017) analysed 17 months of PBM concentrations in Jinan, China together with gaseous pollutants including SO₂, CO and NO_x and inferred coal-fired industries, cement plants and traffic emissions as potential local sources affecting Hg at the site. The source apportionment of speciated atmospheric Hg by Cheng et al (2009) using PMF and PCA suggested industrial sources including chemical production, metal production rather than coal combustion contributed majorly to measured Hg levels in Toronto, Canada.

2.6 Inter-comparison of receptor models

Inter-comparison of receptor models entails the evaluation of the outcomes of two or more source apportionment methods on the same dataset. The application of two or more receptor models for results comparison in source apportionment studies has been suggested (Viana et al., 2008; Callén et al., 2009). For instance, if a receptor model identifies a factor representing two sources, i.e. a factor containing profiles relating to two or more sources, and another model, using the same dataset, could split the mixture into two or more distinct and realistic factors, then the latter has a better performance in resolving the collinearity in source profiles than the former. The main advantage of models comparison is that one receptor model stands a chance to compensate for the other's limitations in the reconstruction of the measured pollutant concentrations. A comparison study by Cheng et al. (2013) utilised PCA, APCS and back trajectories to identify the differences in sources affecting speciated Hg at a coastal site and an inland site. The study revealed major differences in sources and atmospheric Hg processes between a coastal and inland site. The PCA and back trajectory data suggested that the coastal site was affected by evasion of GEM from the ocean. In another study by Caselli et

al. (2006), relative root mean square errors (RRMSE) were used to evaluate the goodness of the reconstruction of the samples, parameters and source profiles derived from an urban atmospheric particulate in the literature. This used two receptor models: Absolute Principal Component Scores (APCS) and Target Transformation Factor Analysis (TTFA). The results were quite different in both methods. The percent errors (Error %) in APCS and TTFA were found to be 79% and 101%, respectively, indicating that APCS rebuilt the source profile better than TTFA. The source contribution to the mean value of the sample was also better described by APCS than TTFA when the contributions from a crustal source (with lowest mean contribution to the samples) were considered. Another comparison study showed that ambient samples were better reproduced by APCS with error of 56% than TTFA with error percentage of 199 (Caselli et al., 2006). In another comparison study, Viana et al (2008) evaluated the comparability of three receptor models (CMB, PCA and PMF) in reconstructing the daily concentrations of PM₁₀ in an industrial area in northeast Spain using three parameters. The study found that dispersion between the modelled and observed PM₁₀ concentration was lowest in CMB ($R^2 = 0.93$, slope 0.93) but minimal in PMF ($R^2 = 0.83$, slope = 0.96) and PCA ($R^2 = 0.86$, slope = 0.86). Similarly, Callén et al (2009) also found reasonable agreement between PCA and PMF reconstructed source profiles in the daily PM₁₀ concentrations data. However, these differences in receptor modeling results are sometimes expected because receptor models are based on markedly different theoretical approaches. The combined use of different types of receptor models would therefore, likely solve the limitations of each of the models by reconstructing a more robust solution based on their strengths (Viana et al., 2008).

CHAPTER 3

METHODOLOGY

3.1 Study Area

The study site (Figure 3.1) is in Flin Flon, Manitoba (55.77° N, 101.88° W, elevation: 304m, Eckley et al., 2013). Manitoba experiences humid continental climate with severely cold mean temperature of -24.5 °C in winter and relatively warmer mean temperature of 23.7 °C in summer (Eckley et al., 2013). Annual precipitation in Flin Flon is 345 mm falling as rain and 146 cm falling as snow (Weather station ID: 5050920, ECCC, 2018). The city has a population of 5363 in Manitoba and 229 in Saskatchewan (Statistics Canada, 2018) with the majority of the city in Manitoba. Residents of Flin Flon travel south into Saskatchewan and north into Manitoba. The Hudson Bay Mining and Smelting (HBM&S) complex is an important industrial site in Flin Flon, which is located in the remote boreal forest environment in West-central Manitoba near the border with Saskatchewan.

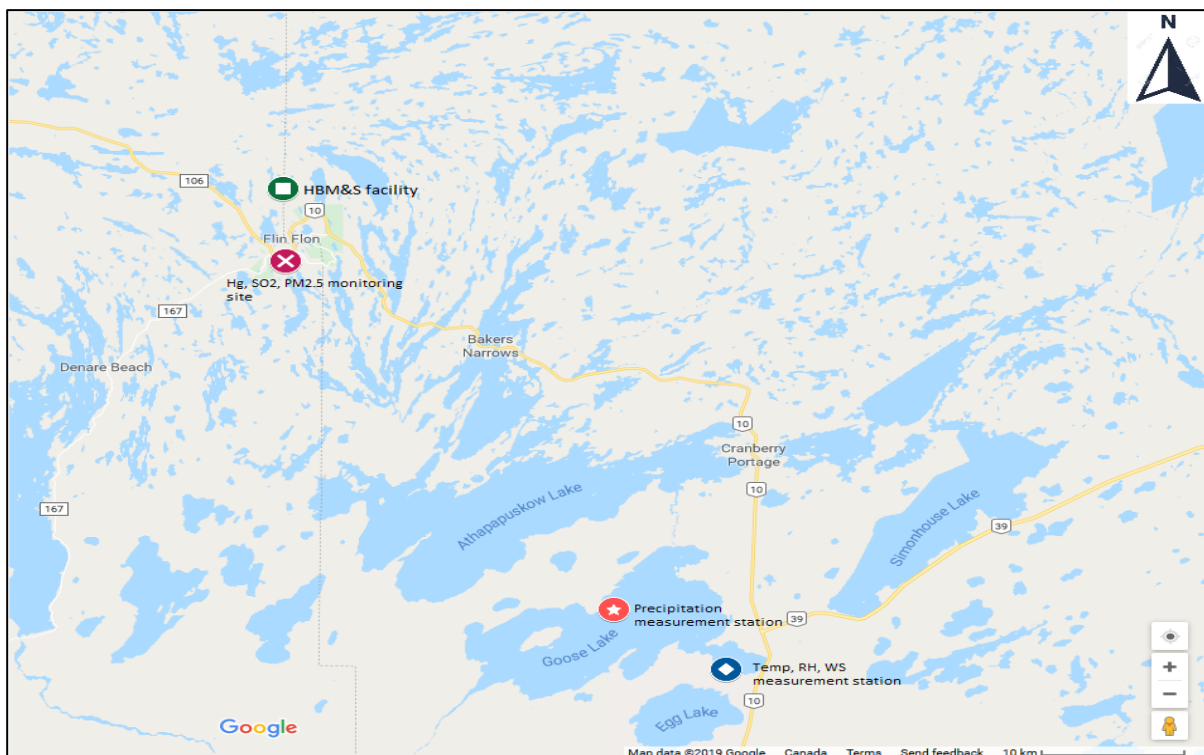


Figure 3.1: Location of Hg, SO₂ and PM_{2.5} sampling sites, HBM&S facility with emission >20kg/yr. based on NPRI, meteorological stations for hourly temperature, RH, WS and daily precipitation.

The HBM&S complex is approximately 600 km northwest of Winnipeg. It was formerly the largest point source of atmospheric Hg in Canada. Other major industrial site of significance in the study area with record of Hg releases to the Canada's National Pollutant Release Inventory (NPRI) is beyond 400 km radius of the sampling site. At Flin Flon, mining operations started in December 1927 followed by smelting in the late 1930 with the natural ore removal from an open pit and refinement at the plant (Franzin et al., 1979). Mercury was a natural constituent of the processed ore. In 1974, the originally designed 30 m stack was replaced with a 251 m stack to ensure effective dispersion of the process emissions in the atmosphere before reaching the ground. Due to the age of the smelter and changes in environmental laws, the facility was closed on July 1st, 2010 after eight decades of active operations. Before the closure, various air pollutants including Hg, SO₂ and airborne particulates containing toxic components were largely emitted into the atmosphere. Based on available information on Hg releases at the study site, past annual air emissions were not documented until the late 1990s. The historical Hg emissions from HBM&S decreased tremendously from 1999 to 2010. The large reduction over the years could be attributed to increased efficiency in control technology and strict enforcement of environmental laws and regulations (CCME, 2011). The estimates of annual air releases from HBM&S facility ranged from 1400 kg/yr. in 1999 to an average of 1019±347 kg/yr. in 2000-2010. However, Environment Canada reported four point sources of atmospheric Hg in Manitoba between 2010 and 2011. These include three metal production plants and a limestone production plant (Listed in Tables A1 and A2). The highest Hg emission in 2010 was reported for HBM&S (Table A1) while the following year (2011) reported zero emission for the same facility (Table A2). Because Flin Flon area is on the border with Saskatchewan, the record of Hg point source emissions in Saskatchewan were also listed included (Listed in Tables A3 and A4). In Saskatchewan, three power generating plants, a metal production plant, two trailer

production plants and a metal smelting plant were reported in 2010 and 2011. Beside Hg emissions, Vale Canada Limited, located at 276 km northeast of site, reported the largest SO₂ emission of 183,397 tonnes between 2010 and 2011. HBM&S also reported 58,306 tonnes of SO₂ during the study period.

3.2 Monitoring data

3.2.1 Speciated Hg

Continuous 2-hr measurements of GEM, GOM and PBM were taken at Flin Flon site from July 21st, 2010 to May 7th, 2011 using a Tekran 1130/1135/2537 ambient speciation system (Tekran Inc., Canada). During the operation of the instrument, ambient air was sampled on Teflon® filter via a KCl-coated annular denuder, and a Quartz fibre filter coupler impactor which is designed to remove <2.5 µg particles at flow rates of 10.0 litres per minute (ECCC, 2016). The sampled air flows over the quartz denuder coated with KCl in the 1130 unit, which collects GOM and PBM, and then passes via a quartz regenerated particulate filter in the 1135 unit where PBM is collected. GEM passes via the 1130 and 1135 collection units and a T-Junction in the sample line then conveys a fraction of the inlet air at a flow rate of 1.0 litre per minute into the 2537 analyser where GEM is pre-concentrated for five minutes prior to analysis by amalgamation on pure gold cartridges used as Hg adsorbent (ECCC, 2016). GEM is removed from the cartridges by thermal desorption and detected using Cold Vapour Atomic Fluorescence Spectrophotometer (CVAFS) (ECCC, 2016). GEM was measured continuously in the 2537 unit every five minutes. The sampling methods are currently the most acceptable methods for measuring GOM and PBM although past studies have reported that these methods may be under the interference of O₃, water vapour and other compounds (Lyman et al., 2010, Huang et al., 2013).

Visual examination of the GEM, GOM and PBM data revealed the following: twenty-two missing data each in July, two in August, one in September and fourteen in October 2010.

In 2011, two data points were missing for each of GEM and PBM, one for GOM in January, nine missing values for each Hg forms in February and twenty-four data each in May. The quality of speciated Hg data was checked using the Environment Canada Research Data Management and Quality Control (RDMQ) module. All the Hg data were obtained from the National Atmospheric Chemistry (NAAtChem) Database and Analysis Facility of the Environment Canada (ECCC, 2010a,).

3.2.2 PM_{2.5} speciation

The PM_{2.5} samples were collected at the monitoring site under the National Air Pollution Surveillance (NAPS) program of the Environment Canada from July 2010 to May 2011. Integrated twenty-four-hour PM_{2.5} (particulate matter with aerodynamic diameter <2.5µg/m³) samples were collected at a flow rate of 16.7 litres per minute on a 47 mm diameter Teflon filter installed on a sequential dichotomous (Dichot) sampler (CCME, 2011) using a 1-in-3 day collection frequency for element characterisation and 1-in-6 day collection frequency for water-soluble ions. In total, forty-two chemical components including elements and ions were measured on each PM_{2.5} samples. The list of components and analytical methods were presented in Table 3.1. All PM_{2.5} samples were routinely analysed by the Analysis and Air Quality Section (AAQS), Air Quality Research Division (AQRD) of the Environment Canada located in Ottawa, Canada. PM_{2.5} mass concentration was determined by gravimetric method using microbalance to weigh the Teflon® filter before and after sampling. The PM_{2.5} mass was divided by volume of air (at ambient conditions) that passed through the filter (CCME, 2011). The particle-loaded Teflon filters were analysed for elemental components using Energy Dispersive X-ray Fluorescence (EDXRF) spectrometry and for soluble anions and cations using Ion Chromatography (IC) (CCME, 2011). The PM_{2.5} data were obtained from the Environment and Climate Change Canada's National Air Pollutant Surveillance (NAPS) program database (ECCC, 2010b).

Table 3.1: PM_{2.5} speciation and analytical instruments

Sampler/Module	Collection medium	Laboratory Analysis	Variable measured
Dichot Partisol Speciation Sampler	47 mm Teflon®	Gravimetry	PM _{2.5} Mass
		X-ray fluorescence	Aluminium, Silicon, Sulphur, Potassium, Calcium, Titanium, Vanadium, Chromium, Manganese, Iron, Nickel, Zinc, Selenium, Bromine, Rubidium, Strontium, Cadmium, Tin, Antimony, Caesium, Barium, Lead
		Ion Chromatography	Sulphate, Nitrate, Chloride, Sodium, Ammonium, Fluoride, Acetate, Formate, Propionate, MSA, Nitrite, Oxalate, Bromide, Phosphate, Lithium, Potassium, Magnesium, Calcium, Strontium, Barium

3.2.3 Sulphur Dioxide (SO₂)

Hourly continuous SO₂ concentrations from July 2010 and May 2011 were measured at the Environment Canada's National Air Pollution Surveillance (NAPS) site in Flin Flon. The detailed sampling protocol for measuring SO₂ concentrations at all the designated NAPS sites across Canada including Flin Flon is provided in the ambient air monitoring protocol for PM_{2.5} and Ozone Canada-wide standards (CCME, 2011). The sampling technique for measuring sulphur dioxide concentration at the site is ultraviolet fluorescence method. The most important primary source of SO₂ in the atmosphere is power generating plant burning coal as fuel. The detection of SO₂ at the site is likely influenced by industrial emissions point sources in the area. SO₂ gas often transforms via oxidation reaction to form secondary product known as sulphuric acid aerosols or sulphates and the reaction takes place in the gas phase, liquid phase or on solid surfaces (CCME, 2011). The hourly SO₂ data collected was converted to daily averages to match with the measurement resolution of other pollutants in the data set. The data was provided by Environment and Climate Change Canada via the NAPS database (ECCC, 2010b).

3.3.4 Meteorological data

The conditions of the atmosphere including seasonality can have significant influence on the variations in ambient concentrations of speciated Hg (Cheng et al., 2015). Meteorological measurements are commonly included in model input to aid source apportionment of speciated Hg and also because change in the ambient concentrations of Hg could occur under certain conditions of the atmosphere (Liao, 2016). Based on weather conditions at the site, the study period can be divided into four seasons, summer (July-August), autumn (September-November), winter (December-February) and spring (March-May). The meteorological data used in this study included hourly temperature, relative humidity, wind speed, and daily precipitation measurements. The hourly data were continuous measurements at a local weather station (climate ID: 5050919) located at a distance of 154.15 km southeast of the sampling site. The station characteristic include latitude 54.41°, longitude 101.41° with elevation of 303.9 m (ECCC, 2010c). Because hourly precipitation data was not available at this station, the daily data were measured at another nearby station (climate ID: 5050920) located at a distance of 148.7 km from the sampling site. The station's information include latitude 54.46°, longitude 101.53° and elevation of 320.0 m (ECCC, 2010c). All meteorological data were extracted from the historical weather data archive available on the Environment and Climate Change Canada's website (ECCC, 2010c).

3.3 Emission Data

Although, air pollutants emitted directly into the atmosphere react and are often conveyed from their origin to various receptors via air mass movement, it is expected that source apportionment of ambient speciated Hg in similar manner to other air pollutants will directly implicate sources identified as important Hg sources at Flin Flon site using emission inventory information. Examining emission inventory is therefore, regarded as a crucial step for conducting source apportionment of speciated Hg. As discussed earlier, adequate

knowledge of the Hg sources at the site may be helpful prior to conducting receptor modeling of ambient speciated Hg for realistic interpretation of the results. For this study, available annual point source emission data including Hg, SO₂, NO₂, NH₃, PM_{2.5}, and Zn emissions from the facilities in Manitoba and Saskatchewan were extracted from the Canada's National Pollutant Release Inventory (Environment Canada's NPRI, 2018) and listed in Tables A1 to A4. Facilities within a radius of 700 km of the sampling site in Flin Flon were considered as the major point sources with significant emissions. The NPRI of Canada is a comprehensive document containing the annual air pollutant releases at the national, provincial and territorial levels and is accessible online free of charge for public use in research and policy formulation.

3.4 Data screening

The screening of the atmospheric concentrations data is an important initial step in apportioning air pollutants to their respective sources or source categories. Recent advances in ambient measurement technology have enabled us to measure air pollutants at very low concentrations. However, due to inherent limitations of analytical sampling methodologies, air pollutant data sets often contain several observations that are reported as missing and below analytical detection limit (Rao et al., 1991). Consequently, measurements below detection limit are commonly excluded from statistical analysis because of their potential effects on modeling results. In the data set used, not all air pollutants, particularly PM_{2.5} components, were useful. This is because some of the components were frequently detected in quantities below their detection limits by the measuring equipment and this might be expected to complicate the statistical analysis resulting in large uncertainty in the results (Cheng et al., 2016). The data screening procedures were carried out in order to treat the inherent features of the data set including below detection limit data, outliers and insufficient species. Firstly, the annual data was counted using the excel function 'count' and the expected annual data for each species was noted. The data counts for the study period are listed in Table 3.2.

Table 3.2: Monitoring data counts and the percentage of data below detection limit (BDL) from July 2010 to May 2011.

Parameter	Total data expected	Total data available	DL	% BDL	% missing				
Hg species									
GEM (ng/m ³)	1790	1790	0.1	0	0				
GOM (pg/m ³)	1790	1790	2	51	0				
PBM (pg/m ³)	1790	1789	2	25	0.06				
1-in-3 days									
Parameters (µg/m ³)	Total data expected	Total data available	DL	% BDL	Parameter (µg/m ³)	Total data expected	Total data available	BDL	% BDL
PM _{2.5}	112	65	0.465	10	Zn	112	65	0.002	17
Al	112	65	0.007	10	Se	112	65	0.005	100
Si	112	65	0.004	19	Br	112	65	0.004	100
S	112	65	0.002	7	Rb	112	65	0.003	100
K	112	65	0.002	10	Sr	112	65	0.004	100
Ca	112	65	0.002	34	Cd	112	65	0.009	100
Ti	112	65	0.002	83	Sn	112	65	0.012	100
V	112	65	0.001	52	Sb	112	65	0.013	100
Cr	112	65	0.002	97	Cs	112	65	0.040	100
Mn	112	65	0.002	62	Ba	112	65	0.031	100
Fe	112	65	0.003	10	Pb	112	65	0.009	100
Ni	112	65	0.002	69					
1-in-6 days									
Parameter (µg/m ³)	Total data expected	Total data available	DL	%BDL	Parameter (µg/m ³)	Total data expected	Total data available	BDL	% BDL
PM _{2.5}	56	32	0.465	20	Nitrite	56	32	0.007	100
SO ₄ ²⁻	56	32	0.007	13	Oxalate	56	32	0.007	19
NO ₃ ⁻	56	32	0.014	17	Br ⁻	56	32	0.014	100
Cl ⁻	56	32	0.007	18	PO ₄ ³⁻	56	32	0.021	100
Na ⁺	56	32	0.002	0	Li ⁺	56	32	0.000	100
NH ₄ ⁺	56	32	0.003	7	K ⁺	56	32	0.004	13
F ⁻	56	32	0.001	93	Mg ²⁺	56	32	0.001	20
Acetate	56	32	0.007	87	Ca ²⁺	56	32	0.001	13
Formate	56	32	0.007	100	Sr ⁻	56	32	0.001	100
Propionate	56	32	0.007	100	Ba ²⁺	56	32	0.001	100
MSA	56	32	0.007	93	Total ions	56	32		
Gaseous									
SO ₂ (ppm)	336	336	0.002	71					
Meteorological data									
Temp(°C)	335	335							
RH(%)	335	335							
Preci (mm)	335	335							
WS (m/s)	335	335							

3.4.1 Below detection limit

The equation used to calculate the percent of data below the detection limit is provided in Equation 3.1 below. Simply explained, the percentage of the data below the detection limit was obtained by dividing the number below detection limit data by the total data available.

$$\% BDL = \frac{\# \text{Belowdetectionlimit}}{\text{Totalavailable}} \times 100 \quad (3.1)$$

With the calculated percentage of BDL for all species, allPM_{2.5} components having greater than 20% of the measurements below their individual detection limits were excluded. Based on this screening threshold, all the components for both years that met and those that did not meet the requirement were selected and listed in Table 3.3.

Table 3.3: PM_{2.5} components data with ≤20% BDL and >20% BDL

BDL ≤20%		BDL >20%	
Element	Ion	Element	Ion
Al	SO ₄ ²⁻	Ti	F-
Si	NO ₃ ⁻	V	acetate
K	Cl ⁻	Cr	formate
Ca	Na ⁺	Ni	propionate
Fe	NH ₄ ⁺	Se	MSA
Zn	Oxalate	Br ⁻	nitrite
S	K ⁺	Rb	Br ⁻
Br	Mg ²⁺	Sr	PO ₄ ²⁻
	Ca ²⁺	Cd	Li ⁺
		Sn	Sr ⁻
		Sb	Ba ²⁺
		Cs	
		Ba	
		Pb	
		Mn	

For this study, speciated Hg and SO₂ data were exempted from the application of the 20% threshold level. This preference was given to speciated Hg because they are the pollutants of focus of this study while SO₂ was preferentially treated due to its relevance in source apportionment of atmospheric Hg. It is worthy of mention at this point that SO₂ is an excellent marker indicative of coal combustion (Reff et al., 2007) and coal combustion is a major

source of GEM, GOM and PBM although they are emitted in different proportions (Cheng et al., 2015)

3.4.2 Linear correlation test

Pairs of PM_{2.5} components including sulphur and sulphate, elemental and soluble calcium, elemental and soluble potassium were respectively present in the ambient monitoring data used in this study. The statistical relationships between each pair of these variables were checked with linear correlation plots. These component pairs measured by both IC and EDXRF were carefully selected by examining their correlation coefficients and data availability. Wherever there was strong agreement between the pair of species, there was no advantage to incorporating both species in the analysis. Common considerations when preparing data set for statistical analysis have been stated by Reff et al. (2007). Sulphur was removed from the data sets due to strong and statistically significant correlation with sulphate (ANOVA, $R^2 = 0.92$, p-value <0.05, Figure 3.2a). In previous source apportionment studies, either SO₄²⁻ or sulphur has been used but not both (Reff et al., 2007). The common justification in the selection for removing one species is to prevent counting sulphur atoms more than once by the receptor models (Kim and Hopke, 2004). The same reason also applies to Ca and Ca⁺. For this pair of species, Ca was discarded due to significant correlation with Ca²⁺ (ANOVA, $R^2 = 0.96$, p-value <0.05, Figure 3.2b). In the case of total K and soluble K⁺, the correlation was weak but statistically significant (ANOVA, $R^2 = 0.42$, p-value <0.05, Figure 3.2c) indicating that separate sources are responsible for the variations in their concentrations. This led to the decision to retain both variables in the analysis of the data set. It is important to note that in source apportionment of air pollutants, soluble K⁺ is an excellent marker for biomass burning while elemental K represents an indicator of crustal or soil dust (Deng et al., 2018).

3.4.3 Outliers

Outliers are observations that deviate markedly from the trend of other measurements in a data set. They occur in ambient data due to errors in measurements or during a power failure affecting the measuring equipment. It is important to identify and remove outliers prior to conducting source apportionment because their presence can lead to large uncertainty in the analysis results (Cheng et al., 2016). In the application of PMF model, the presence of outliers can affect the outputs by making it harder for the model to fit the species of the data set. The visual inspection of the two-hourly data for speciated Hg revealed unusually high data points at some periods during the measurements campaign. The criterion adopted to handle the outliers from the data set was that for a variable, the concentrations measured just before and after a measurement should be less than the annual mean plus six times the standard deviation. For 2010 PBM data set, two outliers including 316.7 pg/m³ on August 18th, 2010 and 221 pg/m³ on October 2010 were detected. GOM had outliers of 45.7pg/m³ on March 31st and 695.1pg/m³ on January 29th, 2011. The data points were removed based on the reason that the concentrations before and after them were above the annual mean plus six times the standard deviation. All SO₂ and PM_{2.5} concentration measurements were within the acceptable levels. The respective species scatter plots for the SO₂ and all PM_{2.5} components selected for this source apportionment study are presented in Tables E1 to E17.

3.5 Data Processing

Data processing in the context of this work involves preparing the screened ambient air pollutants data in one file primarily in the format acceptable by the PMF model and PCA. The post-screening data set was in the initial stage, prepared for input into PMF model and PCA by combining the annual screened data into a single excel file because a count of the sample size fell short of the acceptable size to give reasonable results for both methods. The selected species measurements were adjusted to make the time interval consistent throughout the

measurements period because different measurement intervals were observed in the data set. Because the PM_{2.5}, SO₂ and precipitation data were with daily values, the 2-hr speciated Hg data, and hourly temperature, relative humidity and wind speed were individually calculated into daily averages for consistency. For this analysis, both 1 in 3 days and 1 in 6 days PM_{2.5} data were utilised in order to determine the sources affecting ambient speciated Hg at the site.

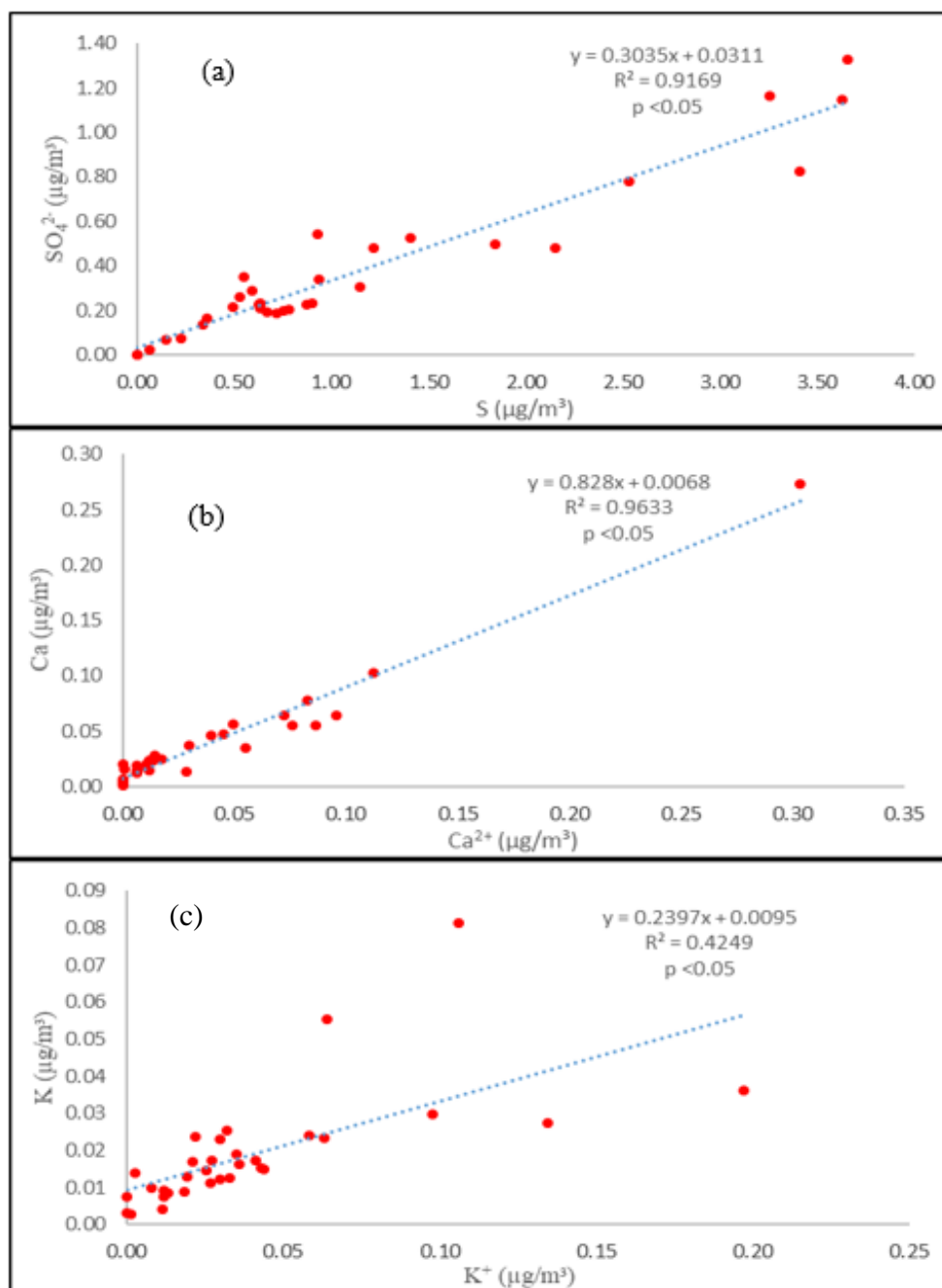


Figure 3.2: Scatter plots of (a) SO₄²⁻(IC) and sulphur (XRF) (b) Ca and Ca⁺ and (c) K and K⁺ from July 2010 to May 2011.

3.6 Treatment of missing data

For the treatment of the missing values in the input concentrations data, conventional exclusion and imputation are the two methods commonly used. In this work, the imputation method was applied in filling up the missing data for GEM, GOM, PBM, PM_{2.5} concentration and components. The following procedures were followed. Step 1: Cross correlations among the three speciated Hg and sixteen PM_{2.5} components including six elements, nine soluble ions and PM_{2.5} mass were initially conducted. Among the three Hg forms, PBM was selected to estimate consecutive missing ($n > 2$) PM_{2.5} components and mass, because PBM significantly correlated with more PM_{2.5} components (nine components) than GOM (correlated with four components) and GEM had no correlations with PM_{2.5} components. Linear regression equations between PBM and each of sixteen PM_{2.5} components were derived using excel data analysis tool. Step 2: For missing one or two consecutive speciated Hg data, PM_{2.5} mass and component samples, the average of equal number of chemical species measurements before and after the missing data were used as imputation. For example, GEM is missing on October 5th, 2010 and October 6th, 2010, imputations for the two consecutive missing GEM data are the average of the four GEM measurements on October 3rd and 4th, 2010 and October 7th and 8th, 2010. Step 3: For missing more than two-consecutive speciated Hg data, mean imputations from the same number of samples before and after the missing data were applied. For example, GEM samples were missing for four consecutive days from November 5th, 2010 to November 8th, 2010, imputations for the four missing GEM data were the averages of the data on all the four days before (November 1st, 2010 to November 4th, 2010) and all four days after (November 9th, 2010 to November 12th, 2010) the missing dates. Step 4: For missing more than 2-consecutive PM_{2.5} mass and component samples, linear regression was used to estimate each missing PM_{2.5} mass and components by using PBM concentration on that day.

After imputation process was completed, there were 292 samples (July 7th, 2010 to May 5th, 2011) in the full dataset. Out of all the 292 samples in the full dataset, there were 97 samples when PM_{2.5} mass and elements were expected to be measured. This reduced data set was denoted as dataset 1. In the 97 reduced samples, there were 16 samples with imputation of Hg data. After removing the 16 samples with Hg imputation, there were 81 samples finally left in the reduced data set. This was then denoted as dataset 2. Dataset 2 was subsequently used for the apportionment of speciated Hg at the site.

3.7 Choice of receptor models

Among numerous receptor models (RMs) currently in use for source apportionment of air pollutants, three commonly and most recently used methods include chemical mass balance (CMB), principal component analysis (PCA) and positive matrix factorization (PMF). The input, output and computation requirements of each model are presented in Table 3.4. The selection of the appropriate receptor modelling method depends on prior knowledge of the sources and source profile. Based on the input-output requirements for CMB, it is the most suitable receptor model to use particularly when the number of sources is well known and their composition profiles measured (Viana et al., 2008). In this study, since the sources and their composition profiles were not available, CMB model was not relevant. However, the PMF and PCA have found numerous applications especially when the sources and their profiles are unknown. As complex as these techniques may be in terms of their mathematical framework, they do not require prior knowledge about the sources and hence do not need source profiles as input (Viana et al., 2008). However, quantitative knowledge of potential sources may be of necessity for easy interpretation of the solution in both methods (Viana et al., 2008). Emission inventory and databases such as SPECIATE databases (USEPA, 2014) may be of importance because they contain information that can help to interpret the modeling results from the PMF model and PCA. In the practical application of PMF and PCA, both

models have their strengths and weaknesses. For instance, PMF requires both concentration dataset and their uncertainties as input whereas PCA allows the inclusion of meteorological data in the input. This is an advantage that PCA has over PMF because some Hg sources and processes are more likely to occur under certain environmental conditions e.g. combustion process occurring in winter due to high heat demand and oxidation of GEM in summer.

Table 3.4: Details input-output requirements of CMB, PCA and PMF (Viana et al., 2008)

	CMB	PMF	PCA
Inputs	<ul style="list-style-type: none"> • Emission profiles • Receptor concentration data • Uncertainty estimates 	<ul style="list-style-type: none"> • Receptor concentration data • Uncertainty estimates 	<ul style="list-style-type: none"> • Receptor concentration data and/or meteorological data
Output	<ul style="list-style-type: none"> • Source contribution • Model performance index 	<ul style="list-style-type: none"> • Source profiles • Source contributions • Model performance index 	<ul style="list-style-type: none"> • Source factors • Performance index
Computation	<ul style="list-style-type: none"> • Specific software downloadable freely on US EPA website • Selection of input source profile- time consuming • Source contribution- time consuming 	<ul style="list-style-type: none"> • Proprietary software downloadable freely on US EPA website • Source identification –fast • Source contribution – fast • Input data preparation – time consuming 	<ul style="list-style-type: none"> • No specific software required • Source identification- fast

3.8 PMF Model setup and performance evaluation

In recent years, PMF model has frequently evolved to address the uncertainty in source apportionment of air pollutants at numerous monitoring site including rural and urban locations (Hopke 2016). For the analysis of the data set, EPA PMF5.0 specifically designed by USEPA for source apportionment of air quality data was used (USEPA, 2014). The application software of the model is available freely for download from USEPA’s website for air quality researchers. The setup of PMF5.0 is presented in Table 3.5. The uncertainty estimates were calculated using the equation-based method. For speciated Hg uncertainty, the error fraction was set at 10% because the concentrations of GOM and PBM were low and have high percentage of below detection limits data (Liao, 2016). For PM_{2.5} and SO₂, the error fraction was set as 10% of their concentrations. In the PMF modeling method, there are two approaches of handling missing data by the model. These approaches include listwise deletion

and pairwise deletion. Listwise deletion removed completely all rows of samples having one or more missing values. This often results in large reduction of the sample size and causes the number to reduce below a sample size expected to yield a satisfactory or realistic solution. Apart from speciated Hg data, all of the PM_{2.5} variables have many missing data at different time of measurement. After imputation and regression analysis were carried out on the data set, the model excluded no sample but reduction in the correlation among the variables was observed. Table C1 contains the cross correlation between input variables before imputation while Table C2 contains correlations after imputation was carried out to treat the missing data. After loading the input data and the uncertainty data in the PMF model, statistical checks provided by the model were used to assess the variations in the data set. The time series plots of the variable concentrations were checked to observe if there were concentration spikes, which could have been caused by real pollution events. No spikes were observed in the time series graphs concentrations for speciated Hg. For the PMF model, categorization of variables is an important step. In this study, all variables used were categorized as strong.

Table 3.5: PMF model handling of missing data and sample size

	Treatment	Missing data handling	Sample size (N)	Minimum sample size*	Other default settings
Data set 2	Imputation of mean and linear regression	Complete data use	81	60	Number of runs (20), random start, listwise deletion

*Hopke, 2016

The S/N ratio as required in PMF model was not used because the uncertainties were set to a fixed fraction of the concentrations (USEPA, 2014). No species was selected as the total variable because the input data contained both particulate matter and gaseous air pollutants but the analysis actually focused mainly on Hg species. The default value of 20 was used as the number of runs to evaluate the stability of the PMF. To determine the number of factors, multiple PMF model runs setting the number of factors from 3 to 9 were performed. A visual display of the Q values by PMF and the individual maximum column mean (IM) and

individual maximum column standard deviation (IS) calculated from the scaled residuals were plotted and visually inspected. The Q values represent the goodness of fit of the data set by PMF model. Each Q_{robust} value was calculated by the model with exclusion of those data points not fit by PMF while the Q_{true} value makes use of all data points (USEPA, 2014). The IM and IS parameters were calculations from the scaled residuals and are used to reduce the range of meaningful solutions in the PMF model (Lee et al., 1999). After inspecting the lines, a range of possible number of factors was chosen.

After each of the runs with 3-9 factors, the Q (robust), Q (true) and the convergence were examined. The converged run showing the lowest Q (robust) value was highlighted and only the converged run was further analysed (USEPA, 2014). All runs in each chosen factor were convergent. Both Q (robust) and Q (true) values had small variations among 20 runs indicating stable PMF results (USEPA, 2014). The run with the minimum Q (robust) value, also identified as the best base run for each factor, was further analysed. In the apportionment of speciated Hg, the model fit and uncertainties were usually evaluated using the scaled residuals to ensure they are randomly distributed within ± 3 standard deviations and/or evaluating the results using regression analysis between the measured and modeled observations. If the number of scaled residuals was between +3 and -3, it is an indication that PMF model fits the variable well (USEPA, 2014). Species with scaled residuals beyond +3 and -3 were further evaluated using observed/predicted scatter plot and time series graphs. The regression statistics used include the coefficient of determination (R^2), slope (S) and the p-value. The R^2 represents the proportion of the variance explained by PMF. The closer R^2 is to one, the better the model performance. If R^2 is closer to one and the slope is closer to zero than one, this shows that the model fits the data well but the variance in the data was small. The p-value for each Hg species is expected to be <0.05 . The right number of factors chosen was based on the performance analysis of PMF and physical meanings of the components

obtained. The factor profiles in the final solution were assigned to sources using source emissions profiles for Hg available from previous Hg apportionment outcomes in the literature.

The contributions of factors to the total predicted Hg concentrations and ratios of predicted Hg concentrations to measured Hg concentrations were calculated to verify the findings derived from Observed/Predicted time series. Factors with average Hg contributions larger than 10% were thought to be the major Hg sources, which have a large impact on ambient Hg concentrations. Special observation of re-emission sources were done in order to know their contributions to the ambient concentrations of Hg at the receptor site. When the average predicted/observed ratio was close to unity, the model was thought to reproduce the measured concentrations well. The PMF factors resolved were assigned to the sources based on the comparison of the major variables contained in the factors and markers of the source profiles in the literature. The variables percentages larger than 0.25 were used as the major variables of the factor. The factors were assigned to the sources with similar major variables.

3.9 PCA setup and performance evaluation

The analysis of the dataset using PCA was conducted using IBM[®] SPSS v25. The data set, with the same treatment of missing data, was used so that comparison of the results could be done. The setup of the data for PCA is presented in Table 3.6. The data set input met the restrictive sample size requirement of $(50+m)$, where m is the number of variables (Thurston and Spengler, 1985). For the dataset, initial PCA was conducted with and without the meteorological data. PCA allows the inclusion of weather parameters whereas the PMF model does not. This is an advantage PCA has over the PMF model because PCA has no constraint of non-negativity of factors profiles and contributions. The suitability of the dataset for PCA was determined using the Kaiser-Meyer-Olkin measure of Sampling Adequacy ($KMO < 0.6$) and Bartlett's test of Sphericity ($p < 0.05$). For the PCA, the number of components to retain

was determined using Kaiser’s Criterion, which states that the components with eigenvalue >1 should be retained.

Table 3.6: PCA handling of missing data and sample size

	Treatment	Handling of missing data	Sample size (N)	Required sample size (50+m)*	Other settings
Dataset 2	Imputation of mean and linear regression	Complete data use	81	70 ^a , 74 ^b	Listwise deletion, eigenvalue (>1), varimax rotation

m is the # of species, ^awithout meteorology factors, ^bwith meteorological factors, *Thurston and Spengler, 1985

Since the imputation ensures the utilization of the complete data input, the default listwise deletion box in PCA was checked. When the input data was imported into SPSS from an excel file, the KMO and Bartlett’s test, coefficient of determination and other user-desired output boxes including components scores, correlation matrix were checked. To determine the number of factors to retain in PCA, the Kaiser criterion (retain principal components with eigenvalue >1) and one more components was used. After obtaining the principal components with eigenvalue >1 from the initial run, the analysis was rerun for the second time with the extracted number of principal components fixed. The extracted principal components were rotated with orthogonal (varimax) rotation.

The communalities and extractions are other two important statistical PCA outputs, shown in form of fractions and the two numbers add up to one. The communality of each species represents the squared loadings on all components extracted. It is the total amount of variance, which an original variable shares with all other variables included in the analysis. This value is analogous to Pearson’s r in regression analysis. If the communality is close to one and the extraction close to zero, the variable shares a large amount of variance with other variables in the data set. The varimax rotated PCA results of the fixed and one added components were also examined. If the result improved with the added component, the result was preferred, else the result for the fixed components was used. Other PCA outputs, categorised as used or unused, are listed in Table B. The interpretability of the principal

components is also an important task in PCA (Lynam and Keeler, 2006; Cheng et al., 2009). The interpretation of the principal components was done by examining the variable loadings on the components. The loadings on the variables indicate the extent of the relationship between the variables and the component. An ideal case is for a loading to be close to positive or negative one. The sign on the loadings (positive or negative) from PCA is indicative of the relationship between the component and a variable. After rotating the result using with varimax rotation, the components were then assigned to Hg sources by examining the variable loadings on source markers and comparison with outcomes of previous studies and NPRI emission data.

3.10 Estimation of PCA components contributions

As the traditional PCA is useful for identifying the factors contributing the ambient Hg, it does not directly provide an apportionment of the mass. However, the overall average contributions of each PCA component to each Hg form and the profiles associated with each component were quantitatively determined for the data set with and without meteorological data. The principal component scores, which is the composite measure created for each observation on each extracted component in PCA, were transformed into absolute values called the Absolute Principal Component Scores, APCS (Thurston and Spengler, 1985). The APCS is determined by calculating the component scores for absolute zero concentrations and uses them to rescale the component scores from PCA. The procedure is briefly explained as follows: the measured concentrations of each chemical species in each sample were normalised using equation 2.4 in section 2.4.2.

The component scores obtained from PCA are in normalized form, with average of zero and standard deviation equal to one. The true zero value for each component was calculated by introducing an artificial sample (Z_0) in which the concentrations of all the species were set to zero. The normalisation of the artificial sample was done using equation 3.2 below:

$$(Z_0)_i = \frac{(0 - C_i)}{s_i} = \frac{-C_i}{s_i} \quad (3.2)$$

The APCS of each component were then estimated by subtracting the component scores for this artificial sample from the component scores of each of the true samples. The concentrations of each of GEM, GOM and PBM were then regressed on the calculated APCS. The resultant regression coefficients were then employed to transform the APCS into the source contributions to each Hg form in each sample. The source contributions to the observed Hg concentration were thereafter calculated using the generated multiple linear regression equation 3.3 below. The average of the product $APCS_p * b_{pi}$ on all samples represents the average contribution of all the sources.

$$C_i = (b_0)_i + \sum_{n=1}^p APSCS_p * b_{pi} \quad (3.3)$$

where,

C_i is the observed concentration of pollutant i

$(b_0)_i$ is the constant term of multiple regression for pollutant i

b_{pi} is the coefficient of multiple regression for the source p for pollutant i

$APCS_p$ is the scaled value of the rotated component p for the considered sample.

$APCS_p * b_{pi}$ is the contribution of source p to the observed concentration C_i in a sample

In APCS, source contribution estimates can be positive or negative because there is no restriction imposed on the results (Miller et al., 2002). However, from engineering point of view, a source cannot have a negative percentage of elements and cannot contribute a negative mass to the receptor concentration of an air pollutant. Therefore, any component with negative mass contribution percentage in APCS was assumed to be zero. The percentage contributions were determined using the equation 3.4:

$$\text{Overall contribution (\%)} = \frac{\text{Component's contribution averaged overall samples}}{\text{Sum of average contributions from all components}} \times 100 \quad (3.4)$$

CHAPTER 4

RESULTS AND DISCUSSION

4.1 PMF Results

4.1.1 Estimation of number of factors

In most cases, deciding the right number of factors in PMF modeling is often challenging. A common strategy is to examine the response of the model's statistical parameters including the Q, IM and IS, plotted against a range of number of factors (Reff et al., 2007). In this study, the calculated Q, and IM and IS values, obtained from PMF simulations initialised with three, four, five, six, seven, eight and nine factors, respectively, are presented in Tables D1 and D2. The plots of these three parameters against the number of factors are shown in Figures. 4.1 and 4.2.

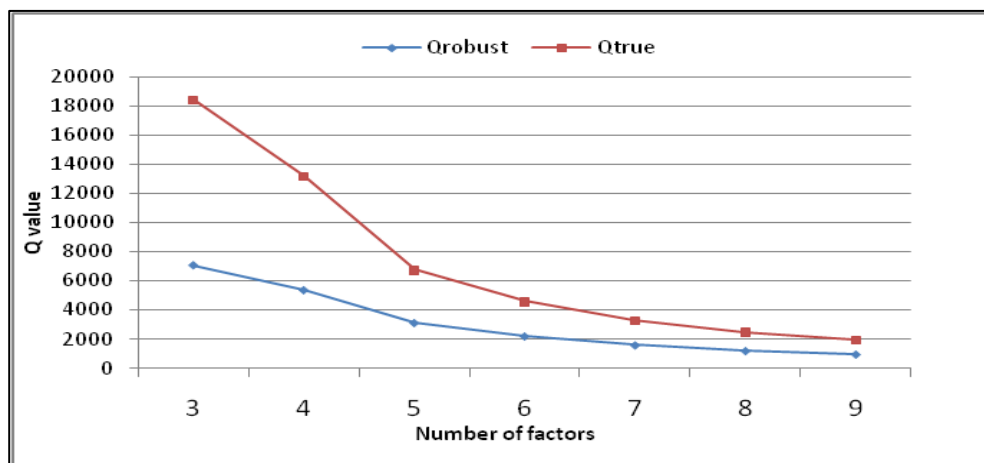


Figure 4.1: Plot of Q_{robust} and Q_{true} against the number of factors

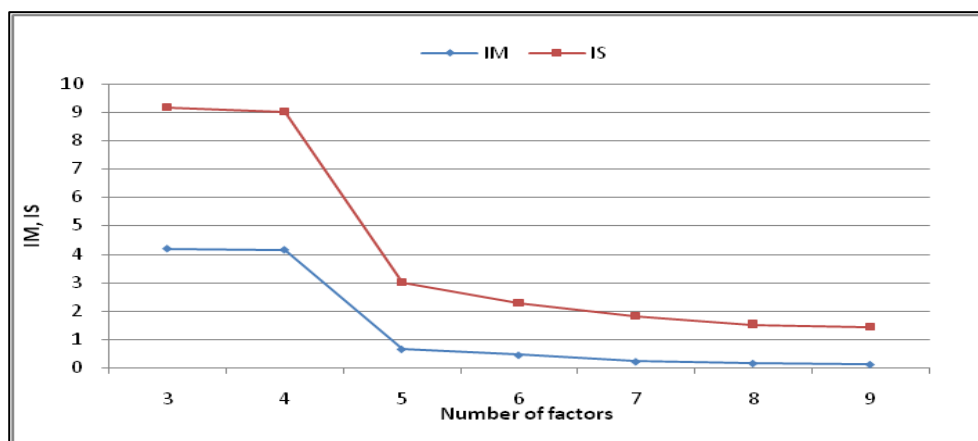


Figure 4.2: Plot of IM and IS against the number of factors

Inspecting the response of the Q values in Figure 4.1, the transition from 4 to 5 factors resulted in a sharp drop in the Q_{robust} and Q_{true} . Further increase of the number of factors from six to nine resulted in a regular decrease of Q_{robust} and Q_{true} . In a similar manner, it can be seen on Figure 4.2 that IS and IM were also sensitive to the changing number of factors. Increasing the number of factors from 4 to 5 led to a sharp drop in IM and IS, similar to the Q-value lines. There was a regular decrease in IS as the number of factors increased above 5. However, the IM nearly became insensitive above 7 factors. It has been reported by Ceasari et al. (2016) that the reasonable number of factors is a compromise of the trends of the lines of Q, and IM and IS. Thus, the comparative analysis of the behaviour of Q, IM and IS in relation to the number of factors suggested that a reasonable number of factor lies within 5, 6 and 7 factors. It is important to know that specifying too many factors in PMF model might further dissociate a real factor into two or more non-existing sources, making it difficult to identify the correct sources. Contrarily, choosing too few factors will likely result in the combination of sources of different nature. This can lead to underestimation of emissions from real sources (Wang et al., 2018). Thus, to choose the real factors to interpret the PMF model results from this study, the solutions of 5, 6 and 7 factors were further explored and compared.

4.1.2 Comparison of 5, 6 and 7-factor profiles

Determination of the real number of factors is a critical step in PMF model data analysis. To choose the final number of factors among 5, 6 and 7, the first method used was to compare the respective factor profiles. The full factor profiles of the 5, 6 and 7 factors are provided in Tables 4.1, 4.2 and 4.3, respectively. In the 5-factor profiles (Table 4.1), F3, which was identified as secondary aerosol, re-emission, and Hg oxidation, was, in the 6 factors, separated into F1 (secondary aerosol and re-emission), and F5 (Hg oxidation) (Table 4.2).

Table 4.1: Profile of five factors (% of species sum) with major variables >25% in bold, blanks <15%)

	F1	F2	F3	F4	F5
GEM			75		15
GOM			58		31
PBM					81
SO ₂				87	
PM	28	23	37		
Al	77		16		
Br			67		22
Fe	54	36			
K	71		24		
Si	90				
Zn		86			
NH ₄ ⁺			85		
Ca ²⁺					85
Cl ⁻					69
Mg ²⁺					71
NO ₃ ⁻					76
Oxalate			38		47
K ⁺			35		52
Na ⁺			16		73
SO ₄ ²⁻			86		
Factor name	Crustal/ soil dust	Industrial	secondary aerosol and re-emission/Hg oxidation	Coal combustion	Road salt/ biomass burning

Table 4.2: Profile of six factors (% of species sum) with major variables >25% in bold, blanks <15%)

	F1	F2	F3	F4	F5	F6
GEM	41				49	
GOM	36			20	41	
PBM				75		
SO ₂						88
PM	18	22	21		29	
Al			66		16	
Br					87	
Fe		31	52			
K			49		44	
Si			79			
Zn		79				
NH ₄ ⁺	78					
Ca ²⁺				84		
Cl ⁻				57	28	
Mg ²⁺				67		
NO ₃ ⁻				63	32	
Oxalate	39			47		
K ⁺	21			41	31	
Na ⁺				59	31	
SO ₄ ²⁻	79					
Factor name	Secondary aerosol and re-emission	Industrial	Crustal/soil dust	Road salt+ biomass burning	Hg oxidation	Coal combustion

Both F1 and F5 have GEM and GOM as major variables of the profiles. The secondary aerosol and re-emission factor (F1) has major variables containing GEM, GOM, NH_4^+ , oxalate and SO_4^{2-} whereas for the Hg oxidation factor (F5), the major variables were GEM, GOM, $\text{PM}_{2.5}$ and Br. The GEM in F3 of 5 factors was apportioned to both F1 and F5 in the 6-factor profiles. In the 5-factor profile, K^+ , found among the major variables in F3, moved to the Hg oxidation profile (F5) in the 6-factor profile. The separation of the secondary aerosol and re-emission (F1), and Hg oxidation (F3) in the 6-factor solution represented a significant improvement in the profiles with easy interpretation of the profiles. Thus, for the 6 factors, the presence of GEM, GOM and source markers in the profiles of the secondary aerosol and re-emission factor (F1) and GEM, GOM, $\text{PM}_{2.5}$ and Br in the Hg oxidation (F5) made it easier to identify the factors as Hg sources. All other major variables used to characterise crustal/soil dust (F1), industrial (F2), coal combustion (F4) and, road salt and biomass burning (F5), respectively in the 5 factors remained in the respective profiles in the 6 factors. A rearrangement of the positions of factors was observed in the 6 factors. However, in the analysis result of the 7 factors (Table 4.3), further dissociation of industrial (F2) into two factors including a zinc factor (F1) and an iron factor (F6) with no other major variables on each profile was observed but this was not useful for the Hg analysis because Hg was not a major variable on either factor. The interpretation of the 7-factor solution was not satisfactory compared with the 5 and 6 factors. Therefore, the 5 and 7-factor solutions were eliminated. The 6 factors were considered the most reasonable.

4.1.3 Comparison 5, 6 and 7 factors' distribution of scaled residual

The second option considered to evaluate the solutions of 5, 6 and 7 factors was the analysis of the distribution of the respective scaled residuals. The scaled residuals are useful in determining how well the PMF model fits each species in a data set. In a data set, if a species

has many scaled residuals, it may be an indication that the species is poorly fit (USEPA, 2014).

Table 4.3: Profile of seven factors (% of species sum) with major variables >25% in bold, blanks <15%

	F1	F2	F3	F4	F5	F6	F7
GEM					51		43
GOM					42		37
PBM			75				
SO ₂				88			
PM		21			22		25
Al		66					
Br					45		23
Fe		35				52	
K		58			25		
Si		74				24	
Zn	68						
NH ₄ ⁺							83
Ca ²⁺			81				
Cl ⁻			57		18		
Mg ²⁺			68				
NO ₃ ⁻			60		28		
Oxalate			46				38
K ⁺			39		29		22
Na ⁺			61		19		
SO ₄ ²⁻							84
Factor name	Zn source	Crustal/soil dust	Road salt+ biomass burning	Coal combustion	Hg oxidation	Iron source	Secondary aerosol and re-emission

A species with good fit is expected to have all the residuals within -3 and +3 standard deviations and a symmetrical distribution (USEPA, 2014). The distribution of scaled residuals of GEM, GOM and PBM for the 5, 6 and 7 factors are presented in Table 4.1. As can be seen on Table 4.1, the PMF solution with 7 factors has the lowest number of scaled residuals for all the three Hg species thus agreeing with the expected threshold boundaries. It is clear from the distribution of the scaled residuals that as the number of factor increased the number of scaled residuals outside +3 and -3 reduced. In this case, because the chemical profiles of the 7 factors showed a higher level of difficulty in interpretation due to the single major variable on some of the factors, the 6-factor solution was preferred.

Table 4.4: Scaled residuals of PMF solutions (N = 81)

Number of factors	Mercury form	Criteria	
		Distribution	Number of scaled residual beyond ± 3
5	GEM	Spread out	10
	GOM	Spread out	5
	PBM	Concentrated at zero	2
6	GEM	Spread out	8
	GOM	Skewed	3
	PBM	Skewed	3
7	GEM	Spread out	3
	GOM	Skewed	3
	PBM	Concentrated at zero	2

4.1.4 Comparison of 5, 6 and 7 factors regression statistics

The regression statistics of the 5, 6 and 7 factors were shown in Table 4.5. The statistical parameters include the coefficient of determination (r^2), slope of regression (S) and p-value for GEM, GOM and PBM and were calculated by the PMF model. These parameters depict how well the model is able to fit the Hg species (USEPA, 2014). They were determined by the model by correlation of the observed concentrations of each Hg form and the predicted concentrations. A satisfactory (e.g. $r^2 > 0.5$) PMF solution is expected to have r^2 values and slope as close to one as possible and p-value < 0.05 since the exact number of sources affecting ambient concentrations of air pollutants at a receptor site is rarely known. As can be seen in Table 4.2, the PMF model had an improvement in r^2 values for GEM and GOM from 5 to 7 factors while the r^2 value for PBM was strong for PBM in all the runs. For the slope and p-value, similar improvement from 5 to 7 factors was also observed for all the Hg forms except GOM. The final decision to retain the 6-factor solution in the PMF analysis focused on the ease of interpreting the factors as compared to the 5 and 7 factors. Hence, the PMF with 6 factors was also resolved to be most acceptable.

Table 4.5: Regression diagnostics of PMF solutions (N = 81)

Number of factors	Mercury form	Criteria		
		Coefficient of determination (r^2)	Slope of regression (S)	p-value
5	GEM	0.146	0.398	0.027
	GOM	0.379	0.336	0.088
	PBM	0.981	0.915	0.005
6	GEM	0.285	0.521	0.132
	GOM	0.440	0.349	0.109
	PBM	0.981	0.942	0.013
7	GEM	0.532	0.650	0.113
	GOM	0.479	0.353	0.090
	PBM	0.983	0.952	0.005

4.1.5 Interpretation of PMF factors

Six factors, which represented the sources of affecting ambient Hg at Flin Flon, were identified in PMF. The profiles of the six factors are presented in Table 4.2. In Table 4.2, the rows represent the percentages of species apportioned to each factor while the columns are the species in each factors. For each factor, the variables emphasized as major variables in the profiles were those >25% (in bold). The time series of the factor contributions to each Hg form with temperature and wind speed are shown in Figures.4.3, 4.4 and 4.5, respectively.

Factor 1 was characterised by the major variables comprising GEM (41%), GOM (36%), NH_4^+ (78%), Oxalate (39%) and SO_4^{2-} (79%). This factor was named secondary aerosol and re-emission. SO_4^{2-} and NH_4^+ were the dominant species of the factor. The gaseous precursor of SO_4^{2-} is SO_2 , which is an excellent marker for identifying coal combustion processes. SO_2 may likely oxidize during atmospheric transport from the source to the sampling site. A search through the NPRI revealed four point sources with significant emissions of SO_2 . These sources include Vale Canada Limited and HBM&S in Manitoba (listed in Tables B1 and B2), and two power-generating stations in Saskatchewan (listed in Tables B3 and B4). Vale Canada Limited, processing non-ferrous metal, is located northeast of the sampling site at a distance of 276 km. The total air emission reported between 2010 and

2011 was 260,014 tonnes per year (sum of SO₂ emissions in Tables B1 and B2). HBM&S, a major iron and steel production plant reported annual air releases of 58,234 tonnes in 2010 (Table B1) and 72 tonnes in 2011 (Table B2). The Boundary Dam and Poplar River power stations in Saskatchewan reported total air releases of 86,247 and 82,147 tonnes per year, respectively.

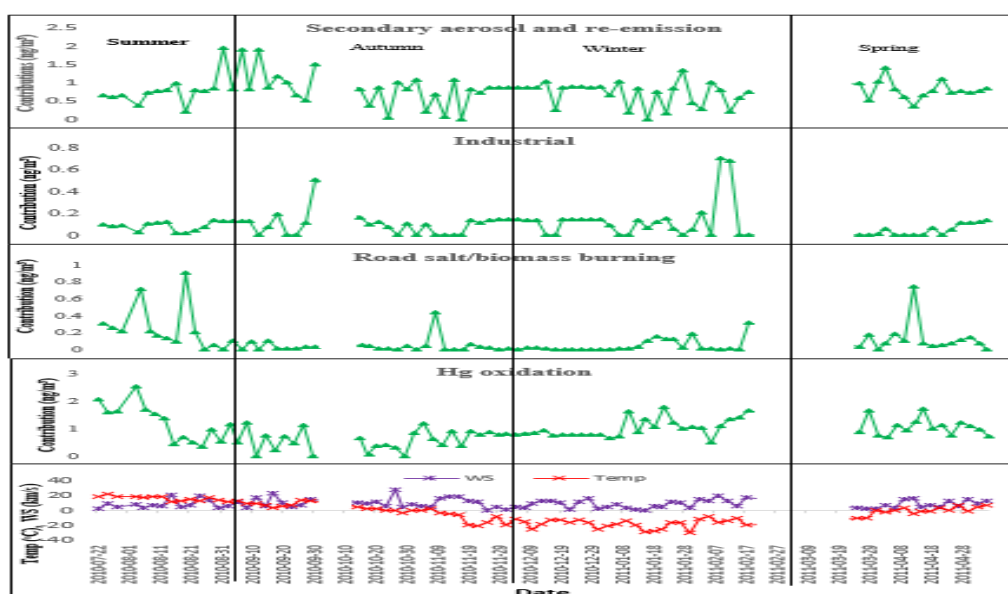


Figure 4.3: Time series relationship of PMF factor contributions to GEM with temperature and wind speed.

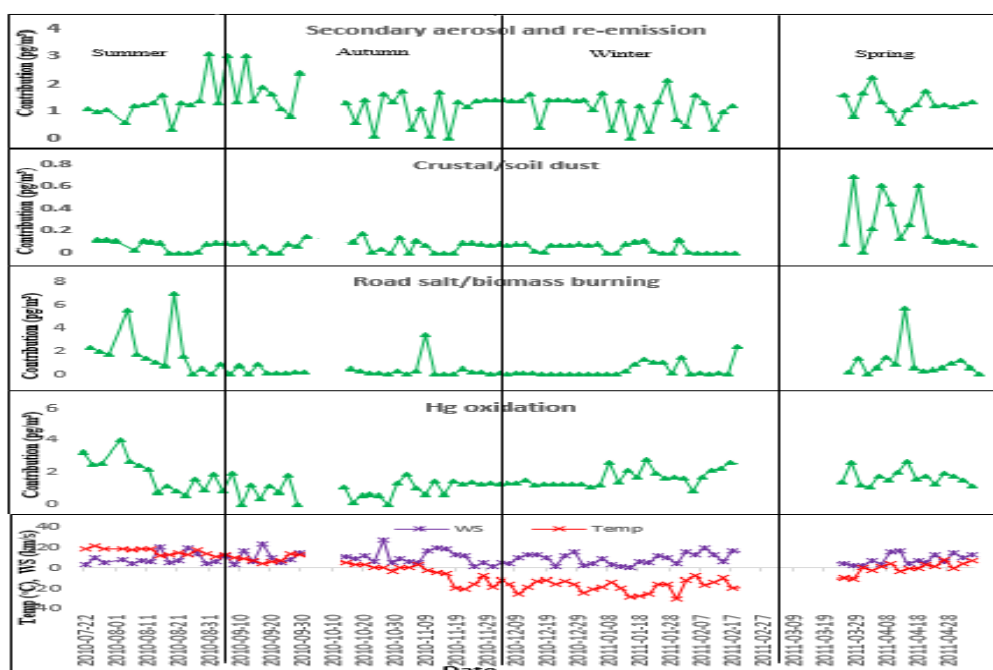


Figure 4.4: Time series relationship of PMF factor contributions to GOM with temperature and wind speed



Figure 4.5: Time series relationship of PMF factor contributions to PBM with temperature and wind speed

GEM and GOM are also major variables of this factor. The presence of GEM is an indication of re-emission because the local soil might be rich in previously deposited Hg (Eckley et al., 2015). The factor contribution time series of GEM and GOM showed similar fluctuation pattern during the study period with peaks in the late summer and early autumn (Figures 4.3 and 4.4). The statistical relationships between the factor contributions to GEM and temperature were very weak and statistically insignificant in the summer ($R^2=0.29$, $p>0.05$, $N=13$), winter ($R^2=0.19$, $p>0.05$, $N=26$) and spring ($R^2=0.10$, $p>0.05$, $N=15$) and moderately weak in the autumn ($R^2=0.32$, $p>0.05$, $N=26$). The overall correlation coefficient between the factor contributions to GEM and temperature was very weak and statistically insignificant ($R^2=0.19$, $p>0.05$, $N=81$). This indicates that re-emission is not likely the dominant source contributing to GEM but other sources of GEM, which are not reported in NPRI may be present. The contributions to GOM (Figure. 4.4) and PBM (Figure. 4.5) also

varied across seasons peaking at the same season with GEM. GOM formation is suspected to occur from atmospheric oxidation of GEM but marker species to confirm this process are available. NH_4^+ in this factor suggests the transformation of NH_3 from agricultural activities (Liao, 2016) and emissions from fertilizer production. A major source of NH_3 , based on NPRI, was Kosh Fertilizer Canada located southeast of the site. NH_3 is an essential species for neutralization of acidic components of the atmospheric air including H_2SO_4 (Pichfor et al., 2009; Hoet et al., 2018) yielding NH_4^+ micro-particles. Oxalate is also an emphasised variable of the factor. A study by Jiang et al. (2011) has shown a strong correlation between oxalate, and SO_4^{2-} and NH_4^+ , indicating common process of formation.

Factor 2 displayed two major variables including high percentage of Zn (79%) and moderate percentage of Fe (31%). This was named industrial because these species are the air pollutant markers of industrial processes relating to metal production (Song et al., 2006). Zn is the dominant chemical species in this factor and 79% of the variance is explained. Based on the NPRI data, HBM&S is a major source of Zn with annual air emissions of 62 tonnes in 2010 (quoted from Table B1) and 1.5 tonnes, representing 98% reduction, is reported in 2011. The presence of Fe in this factor is consistent with metal processing. An important source of Fe in the atmosphere is metal processing emissions. From the emission data on the NPRI, Fe was not in the sources used in this study because some sources that could be emitting Fe were not considered. The absence of Hg in this factor is unexpected because HBM&S emitted both Hg and Zn, according to the NPRI data. Thus, it may be necessary to speculate that the Hg emitted from HBM&S has been washed out via wet deposition processes during plume aging in the air (Lindberg, 1980). The speciation of Hg in the plume enhances Hg deposition with GOM and PBM more susceptible to rapid wash out because of their high solubility (Poissant et al., 2004). Therefore, the absence of Hg is an indication that the factor may be contributing little or no Hg to the ambient concentrations. The time series check of the factor contributions

to GEM and PBM showed clear seasonal variations with peaks once in the autumn and twice in the winter.

Factor 3 was identified as crustal/soil dust because it accounted for high percentages of the variability in Al (66%), Fe (52%), K (49%) and Si (79%). All the dominant elements of this factor (Al, Fe, K and Si) are abundant elements in crustal and soil dust resuspension (Xiong et al, 2017). The factor contribution to ambient Hg was statistically insignificant ($p > 0.05$). No Hg form was apportioned to this factor indicating that the factor contribute little or no Hg at the site.

Factor 4 was identified as road salt and biomass burning. This factor explains high variability in PBM (75%), Ca^{2+} (84%), Cl^- (57%), Mg^{2+} (67%), NO_3^- (63%), oxalate (47%), K^+ (41%) and Na^+ (59%). Mg^{2+} , Na^+ and Cl^- are markers of marine aerosol but the Flin Flon site is not in close proximity to the ocean. Therefore, these pollutant markers are likely related to the application of salt used in road snow control (Cheng et al., 2012; Deng et al., 2018). The presence of K^+ indicates biomass burning emission because it is commonly used to identify the contribution from biomass burning related activities (Deng et al., 2018). Biomass burning, such as residential wood burning, was identified as a source of PBM in the winter (Dicosty et al., 2006; Simone et al., 2017). However, there is tendency for high uncertainty in this factor because NPRI data on road salt/biomass burning are not available. Comparison of the factor profile with past Hg studies was therefore the option available to interpret the factor. In the laboratory and field studies by Obrist et al. (2007), up to 30% of PBM was found to be present in the Hg released by biomass burning. Determining the speciation and whether PBM is a direct emission or if it is a product of GEM oxidation within the plume were not known. However, PBM mass emissions were found to correlate strongly ($R^2=0.67$) with particulate matter (Obrist et al., 2007). Further investigation of this factor using the time series of the factor contributions to PBM showed that there were spikes in the summer and

spring, and this seasonal trend showed a disconnection with residential wood burning emissions. A critical examination of the predicted seasonality in the factor contributions to PBM points to contributions from forest fires or occasional crop residue burning. According to the Manitoba Newsletter (Manitoba Co-operator, 2017), crop residue burning is a common agricultural practice in Manitoba although authorization for such practices, for those who choose to burn crop residue, is an important requirement. Open burning in the daytime are allowed by law between November 16 and July 31 of every year.

F5 was named Hg oxidation. This factor accounted for high percentages of GEM (49%), GOM (41%), PM_{2.5} (29%) and Br (87%) and moderate percentages of K (44%), Cl⁻ (28%), NO₃⁻ (32%), K⁺ (31%) and Na⁺ (31%) variations. As can be seen from the factor profile, Br is the dominant species with the highest percentage. This is an indication of an environment that is rich in bromine. Although, the results of previous Hg studies showed that the oxidation of Hg is facilitated by ozone but there were high uncertainties with this reaction. However, the oxidation rates of Hg by bromine have been shown to be very fast, which explains Hg depletion events (Goodsite et al., 2004). The source of Br at Flin Flon is uncertain because Br emission data was not available in the NPRI. Atmospheric bromine has previously been associated with traffic emissions, as this element is a major component in fuel additives (Khodeir et al., 2012), but Flin Flon is a small city with low population and may likely not be affected by traffic emissions. The time series of Br concentration in the atmospheric PM_{2.5} showed that the concentrations were high in the spring, which is likely to support GEM oxidation to GOM. A thermodynamic study of GEM conversion in the atmosphere has shown that the rate of GEM oxidation by atomic bromine is faster than oxidation by O₃ (Holmes et al., 2010). As can be seen from Figures 4.3 and 4.4, contributions from this source to GEM and GOM concentrations varied with highest contributions in summer 2010 and spring 2011.

F6 was identified as coal combustion. This factor explained high percentage of the variation in SO₂. This species only was apportioned by PMF to this factor. SO₂ is a known marker for coal combustion source (Zhu et al., 2018). Coal combustion source identified by Lee et al (2003) contained SO₂, SO₄²⁻ and NH₄⁺ as major variables of the factor but the PMF model, in this case, failed to associate SO₄²⁻ and NH₄⁺ with this factor. In the input correlation table (Table C2), SO₂ correlated significantly positively with SO₄²⁻ indicating that transformation of SO₂ to sulphate during transport is a likely reaction. Since coal combustion is an important source of atmospheric Hg (Carpi, 1997), the factor profile shows a lack of Hg. A check of the Canada's NPRI revealed that the closest significant Hg point source in Manitoba in 2010 was HBM&S (Hg = 283 kg/yr), which coincidentally emitted significant amount of SO₂ (58,234 tonnes). In the following year (2011), the Hg emission from the plant drastically reduced to zero and SO₂ emission was 72 tonnes. Aside HBM&S, other major source of SO₂, based on the NPRI data, is Vale Canada limited, a metal processing plant located at 276 km northeast of the sampling site, which had high emissions in 2010 (134,617 tonnes) and also in 2011 (125,379 tonnes). Regional emission of SO₂ is also a likely source affecting the site but the verification of this is beyond the scope of this work. The time series of SO₂ concentrations clearly shows large fluctuations in 2010 but the variation was less in 2011. In a larger regional west coast in New York, analysis of the trend of Hg showed lower Hg concentrations alongside reduced SO₂ concentrations (Zhou et al., 2017).

4.1.6 Seasonal and overall source contributions

The four seasons, spanning the entire ambient Hg data and the data size in each season, were the summer (July-August, 2010, N=13), autumn (September-November, 2010, N=26), winter (December 2010 – February 2011, N=27) and spring (March – May, 2011, N=15). The average seasonal contributions of PMF resolved factors to GEM, GOM and PBM in all the four seasons are shown in Figures 4.6, 4.7 and 4.8, respectively. According to Duan et al.

(2017), the pattern of variations in factor contributions to ambient Hg often depends on the type and magnitude of source contributions, prevailing meteorological conditions and other important factors. In this study, distinct variations in the seasonal average contributions of the PMF factors to speciated Hg were observed (ANOVA, $p < 0.05$). For GEM (Figure 4.6), the Hg oxidation, and secondary aerosol and re-emission factors were respectively, the dominant contributing factors in the summer, winter and spring. In summer, both factors contributed approximately 1.2 and 0.7 ng/m³, respectively, to GEM. Among all the factors, the average contribution from the Hg oxidation was highest in summer and lowest in autumn. Although re-emission contributed the most in spring, its seasonal variation was small. However, the GOM contributions in the summer from Hg oxidation and road salt/biomass burning factors were nearly the same (~2 ng/m³) but varied in other seasons (Figure 4.7). For PBM (Figure 4.8), Hg oxidation factor was the dominating factor in the summer, winter and spring.

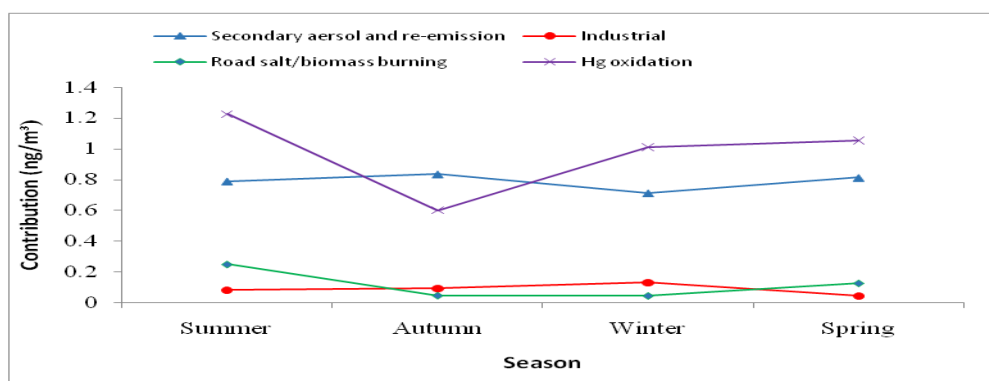


Figure 4.6: Average seasonal contributions of PMF resolved factors to GEM

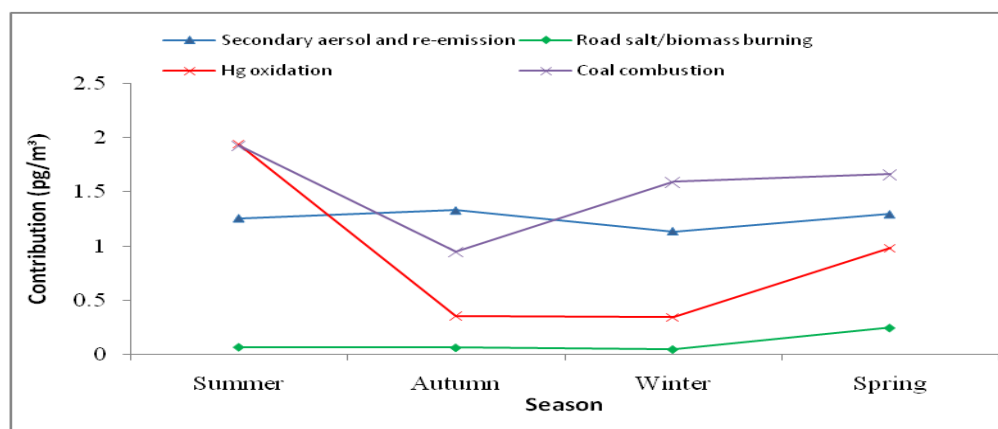


Figure 4.7: Average seasonal contributions of PMF resolved factors to GOM

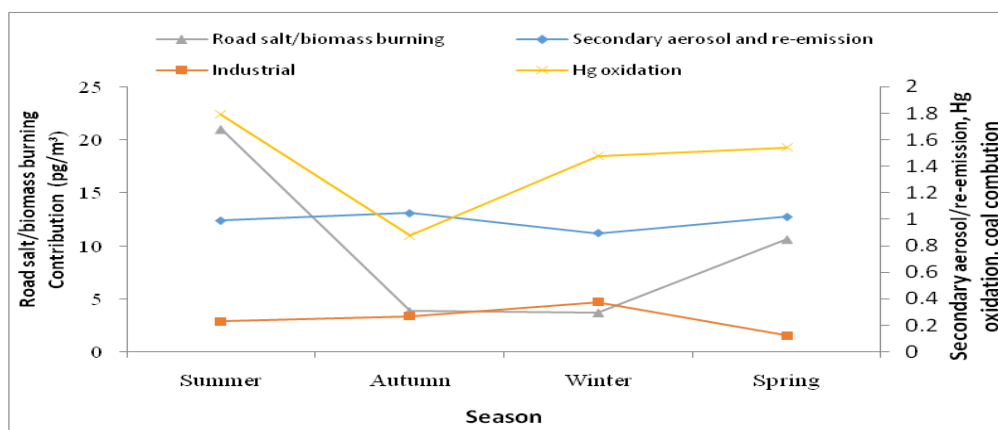


Figure 4.8: Average seasonal contributions of PMF resolved factors to PBM

The overall contributions of each factor to the three Hg forms and their ranks are presented in Table 4.4. As can be seen on Table 4.4, the Hg oxidation contributed the largest to GEM with an average of 48%. This was followed by the secondary aerosol and re-emission (average 42%) and industrial (average 5%) factors, among all the six PMF factors. The Hg oxidation factor contribution to GOM was the greatest with an overall average contribution of 43%. This was followed by the secondary aerosol and re-emission (average 40%), and road salt and biomass burning (average 15%) factors. Among all the six factors identified, the road salt and biomass burning factor dominated the overall contribution to PMB with an average of 48%. Since neither road salt application nor wood burning for heat generation is applicable in the summer season, and this factor dominated the PBM contributions in summer, the high PBM in summer is speculated to be forest fire or seasonal open burning of crop residue and weeds, which is a common land preparation practice in agriculture for new planting season. Such practice is capable of mobilising Hg-rich soil particles from surfaces to the atmosphere. This seasonality in biomass burning was observed by Cheng et al., 2014. The factor contribution to PBM was followed by the Hg oxidation factor (average 25%) and then the secondary aerosol and re-emission (average 22%).

Table 4.6: Estimated annual source contributions to speciated Hg (rank in bracket)

		Secondary aerosol and re-emission	Industrial	Crustal/soil dust	Road salt+biomass burning	Hg oxidation	Coal combustion
GEM (%)	Min	0	0	0	0	0	0
	Max	100	30	0	50	98	0
	Average	42(2 nd)	5(3 rd)	0	4(4 th)	48(1 st)	0
	Median	45	4	0	2	47	0
GOM (%)	Min	0	0	0	0	0	0
	Max	99	0	16	83	95	1
	Average	40(2 nd)	0	3(4 th)	15(3 rd)	43(1 st)	1(5 th)
	Median	40	0	2	8	45	0
PBM (%)	Min	0	0	0	0	0	0
	Max	100	43	44	98	86	1
	Average	22(3 rd)	6(4 th)	0	48(1 st)	25(2 nd)	0
	Median	15	2	3	51	22	0

4.1.7 Performance of PMF using pred/obs scatter plot

In order to measure the performance of PMF model in source apportionment of air pollutants, an important criterion is that the model must reproduce the original data (Hopke, 2016). One of the methods to achieve this is to check the correlation coefficient between predicted and observed concentrations. The scatter plots of the predicted and observed concentrations of GEM, GOM and PBM are shown in Figures 4.9, 4.10 and 4.11 respectively. As can be seen in these Figures, the correlation coefficient between the predicted and observed GEM concentrations (Figure 4.9) was very weak among the three Hg species ($R^2 = 0.28$, slope 0.54, p-value <0.05). Based on these performance indices, the re-emission of GEM was not well extracted in PMF analysis most likely because the input dataset consisted mostly of PM_{2.5} speciation and more emphasis was placed on PM_{2.5} by the model. It is important to note that GEM re-emission does not depend on PM_{2.5} and the limitations of the non-availability of data for other gaseous species might result in high uncertainty in the PMF result. The correlation coefficient between the predicted and observed GOM concentrations (Figure 4.10) was relatively weak but significant ($R^2 = 0.44$, slope = 1.26, p-value <0.05). However, the correlation coefficient between the predicted and observed concentrations of

PBM (Figure 4.11) was the strongest and significant ($R^2 = 0.98$, slope = 1.05, p-value <0.05) indicating that PMF model reproduced PBM better than GEM and GOM.

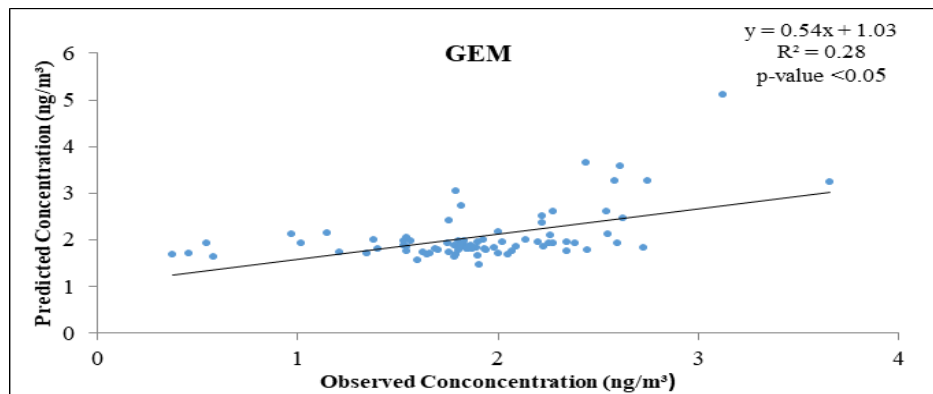


Figure 4.9: Pred/Obs concentrations scatter plot for GEM in PMF model

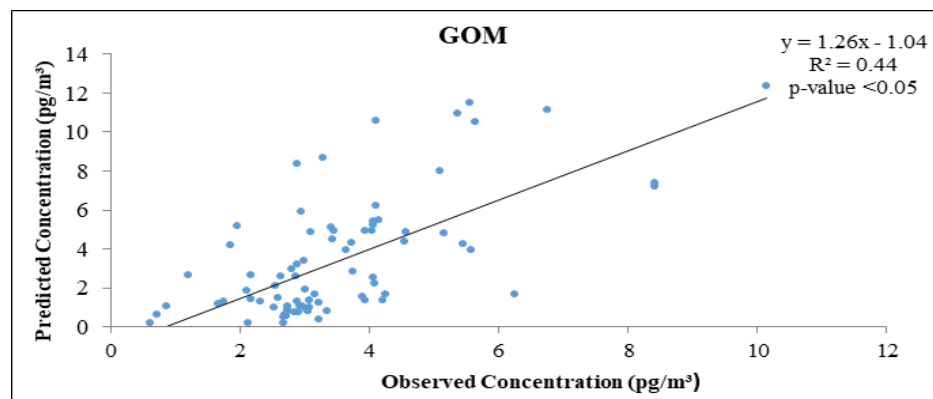


Figure 4.10: Pred/obs concentration scatter plot for GOM in PMF model

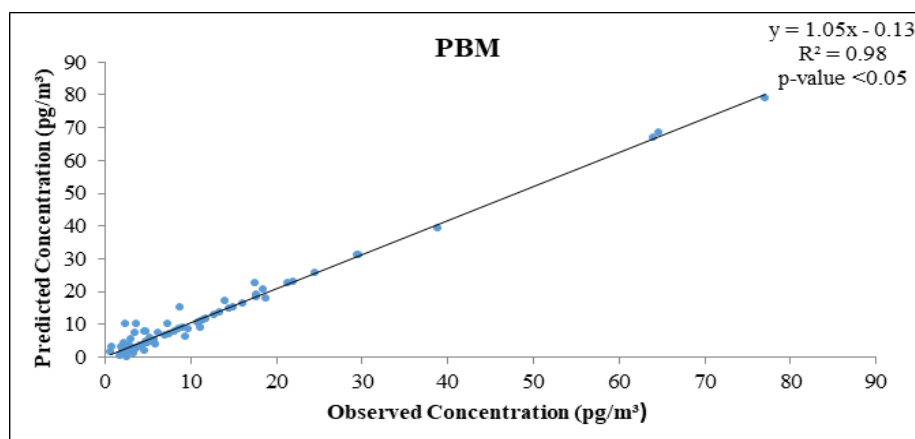


Figure 4.11: Pred/obs concentration scatter plot for PBM in PMF model

4.1.8 Performance of PMF using pred/obs time series plot

The time series of the predicted/observed GEM, GOM and PBM concentrations were plotted to further assess the performance of PMF in reproducing the daily concentrations. The time series of GEM, GOM and PBM are shown in Figs. 4.12, 4.13 and 4.14, respectively. According to the PMF5.0 user guide (USEPA, 2014), the model performance is high and acceptable when the observed daily concentrations of pollutant species are well tracked. By visual inspection of the time series, GEM concentrations were mostly under-predicted in October and November, over-predicted in March and April and relatively tracked the concentrations in July and August. There were large fluctuations in the model predicted GEM concentrations in the summer (July-August) and autumn (September-October) but less in winter (December-February) and spring (March-April) as shown in Figure 4.12. In some instances, the concentrations of GEM were frequently high during the summer due to high temperature resulting from high solar radiation that increases soil temperature, thereby enhancing re-emission of GEM from surfaces (Maxwell et al., 2013; Tao et al., 2017). High fluctuations in GEM were observed in spring and autumn in Miyun County in China (Zhang et al., 2013). Blanchard et al., 2002) found a winter maximum for GEM and this is consistent with the findings of Stamenkovic et al. (2007) in the Reno airshed in the USA. Many other studies found different seasonal fluctuations in GEM concentrations. As a result, there is no consensus on the season with highest fluctuations (Han et al., 2004). However, these fluctuations in GEM concentrations might relate to the monthly changes in weather conditions at the site, wind speed can be another factor that can affect the seasonal concentrations of GEM at a receptor site. High wind speed autumn has been found to cause fluctuations in GEM concentrations (Han et al., 2004). There were large variations in predicted GOM concentrations (Figure 4.13) with large over-prediction from November to February.

However, the predicted PBM daily averages were consistent with the observed values and thus, can be concluded that PBM was better reproduced by the PMF than GEM and GOM.

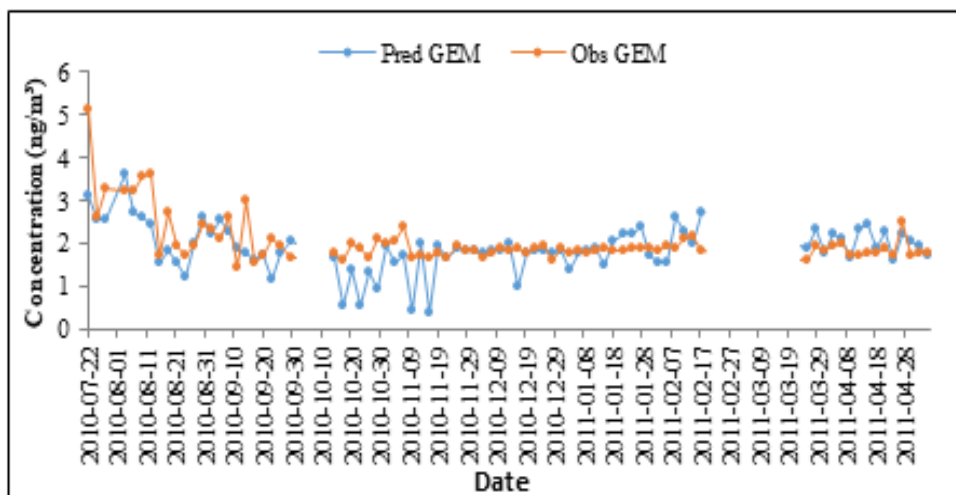


Figure 4.12: Pred/Obs concentration time series for GEM concentrations

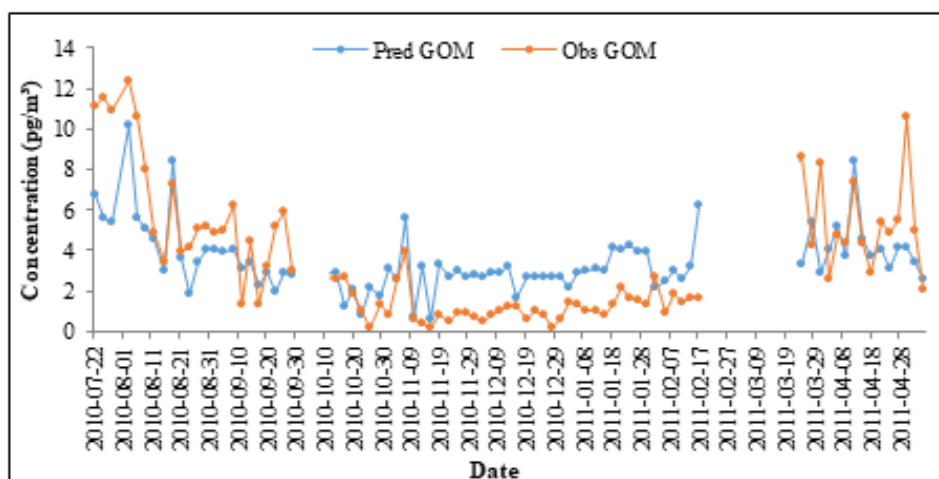


Figure 4.13: Pred/Obs concentration time series for GOM concentrations

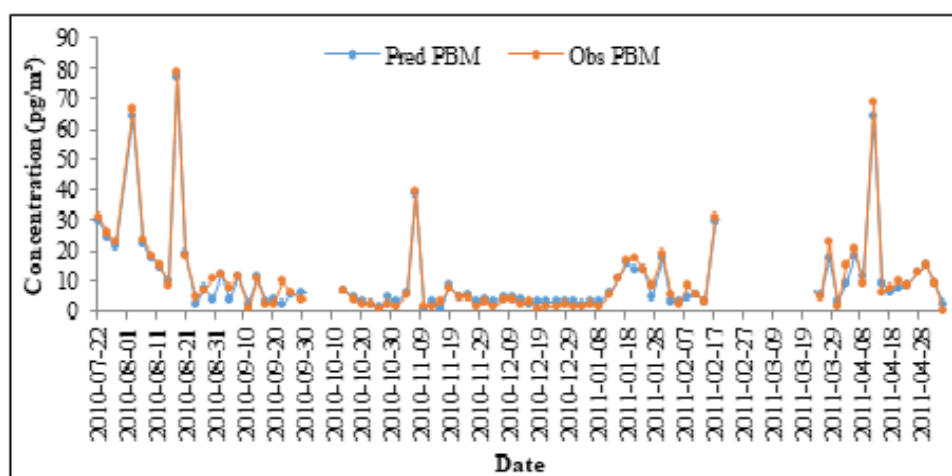


Figure 4.14: Pred/Obs concentration time series for PBM concentrations

The ratio of the overall predicted to the observed concentrations (Pred/Obs) of Hg can be used to verify the results obtained from the predicted/observed concentrations time series. The predicted PBM concentrations can be said to track the observed PBM well because the range of the Pred/Obs ratio was narrow (Table 4.7, 0.23-3.35). The observed PBM concentrations were also reproduced well on an annual basis because the ratio of annual mean concentration predicted to annual mean concentration observed (annual Predmean/Obsmean, 0.97) is closest to 1. The narrower range of the Pred/Obs ratio of GOM and the annual Predmean/Obsmean ratio for GOM closer to 1 compared with GEM (0.35-13.25 vs 0.22-1.49, 0.91 vs 0.87, respectively, Table 4.7) indicated that the GOM concentrations were better reproduced than GEM by PMF. The performance derived from pred/obs ratios are consistent with the performance derived from Pred/Obs time series.

Table 4.7: Ratios of PMF predicted to observed Hg concentrations

Hg form		
GEM	Min	0.22
	Max	1.49
	Average	0.94
	Median	0.97
	Ratio of annual mean	0.87
GOM	Min	0.35
	Max	13.25
	Average	2.06
	Median	1.28
	Ratio of annual mean	0.91
PBM	Min	0.23
	Max	3.35
	Average	1.10
	Median	1.03
	Ratio of annual mean	0.97

4.2 PCA Results

4.2.1 Suitability of dataset

The two statistical parameters often used to determine if a dataset is suitable for PCA include the KMO Measure of Sampling Adequacy and Bartlett's Test of Sphericity. A KMO

value greater than 0.60 and a small value of Bartlett's test (<0.05) of the significance level generally indicate that PCA could be a useful tool to analyze a dataset (Jolliffe, 2010). Thus, the suitability assessment results of PCA of the dataset in this study, shown in Table 4.8, provided satisfactory statistical outcomes. As seen on Table 4.8, since the KMO value of 0.739 (>0.60) and Bartlett's Test of Sphericity <0.05 were obtained, the conclusion is that the dataset is appropriate for the PCA method.

Table 4.8: KMO and Bartlett's Test Results

KMO Measure of Sampling Adequacy		0.739
Bartlett's Test of Sphericity	Approx. Chi-Square	3404.035
	df	276
	Sig.	0.000

4.2.2 Selection of components to retain in PCA of dataset

The full rotated component loadings of the initial five extracted components, when the restriction to retain the components with eigenvalue >1 was imposed, is shown in Table G1. The component loadings for an additional component added (six components), with eigenvalue close to one (0.9) is presented in Table G2. By comparing the five and six rotated component loadings, it was found that using six components, with total explained variance of 93.9%, were reasonable and more physically realistic than the five components (to be explained in section 4.2.3), with a total explained variance of 89.5%. An assessment of the communalities of the chemical species in the six component analysis showed reasonably high values (lowest value, 0.77) compared with that using five components (lowest value, 0.51). Generally, the communality is reasonable when it is closer to one than to zero (Jolliffe, 2010). Based on the assessment of the eigenvalues (total variance explained) and the source and process-related interpretability of the components, the varimax rotated six-component solution was chosen for the PCA method.

4.2.3 PCA results from concentration dataset

From the PCA of this concentration dataset, PCA's major loadings as well as the main statistical parameters including the communalities, eigenvalues, percent variance explained and the cumulative variance of the six components are presented in Table 4.9. The Loadings are the extent of the relationship between the factor scores and the original input variables, which help in the factor interpretation (Thurston et al., 2012). Loadings with modulus >0.25 were emphasized as major loadings of the factors. The factors were interpreted by physical comparison of the elements with highest loadings in each factor with species emitted in large proportion (emission inventory, Tables B1-B4) and in the previous Hg source apportionment studies.

PC1 was mainly characterized by strong positive loadings on PBM (0.97), Ca^{2+} (0.96), Cl^- (0.97), NO_3^- (0.97), Mg^{2+} (0.98), oxalate (0.94), K^+ (0.97) and Na^+ (0.97), and moderate loadings on GEM (0.32) and GOM (0.48). This component was named road salt/biomass burning because the air pollutant markers are all contained in this factor. This factor accounted for 43.9% of the variance in the dataset. PC1 correlated with all the three Hg forms and pollutant markers of road salt and biomass burning (Kamp et al., 2018). Although, Na^+ , Mg^{2+} and Cl^- are air pollutant markers of marine aerosol (Cheng et al., 2013), because Flin Flon is not near the ocean, these species suspected as to be of road salt origin. However, it is uncertain if road salt is used in Flin Flon due to non-availability of emission data for the source markers in the NPRI. Personal communication with atmospheric modeling experts revealed that the use of sand likely dominates road snow control in the town. In Cheng et al. (2012), road salt particles were identified as potential source of PBM because of its influence on PBM, Na^+ and Cl^- . This factor contains high loading on K^+ , which is a common marker for biomass burning (Zhang et al., 2008). Biomass burning is a primary source of K^+ , mainly in form of KCl , KNO_3 and K_2SO_4 (Li et al., 2003).

Table 4.9: Varimax rotated component loadings for dataset (major variables >0.25 in bold, blanks \leq abs 0.25)

	PC1	PC2	PC3	PC4	PC5	PC6	Comm
GEM	0.32			0.87			0.88
GOM	0.48			0.73			0.80
PBM	0.97						0.98
PM _{2.5}		0.63	0.47		0.52		0.92
Al		0.96					0.96
Br						0.95	0.97
Fe		0.87			0.26		0.88
K		0.90					0.93
Si		0.98					0.98
Zn			0.27		0.94		0.97
NH ₄ ⁺			0.97				0.95
Ca ²⁺	0.96						0.97
Cl ⁻	0.97						0.96
Mg ²⁺	0.98						0.99
NO ₃ ⁻	0.97						0.99
Oxalate	0.94						0.96
K ⁺	0.97						0.99
Na ⁺	0.97						0.98
SO ₄ ²⁻			0.95				0.96
SO ₂			0.82				0.77
Eigenvalue	8.8	4.1	2.9	1.1	1.0	0.9	
% Var. Exp	43.9	20.7	14.2	5.6	5.1	4.4	
Commu (%)	43.9	64.6	78.9	84.4	89.5	93.9	
Factor name	Road salt + biomass burning	Crustal/ soil dust	Coal combustion + agriculture	Long-range transport of Hg	Industrial	Bromine source	

KCl occurs predominantly in fresh smoke whereas K₂SO₄ and KNO₃ are present in aged smoke, due to the substitution of chloride by sulfate and nitrate. Biomass combustion can emit all the three forms of Hg although there are uncertainties in whether PBM is emitted directly or formed from GEM oxidation in the plume (Obrist et al., 2007). The presence of GEM suggests emission from biomass burning including residential wood burning, forest fires and crop residue burning. The confirmation of the type of biomass burning depends on the seasonal evaluation of the factor contributions. Active residential wood burning usually occurs in winter and spring whereas forest fires and crop residue burning are often associated with the summer. The time series of the daily contribution estimates of GEM and GOM showed negative values indicating no contributions to GEM and GOM. The temporal variations of the ambient concentrations of K⁺ showed that there were high concentrations

during the late winter period to early spring but the time series to be discussed in section 4.2.5 will be used to check the likely biomass process. The presence of NO_3^- and oxalate relate to aerosol particle formation and Ca^{2+} is from particles mobilized from surfaces.

PC2 has high positive loadings on $\text{PM}_{2.5}$ (0.63), Al (0.96), Fe (0.87), K (0.90) and Si (0.98). This was named crustal/soil dust (Zhang et al., 2009). It explained 20.7% of the variance in the dataset. All the species including Al, Fe, K, Si and $\text{PM}_{2.5}$, were found in the similar factor in PMF were present as major variables in this component. From the correlation coefficients, since there is no association between the factor and Hg, this suggests that Hg from crustal/soil dust is not significant to affect atmospheric Hg concentrations.

PC3 has high positive loadings on NH_4^+ (0.97), SO_4^{2-} (0.95) and SO_2 (0.82) and moderate loadings on $\text{PM}_{2.5}$ (0.47) and Zn (0.27). The factor was named coal combustion and agriculture. It explained a total variance of 14.2%. SO_2 is a marker for coal combustion process and SO_2 is a gaseous precursor for the formation of SO_4^{2-} during transport of aerosol particles. The major point sources of SO_2 , located within 700km radius that are likely affecting the site, are listed in Tables A1 and A2 in Manitoba and Tables A3 and A4 in Saskatchewan. Regional transport of SO_2 is also a possible source. Although agricultural emission data was not available, the presence of NH_4^+ may relate to the transport of agricultural emissions and consequent reaction of NH_3 and an acidic component of the atmosphere yielding $(\text{NH}_4)_2\text{SO}_4$ (Pichfor et al., 2009). Zn in this factor is an indication of the influence of industrial sources (Duan et al., 2016). There is no association between this factor and Hg although it is expected that coal combustion will correlate highly with Hg. The absence of Hg in coal combustion source found in PMF is consistent with this component.

PC4 has high positive loadings on GEM (0.87) and GOM (0.73). This factor was identified as long-range transport of Hg. The factor explained 5.6% of the variance. Because of the atmospheric behaviour of GEM, it can travel several thousands of kilometres from

locations that are upwind of site while atmospheric reactions, such as oxidation, are likely to convert GEM to GOM. This factor could not be assigned to a specific Hg source because of lack of correlations with air pollutant markers and several sources of GEM and GOM exist (Paatero et al., 2005). When a component associated with Hg exists in PCA and does not have other air pollutants to characterise the sources, it becomes difficult to assign to a specific Hg source. Statistical investigation of this factor can be used to assess the relationship with meteorological parameters. In the later section of the PCA technique, temperature and time series are included in the analysis of the result to assess the relationship between these factors and their influence on atmospheric Hg. However, further analysis using wind rose and trajectory could be used to locate the regional sources through which the air mass passed before reaching the site.

PC5 accounted for high loadings of Zn (0.94) and moderate loadings of PM_{2.5} (0.52) and Fe (0.26). This factor was identified as industrial and it explained 5.1% of the total variance in the dataset. The presence of Zn and Fe is consistent with emission from industrial processes. This factor with the same major variables was also resolved by PMF model. Historically, Fe and Zn have been associated with open incineration of refuse and automobile emission, respectively, but the enforcement of regulations to phase out open burning has essentially eliminated the sources of these elements in Canada and the US allowing for a general interpretation of this factor to be industrial emissions (Thurston et al., 2012). Zn can originate from combustion of lubricating oil in heavy industrial machineries used in moving material within industrial premises (Pokorna et al., 2015). This factor does not have any correlation with the Hg.

PC6 was predominantly characterised with high loading on Br (0.95). This factor was identified as a bromine source and explained 4.4 % of the total variance. The source of bromine in Flin Flon is uncertain because NPRI has no information concerning the element.

This element has been reported as a significant constituent of automobile fuel additives as well as a major constituent in consumer plastics (Khodeir et al., 2012). An examination of the concentration time series of Br at the sampling site shows a spike in the late part of winter but less variation in the spring. This factor was not associated with Hg.

4.2.4 PCA factors contributions to ambient Hg

The statistical analysis results of the APCS applied to the six extracted factors are shown in Table 4.7, in which the contributions from the sources were obtained. The contribution estimates in Table 4.7 were the overall average source contributions calculated over all daily samples. Source contributions could depend on atmospheric conditions and the strength of the sources (Paatero et al., 2005). Factor contributions in APCS can be positive or negative estimates because imposition of non-negativity is not present in the algorithm (Miller et al., 2002). However, from engineering point of view, a source cannot have negative contributions to Hg concentration at the receptor. Therefore, all negative factor contribution estimates presented in Table 4.7, as obtained from APCS calculations, were assumed zero.

Table 4.10: Contributions of PCA factors with concentration dataset (N =81)

PC	Name of factor	Average contribution \pm SD (%)		
		GEM	GOM	PBM
PC1	Road salt/biomass burning	-35.0 \pm 0.4	-35.7 \pm 2.0	146.7 \pm 18.0
PC2	Crustal/soil dust	2.9 \pm 0.0	-12.3 \pm 0.6	2.7 \pm 0.3
PC3	Coal combustion/agriculture	-9.5 \pm 0.1	15.6 \pm 0.7	-7.1 \pm 0.7
PC4	Long-range transport of Hg	146.1 \pm 0.8	119.5 \pm 3.6	11.1 \pm 3.6
PC5	Industrial	9.7 \pm 0.1	-8.6 \pm 0.4	-0.1 \pm 0.0
PC6	Bromine source	-14.2 \pm 0.2	-21.6 \pm 0.2	-53.4 \pm 6.6
R ²		0.88	0.82	0.95

In setting all the negative contribution estimates to zero, the factor contributions to GEM, GOM and PBM, scaled to total 100% after removal of negative factor contributions, are shown in Table 4.8. As can be seen on Table 4.8, the long-range transport of Hg was the major contributor to GEM (average 92.1 \pm 0.8 %) and GOM (average 76.3 \pm 3.6 %)

concentrations at the site. PBM concentration (average 91.4 ± 18.0 %) was dominantly contributed by the road salt/biomass burning factor. The R^2 values represent the fractions of the measured concentration variance that is attributable to variance in the predicted concentrations. All the three Hg forms had a R^2 value greater than 0.80, indicating a good fit between the predicted and the observed concentrations (Guo et al., 2004).

Table 4.11: PCA components contribution rescaled after removing negative contribution estimates (N =81)

PC	Name of factor	Average contribution \pm SD (%)		
		GEM	GOM	PBM
PC1	Road salt/biomass burning	-	-	91.4 ± 18.0
PC2	Crustal/soil dust	1.8 ± 0.1	-	1.7 ± 0.3
PC3	Coal combustion/agriculture	-	9.9 ± 0.7	-
PC4	Long-range transport of Hg	92.1 ± 0.8	76.3 ± 3.6	6.9 ± 3.6
PC5	Industrial	6.1 ± 0.1	-	-
PC6	Bromine source	-	13.8 ± 1.2	-
R^2		0.88	0.82	0.95

4.2.5 Statistical relationship between Hg and meteorological factors

Figures 4.15, 4.16 and 4.17 show the respective time series of GEM, GOM and PBM contributions from the Hg-associated factors present in the PCA of this concentration dataset. The time series plots revealed clear variations in the daily factor contributions to the ambient Hg in all seasons from the sources. For GEM, three factors including crustal/soil dust, long-range transport of Hg and industrial were predominant. The crustal/soil dust contributions were higher in the spring but lower in summer, autumn and winter (Figure 4.15). Overall correlation of GEM contributions from crustal/soil dust with temperature showed a very weak correlation and statistically insignificant (ANOVA, $r=0.05$, $p\text{-value} > 0.05$, $N=81$). For the long-range transport of Hg, the contributions to GEM were higher in the summer when temperature was constantly above zero degree. Statistically, a strong positive correlation coefficient between the factor contributions and temperature was obtained and this was

statistically significant (ANOVA, $r=0.52$, $p\text{-value} < 0.05$, $N=81$). The strong positive correlation coefficient suggested that this factor contributed significantly the GEM concentration and this can be linked to regional contributions to GEM. The industrial factor's contributions to GEM was observed to be highly variable in the winter but statistically, the correlation with temperature was not significant (ANOVA, $r=0.06$, $p\text{-value} > 0.05$). The contributions of the PCA factors to GOM and PBM are shown in Figs. 4.16 and 4.17. As can be seen in Figure 4.16, GOM contributions from coal combustion and agriculture had highest variations in early autumn and later part of the winter. The time series of GOM contributions from bromine source showed high variations in summer, winter and spring with many peaks in the summer, winter and spring. The peaks of PBM contributions from road salt and biomass burning, crustal/soil dust and Hg component occurred in summer and spring (Figure 4.17).

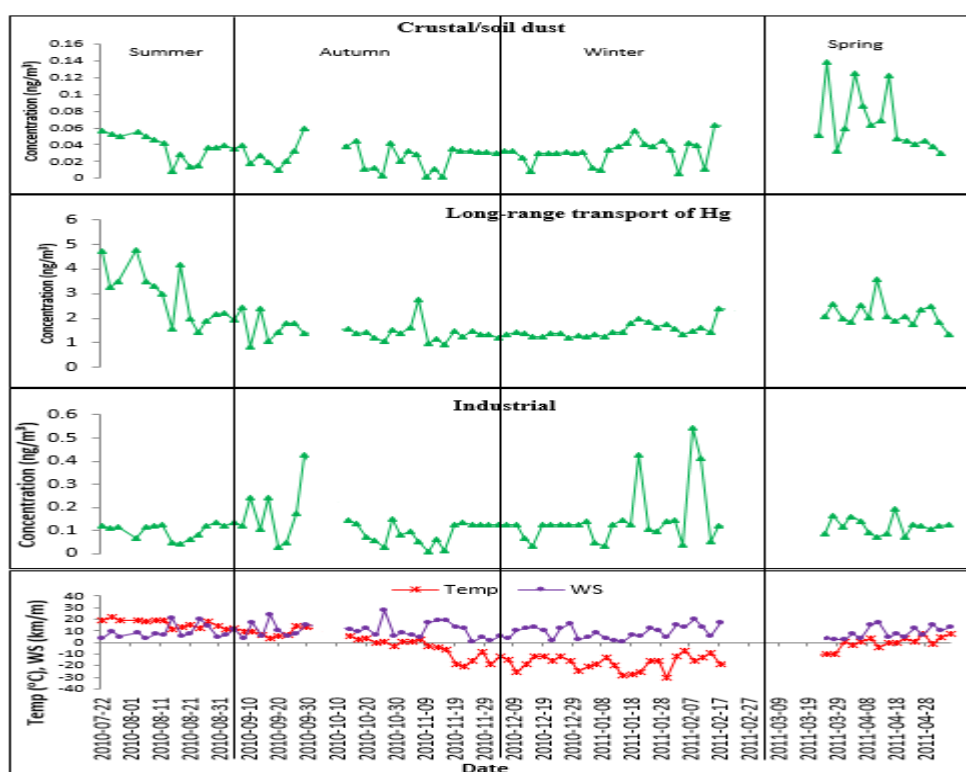


Figure 4.15: Time series of source contributions to GEM with temperature and wind speed

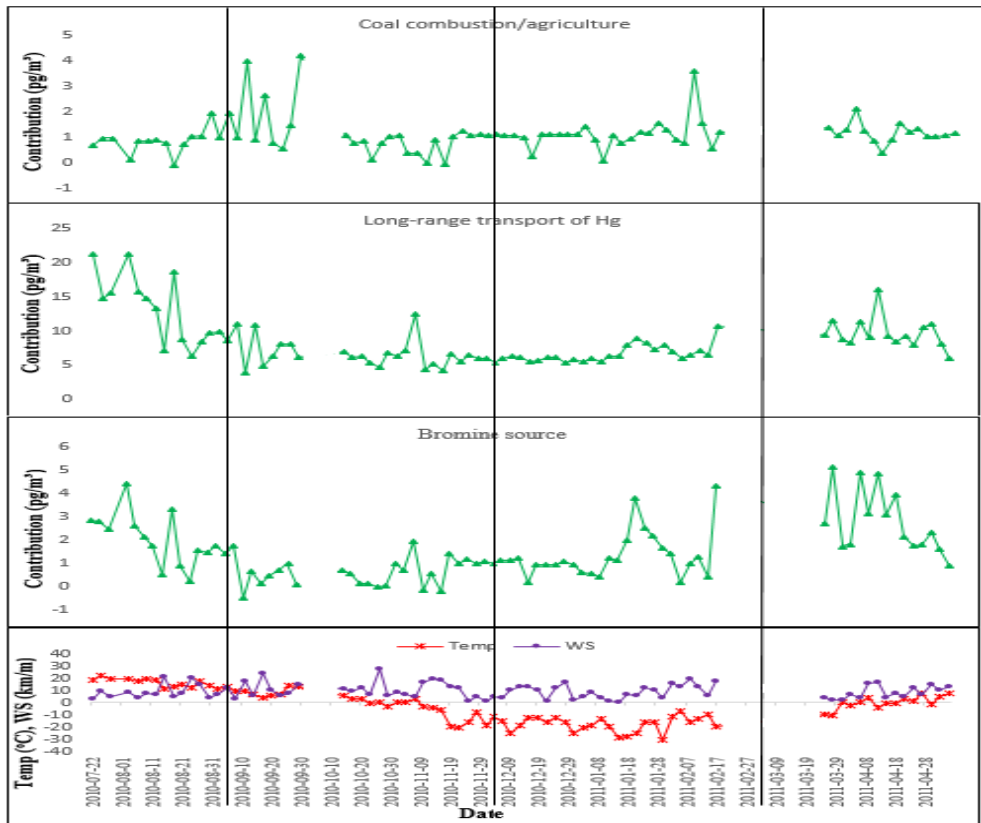


Figure 4.16: Time series of source contributions to GOM with temperature and wind speed

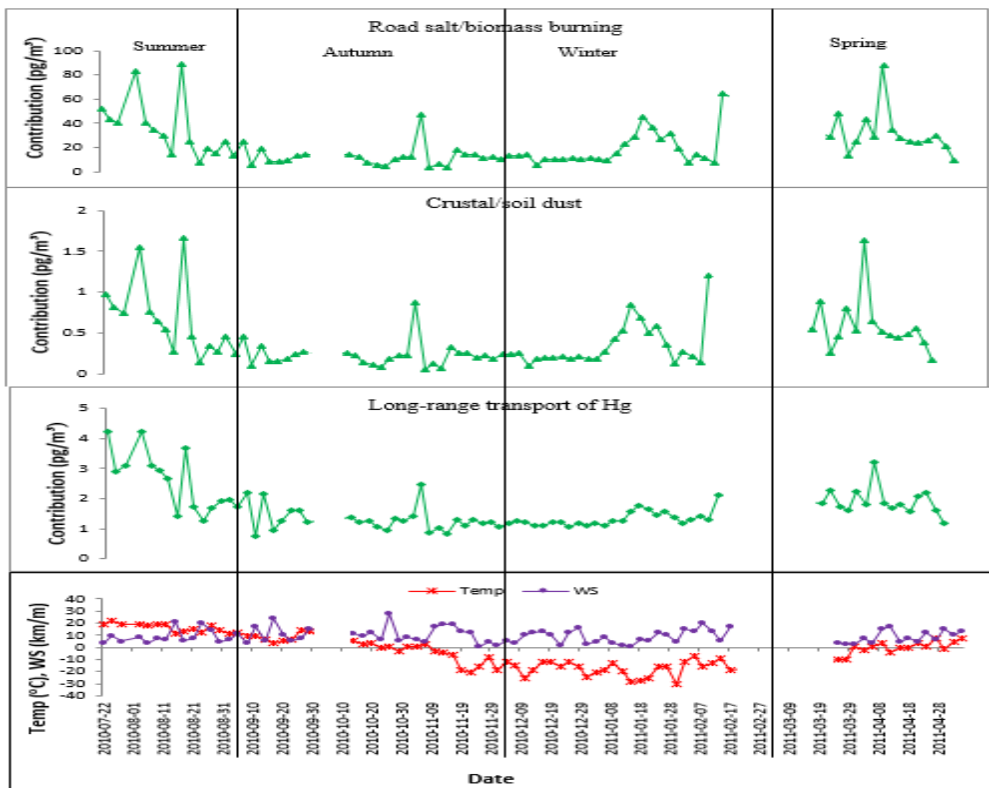


Figure 4.17: Time series of source contributions to PBM with temperature and wind speed

4.2.6 Performance of PCA of concentration dataset on Hg

The performance of PCA of the concentration dataset on GEM, GOM and PBM was assessed using the predicted/observed time series graphs shown in Figures 4.18, 4.19 and 4.20, respectively. The time series graphs show how well PCA reproduced the observed daily concentrations of speciated Hg. The time series graphs were divided into three data periods including July to September 2010, October 2010 to February 2011 and March to May 2011 due to the missing data gaps. As can be seen from Figures 4.18 and 4.19, PCA under-predicted the daily concentrations of GEM all through the study period but majorly over-predicted the daily GOM concentrations except a point when it tracked the GOM in March and under-predicted the concentration once in April. However, from the overall statistical examination of the daily predictions of speciated Hg, PCA most closely tracked the peak values of PBM ($R^2 = 0.98$), indicating a better performance for PBM than GEM ($R^2 = 0.86$) and GOM ($R^2 = 0.81$).

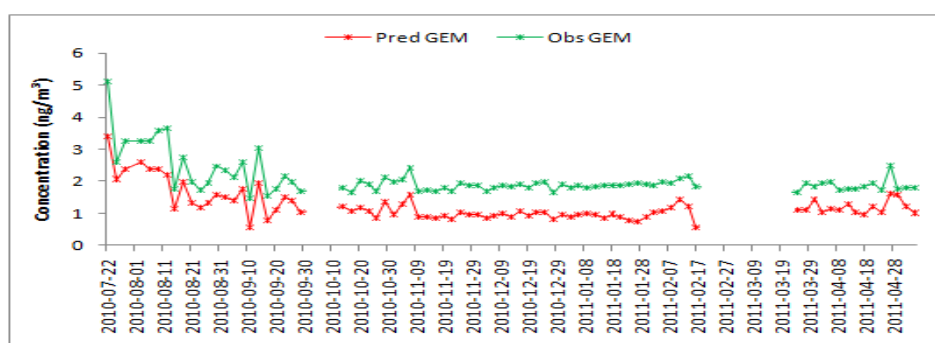


Figure 4.18: Pred/Obs GEM concentrations time series for components from PCA of dataset

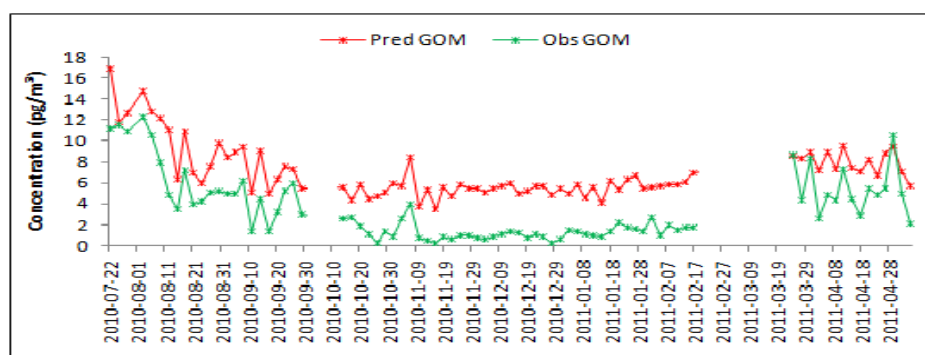


Figure 4.19: Pred/Obs GOM concentrations time series for components from PCA of dataset

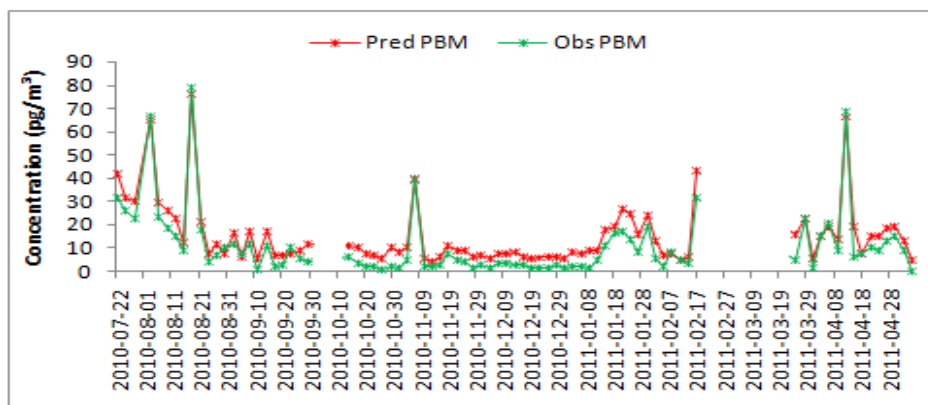


Figure 4.20: Pred/obs PBM concentrations time series for components from PCA of dataset

4.2.7 Including meteorological parameters

The PCA of the dataset including meteorological data extracted six factors (Table H3) for the first run. After comparing this with the seven-factor solution (Table 4.12), the seven-factor solution was preferred because it has more physically reasonable interpretation than the six factors. Table 4.12 shows the PCA results of seven factors with major variable loadings. The statistical parameters including the communalities, eigenvalues, percent of variance explained and cumulative percentages were also included in Table 4.8. All the factors identified by PCA of concentrations dataset were also present when meteorological data were included. All the seven factors except coal combustion/agriculture had one or two loadings on meteorological variables and their communalities were all reasonable as well (>0.70). PC1, PC2, PC3, PC5 and PC7 were all consistent with road salt/biomass burning, crustal/soil dust, coal combustion and agriculture, industrial and bromine source, respectively. The long-range transport of Hg, which was previously found from PCA of the concentration dataset, was identified as re-emission because it has an additional positive loading on temperature and negative loading on relative humidity. The clustering of these variables on this factor in GEM re-emission being significantly enhanced by at high temperature conditions (Lin et al., 2012; Kamp et al., 2018).

Table 4.12: Varimax rotated factor loadings of PCA components including meteorological parameters (major variables >0.25 in bold, blanks ≤abs 0.25)

	PC1	PC2	PC3	PC4	PC5	PC6	PC7	Com
GEM	0.34			0.65		0.50		0.81
GOM	0.47			0.76				0.86
PBM	0.97							0.98
PM _{2.5}		0.62	0.50		0.49			0.90
Al		0.97						0.96
Br		0.29			0.30		0.70	0.78
Fe		0.84						0.82
K		0.91						0.92
Si		0.98						0.98
Zn			0.32		0.88			0.89
NH ₄ ⁺			0.95					0.93
Ca ²⁺	0.97							0.96
Cl ⁻	0.96							0.96
Mg ²⁺	0.97							0.99
NO ₃ ⁻	0.97							0.99
Oxalate	0.93							0.96
K ⁺	0.97							0.99
Na ⁺	0.97							0.98
SO ₄ ²⁻			0.94					0.95
SO ₂			0.83					0.75
Temp				0.88				0.90
RH	-0.27	-0.55		-0.43	-0.31			0.72
WS						-0.87		0.86
Precip					-0.29		0.73	0.71
Eigenvalue	8.1	4.4	3.1	2.1	1.5	1.2	1.1	
% var. exp	33.8	18.4	12.7	8.9	6.1	5.1	4.8	
Cummu	33.7	52.1	64.9	73.8	79.9	84.9	89.7	
Factor name	Road salt/ biomass burning	Crustal/ soil dust	Coal combustion/ agriculture	Re- emission	Industrial	Dispersion	Bromine source	

From laboratory studies carried out under controlled conditions, results showed that GEM re-emission was greatly enhanced by increased temperature of the soil sample (Omine et al., 2012). Another study, in which the temperature of soil slurry was monitored, showed that increasing the temperature of a soil slurry increases the potential for GEM re-emission (Wu et al., 2010). GEM flux from a soil surface depends on the intensity of solar radiation (Gustin et al., 2002). GOM in soil is converted to GEM via reactions facilitated by light and re-emitted into the atmosphere (Liang et al., 2014). The loadings on relative humidity and precipitation in PC5 were low compare to other variables of the factor. Thus, the component, industrial, was not affected by the loadings on these variables. PC6 was identified as dispersion because it had a positive loading on GEM and a negative loading on wind speed (WS). The dispersion

of GEM in the atmosphere often depends on the wind speed (Gworek et al., 2017). Therefore, the strong positive correlation between PC6 and GEM, and inverse relationship with wind speed indicate a dominance of local sources whose emission data were not available in NPRI. Wind speed plays a leading role in how GEM behaves in the atmosphere. Strong winds disperse GEM out of the atmosphere, whereas low wind speed allows GEM levels to increase.

4.2.8 PCA factor contributions in PCA including meteorological data

The statistical analysis results of the factor contribution when meteorological data were added to the input were shown in Table 4.9. As can be seen from Table 4.9, two, three and four out of the seven factors had negative contribution estimates for GEM, GOM and PBM, respectively. This implies that these factors with negative estimates were not contributing to ambient Hg based on the reason stated earlier in factor contributions of PCA of concentration dataset. The R² values were all above 0.80, indicating good modelled Hg species.

Table 4.13: Contributions of PCA components with inclusion of meteorological factors (N=81)

PC	Name of factor	Average contribution \pm SD (%)		
		GEM	GOM	PBM
PC1	Road salt/biomass burning	-27.5 \pm 0.18	-184.7 \pm 0.91	105.5 \pm 16.32
PC2	Crustal/soil dust	-17.7 \pm 0.23	-14.1 \pm 0.13	-5.8 \pm 1.72
PC3	Coal combustion/agriculture	0.6 \pm 0	-159.6 \pm 0.55	7.5 \pm 0.81
PC4	Re-emission	38.2 \pm 0.47	351.5 \pm 3.19	-5.2 \pm 1.34
PC5	Industrial	6.5 \pm 0.09	55.4 \pm 0.59	-2.0 \pm 0.68
PC6	Dispersion	99.3 \pm 0.31	24.7 \pm 0.06	-0.3 \pm 0.02
PC7	Bromine source	0.7 \pm 0.01	26.8 \pm 0.31	0.2 \pm 0.08
R ²		0.81	0.86	0.98

^aValues are presented as percentages of mass apportioned to each source followed by the percentage standard deviation. R² is correlation coefficient

When the factors with negative estimates of Hg contributions were removed and other factor contributions scaled to total 100%, the real factors contributing to ambient Hg are presented in Table 4.10. In Table 4.10, there was a shift of factor contributing the largest GEM. The factor, dispersion dominated the contributions to GEM with an average of 68.4 \pm 0.31%, followed by the re-emission factor with an average of 26.3 \pm 0.09. For GOM and

PBM, the predominant factors contributing to these Hg forms were respectively consistent with the results of PCA of the concentration dataset.

Table 4.14: PCA components contributions to Hg rescaled after removing negative contribution estimates (N=81)

PC	Name of factor	Average contribution \pm SD (%)		
		GEM	GOM	PBM
PC1	Road salt/biomass burning	-	-	93.2 \pm 16.32
PC2	Crustal/soil dust	-	-	-
PC3	Coal combustion/agriculture	0.4 \pm 0	-	6.6 \pm 0.81
PC4	Re-emission	26.3 \pm 0.47	76.7 \pm 3.19	-
PC5	Industrial	4.4 \pm 0.09	12.1 \pm 0.59	-
PC6	Dispersion	68.4 \pm 0.31	5.4 \pm 0.06	-
PC7	Bromine source	0.4 \pm 0.01	5.8 \pm 0.31	0.2 \pm 0.08
R ²		0.81	0.86	0.98

^aValues are presented as percentages of mass apportioned to each source followed by the percentage standard deviation. R² is correlation coefficient

4.2.9 Factor contribution pattern with inclusion of meteorological parameters

The time series of factor contributions to GEM, GOM and PBM including meteorological data were shown in Figures 4.19, 4.20 and 4.21, respectively. There were clear fluctuations in Hg emissions in different seasons. For GEM contributions in Figure 4.19, re-emission had more fluctuations variations in the summer compared with other factors, however contributions to concentrations were rarely above the background levels of 1.2 ng/m³ (Eckley et al., 2013). The dispersion factor contributions varied had frequent fluctuations in all seasons. In winter, coal combustion and agriculture, industrial and bromine source factor contributions increased suddenly and dropped afterwards. For GOM contributions (Figure 4.20), the re-emission factor was predominant whereas the dispersion factor, among other factors, had frequent fluctuations, similar to GEM, throughout the study period. When temperature was lower (negative temperature), industrial and bromine source factors contributions peaked at two different times. The contributions to GOM from re-emission factor in late autumn and all through winter showed no variation. In the case of PBM (Figure

4.21), road salt and biomass burning factor contribution attained its highest in summer showing that road dust suspected to be rich in particulate Hg were more in summer than in other seasons. The bromine source factor also showed frequent fluctuations, which peaked in winter when temperature was below zero degrees.

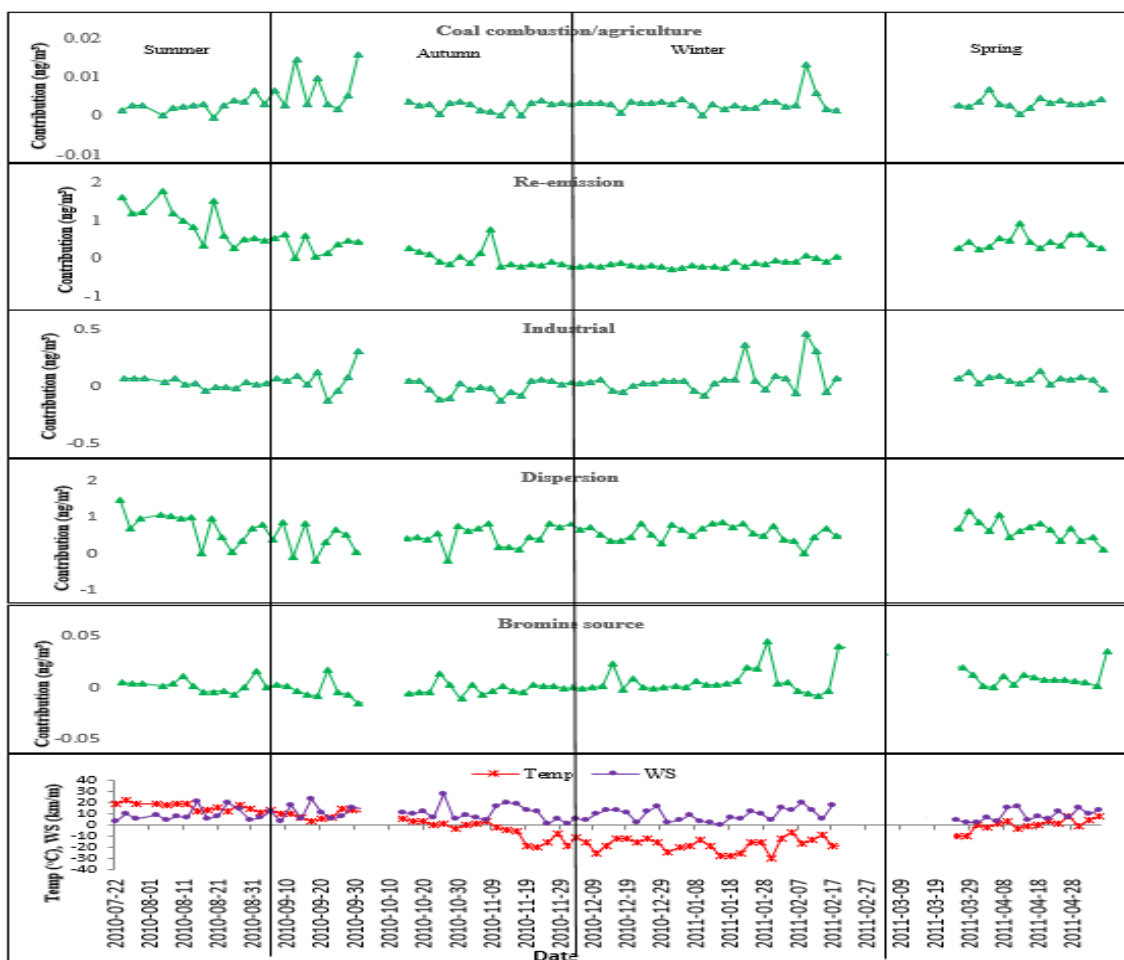


Figure 4.21: Time series GEM contribution patterns of PCA factors with temperature and wind speed

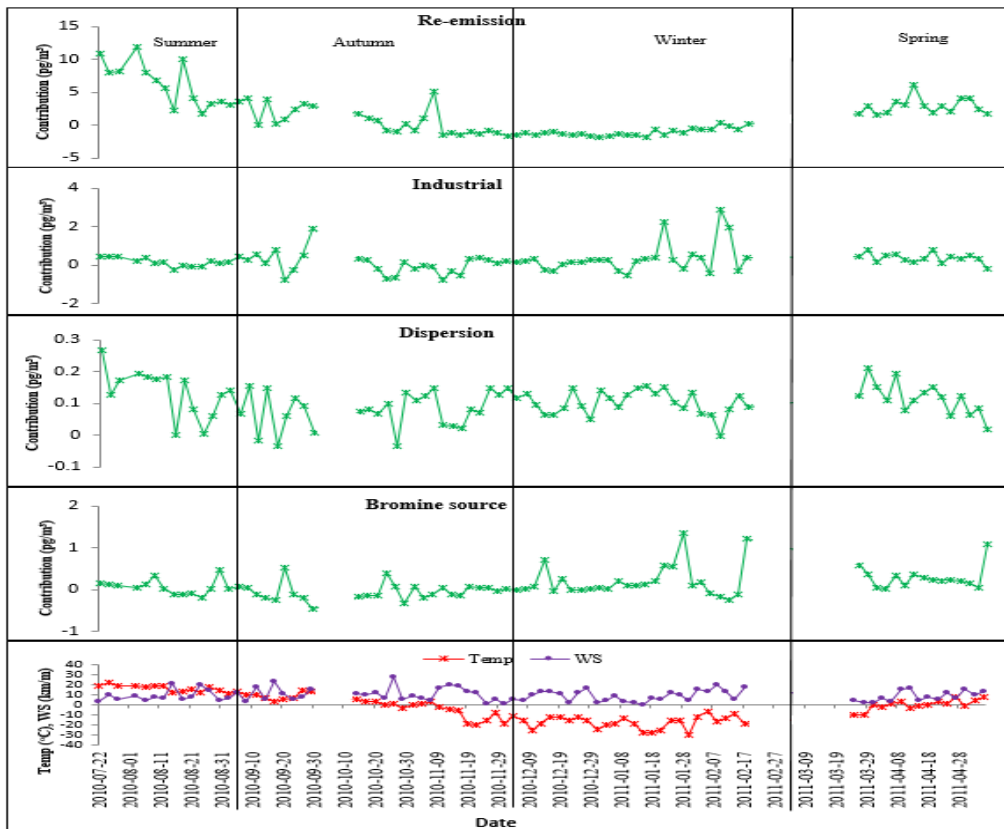


Figure 4.22: Time series GOM contribution patterns of PCA factors with temperature and wind speed



Figure 4.23: Time series PBM contribution patterns of PCA factors with temperature and wind speed

4.2.10 Performance assessment of PCA

The performance of PCA was assessed using the time series of the daily predicted/observed concentrations of ambient Hg contributed by all components. The time series of the predicted/observed GEM, GOM and PBM is represented in Figure 4.24.

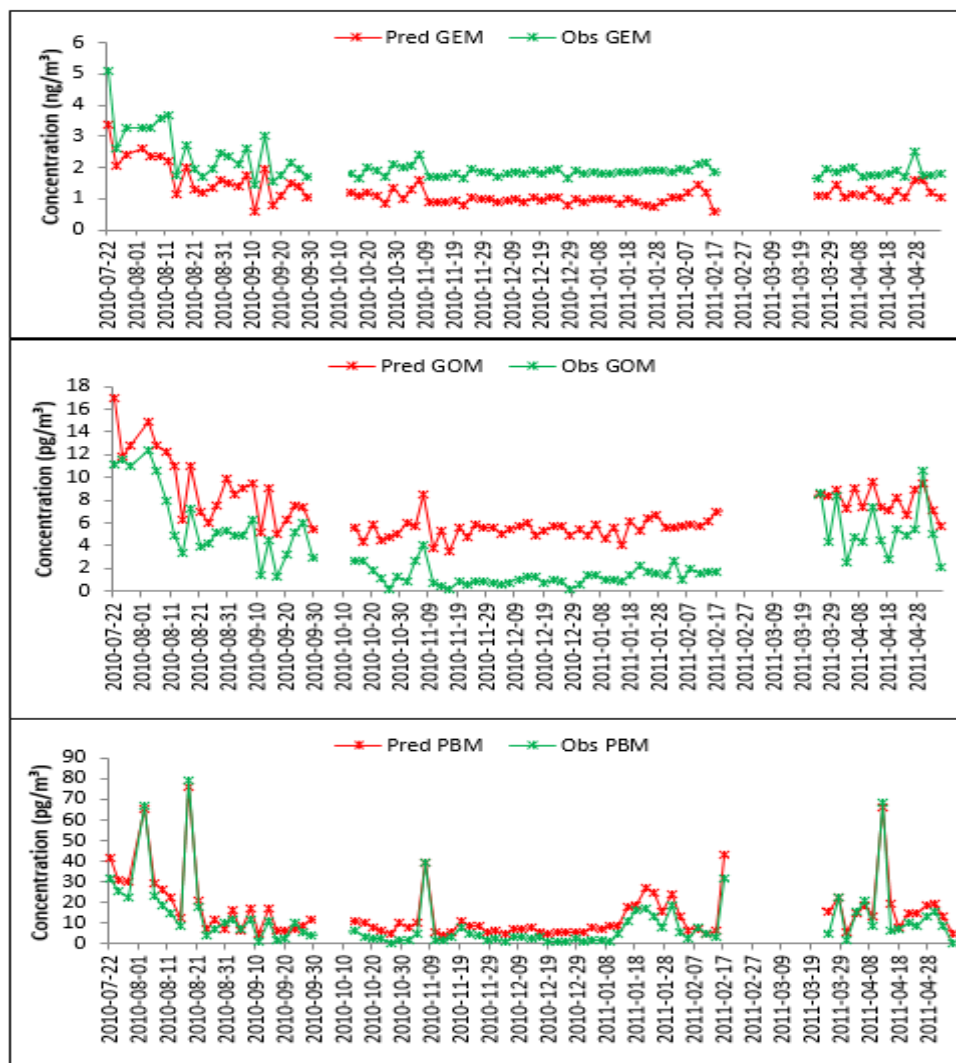


Figure 4.24: Time series of predicted/Observed GEM, GOM and PBM concentration in PCA

The broken portions of the lines were due to unavailable data during the period of study. The model predictions reproduced the observed data well in terms of magnitude although, a tendency toward under-prediction of GEM and over-prediction of GOM concentrations appeared throughout the modeled period. As can be seen from Figure 4.24, the daily

concentrations of GEM were frequently under-predicted throughout the study period. The variations in the concentrations were high in summer as expected but constantly less in the other seasons. By visual inspection of the GOM concentration time series, the daily concentrations were frequently over-predicted, tracked one observed GOM in March and under-predicted GOM once in April. Nevertheless, the predicted daily GEM and GOM concentrations pattern are all consistent with the observed concentrations. Overall, the predicted daily PBM concentrations closely tracked the observed measurements ($R^2 = 0.98$) indicating that PCA had a better performance in reproducing the observed concentrations of PBM, than GOM ($R^2 = 0.86$) and GEM ($R^2 = 0.81$).

4.3 Comparison of PMF model and PCA results

The Hg sources and processes identified using PMF and PCA techniques are listed in Table 4.15 for comparison. It is important to note that the outputs from both models can be different because their mathematical framework are not the same. For the data analysis in this study, the comparisons of the PMF and PCA results mainly focused on the input of concentration dataset because PMF model is unique in that it does not allow the inclusion of meteorological data in the input. Six factors each, with the factors associated Hg one, two and all the three Hg forms were found by both methods (Table 4.15).

Among the factors identified, four factors including road salt/biomass burning, crustal/soil dust, industrial and bromine source were the same because the air pollutant markers for these sources were all the same. The road salt/biomass burning factor in PMF had only PBM in its profile but the PCA factor had strong positive correlations with GEM, GOM and PBM. In the PMF results, the Hg oxidation factor profile contained GEM and GOM, among other major variables of the factor including Br. However, the PCA factor that contains bromine as the only major variable was not associated with any Hg forms. While the source of bromine at the site is uncertain and available as the only variable with major loading

on the factor, the factor was named as bromine source. The factors identified separately as secondary aerosol and re-emission, and coal combustion in the PMF result were both in one factor with all the major variables of the two factors. This led to the naming of the factor as named coal combustion and agriculture in PCA. A PCA factor that was identified as long-range transport of Hg because of its strong positive correlation only GEM and GOM, was named re-emission when meteorological data were included in the input and an additional component, dispersion was identified. Overall, PMF identified three main sources and processes affecting speciated atmospheric Hg whereas PCA was able to identify four sources and processes including re-emission of GEM at the site.

Table 4.15: Factor comparison in PMF model and PCA

PMF factors	PCA factors
Secondary aerosol and re-emission (GEM, GOM)	Road salt/biomass burning (GEM, GOM, PBM)
Industrial	Crustal/soil dust
Crustal/soil dust	Coal combustion/agriculture
Road salt/biomass burning (PBM)	Long-range transport (GEM, GOM)
Hg oxidation (GEM, GOM)	Industrial
Coal combustion	Bromine source
	Re-emission* (GEM, GOM)
	Dispersion*(GEM)

*after including meteorological data in the PCA input

CHAPTER 5

CONCLUSION AND RECOMMENDATIONS

5.1 Conclusions

Source apportionment of ambient Hg was conducted using the PMF model and PCA. Eighty-one (81) daily samples with twenty (20) chemical species as well as meteorological parameters were analysed. The input concentration dataset, comprising GEM, GOM, PBM, SO₂, PM_{2.5} and its components as well as meteorological parameters, measured from July 2010 to May 2011 in Flin Flon, Manitoba, was utilised.

Six factors identified by PMF include secondary aerosol and re-emission, industrial, crustal/soil dust, road salt/biomass burning, Hg oxidation and coal combustion. Among these six factors, three factors including secondary aerosol and re-emission, road salt/biomass burning and Hg oxidation contained one or two Hg forms. The average GEM contributions by factors in the summer, winter and spring were dominated by the Hg oxidation factor with 1.2, 1.0 and 1.1 ng/m³, respectively. Among the six sources and processes resolved by PMF, the Hg oxidation factor had the greatest overall percentage contribution to GEM (average 48%) and GOM (average 43%). The overall predicted GEM contribution from the secondary aerosol and re-emission factor was 42% based on the PMF findings. The road salt/biomass burning factor contributed the highest to PBM (48%). For the performance of PMF on speciated Hg, the measured peak daily PBM concentrations were closely predicted ($R^2 = 0.98$) followed by GOM ($R^2 = 0.44$) and GEM ($R^2 = 0.28$) as revealed by the scatter plots.

PCA of the same concentration dataset extracted six principal components. These components were largely consistent with PMF resolved factors. Four of the six components were assigned the same names because they contained the same major variables. A component named as long-range transport of Hg, which contains high positive loadings on GEM and GOM only, was identified by PCA. This component was split into re-emission and

an additional component, named dispersion when meteorological data was included in the input. The re-emission component strongly positively correlated with temperature whereas the dispersion component was negatively related with wind speed. Therefore, including meteorological parameters in the PCA input provided a better reasonable solution in terms of source identification than using concentration dataset only. For PCA of concentration dataset, the long-range transport of Hg contributed the highest to GEM (average $92.1 \pm 0.8\%$) and GOM ($76.3 \pm 3.6\%$) whereas the road salt and biomass burning factor contributed the highest to PBM ($91.4 \pm 18.0\%$). When meteorological data was added, the predominant contributor to GEM, among other factors, was the dispersion factor with an average contribution of $68.4 \pm 0.3\%$. The contribution of the re-emission component to the overall GEM concentration was $26.3 \pm 0.47\%$. The highest contributors to GOM and PBM concentrations remained the same as in the case of PCA of the dataset. The performance assessment of PCA showed that the observed daily concentrations of PBM were more closely tracked than GEM and GOM regardless of whether meteorological parameters were included or not. Therefore, PCA analysis of the data set provided a better atmospheric Hg apportionment result than PMF model.

5.2 Recommendations

A large proportion (76%) of the speciated Hg data was lost during the process of combining the consecutive daily Hg data with every 3- and 6- days $PM_{2.5}$ data. This resulted in the use of small a sample size ($N=81$) compared with the original ample size ($N=335$). Based on this limitation and the results obtained in this study, the following recommendations could help in future studies:

- Multiple years (2 or 3 years) of ambient Hg and $PM_{2.5}$ data or a combination of ambient data from different sampling locations should be used in order to have a robust model comparison.

- Comparisons of source apportionment studies using the PMF model and PCA on ambient speciated Hg concentrations data set are still very few. Therefore, future research should focus on comparison of these modeling techniques for atmospheric speciated Hg source apportionment.
- Although, carbon monoxide (CO) and ozone (O₃) concentrations data could not be used in this study because they were not available at the site, it is recommended for future research to include these chemical species in source apportionment of atmospheric Hg. This is because CO is an excellent air pollutant marker for combustion process while O₃ is an important atmospheric oxidant that can aid the identification of photochemical reaction involving conversion of GEM to GOM in the atmosphere, especially during the summer season.
- The input data set contained too many parameters on PM components. The full Hg data set can be used for source apportionment analysis using methods that are different from PMF and PCA and do not require PM_{2.5} data. This can be considered in future studies.
- Although wind direction is an essential meteorological parameter in receptor modeling, wind direction could not be used in the PMF model and PCA. Other receptor models utilizing wind direction including back trajectory and wind rose are highly recommended for future research in source apportionment of mercury to verify the factors identified by the PMF model and PCA.

REFERENCES

- Al-Zubaidi, E. S., & Rabee, A. M. (2017). The risk of occupational exposure to mercury vapor in some public dental clinics of Baghdad city, Iraq. *Inhalation Toxicology*, 29(9), 397-403. doi:10.1080/08958378.2017.1369601.
- Ariya, P. A., Amyot, M., Dastoor, A., Deeds, D., Feinberg, A., Kos, G., . . . Toyota, K. (2015). Mercury Physicochemical and Biogeochemical Transformation in the Atmosphere and at Atmospheric Interfaces: A Review and Future Directions. *Chemical Reviews*, 115(10), 3760-3802. doi:10.1021/cr500667e.
- Ariya, P. A., Jobson, B. T., Sander, R., Niki, H., Harris, G. W., Hopper, J. F., & Anlauf, K. G. (1998). Measurements of C₂-C₇ hydrocarbons during the Polar Sunrise Experiment 1994: Further evidence for halogen chemistry in the troposphere. *Journal of Geophysical Research: Atmospheres*, 103(D11), 13169-13180. doi:10.1029/98jd00284.
- Ariya, P. A., Khalizov, A., & Gidas, A. (2002). Reactions of Gaseous Mercury with Atomic and Molecular Halogens: Kinetics, Product Studies, and Atmospheric Implications. *The Journal of Physical Chemistry A*, 106(32), 7310-7320. doi:10.1021/jp020719o.
- Balabanov, N. B., & Peterson, K. A. (2003). Mercury and Reactive Halogens: The Thermochemistry of Hg {Cl₂, Br₂, BrCl, ClO, and BrO}. *ChemInform*, 34(50). doi:10.1002/chin.200350012.
- Bernhoft, R. A. (2012). Mercury Toxicity and Treatment: A Review of the Literature. *Journal of Environmental and Public Health*, 2012, 1-10. doi:10.1155/2012/460508.
- Bhuiyan, M. A., Parvez, L., Islam, M., Dampare, S. B., & Suzuki, S. (2010). Heavy metal pollution of coal mine-affected agricultural soils in the northern part of Bangladesh. *Journal of Hazardous Materials*, 173(1-3), 384-392. doi:10.1016/j.jhazmat.2009.08.085.
- Blanchard, P., Froude, F., Martin, J., Dryfhout-Clark, H., & Woods, J. (2002). Four years of continuous total gaseous mercury (TGM) measurements at sites in Ontario, Canada. *Atmospheric Environment*, 36(23), 3735-3743. doi:10.1016/s1352-2310(02)00344-8.
- Brown, S. G., Frankel, A., & Hafner, H. R. (2007). Source apportionment of VOCs in the Los Angeles area using positive matrix factorization. *Atmospheric Environment*, 41(2), 227-237. doi:10.1016/j.atmosenv.2006.08.021.
- Caesari, D., Amato, F., Pandolfi, M., Alastuey, A., Querol, X., & Contini, D. (2016). An inter-comparison of PM₁₀ source apportionment using PCA and PMF receptor models in three European sites. *Environmental Science and Pollution Research*, 23(15), 15133-15148. doi:10.1007/s11356-016-6599-z.

- Callén, M. S., López, J. M., & Mastral, A. M. (2012). Influence of organic and inorganic markers in the source apportionment of airborne PM₁₀ in Zaragoza (Spain) by two receptor models. *Environmental Science and Pollution Research*, 20(5), 3240-3251. doi:10.1007/s11356-012-1241-1.
- Canada Council of Ministers of the Environment (2011). Ambient Air Monitoring Protocol for PM_{2.5} and Ozone Canada-wide Standards for Particulate Matter and Ozone [Online]: Accessed on July 20th, 2018, from https://www.ccme.ca/files/Resources/air/pm_oz/pm_oz_cws_monitoring_protocol_pn_1456_e.pdf.
- Carpi, A. (1997). Mercury from combustion sources: A review of the chemical species emitted and their transport in the atmosphere. *Water, Air, and Soil Pollution*, 98(3-4), 241–254. doi: 10.1007/bf02047037.
- Caselli, M., Gennaro, G. D., & Ielpo, P. (2006). A comparison between two receptor models to determine the source apportionment of atmospheric pollutants. *Environmetrics*, 17(5), 507-516. doi:10.1002/env.788.
- Chan, T. W., & Mozurkewich, M. (2006). Application of absolute principal component analysis to size distribution data: Identification of particle origins. *Atmospheric Chemistry and Physics Discussions*, 6(5), 10493-10522. doi:10.5194/acpd-6-10493-2006.
- Chang, C., Wang, J., Lung, S. C., Liu, S., & Shiu, C. (2009). Source characterization of ozone precursors by complementary approaches of vehicular indicator and principal component analysis. *Atmospheric Environment*, 43(10), 1771-1778. doi:10.1016/j.atmosenv.2008.12.023.
- Chen, C., Liu, S., Gao, Y., & Liu, Y. (2014). Investigation on Mercury Reemission from Limestone-Gypsum Wet Flue Gas Desulfurization Slurry. *The Scientific World Journal*, 2014, 1-6. doi:10.1155/2014/581724.
- Cheng, I., Lu, J., & Song, X. (2009). Studies of potential sources that contributed to atmospheric mercury in Toronto, Canada. *Atmospheric Environment*, 43(39), 6145-6158. doi:10.1016/j.atmosenv.2009.09.008.
- Cheng, I., Zhang, L., Blanchard, P., Dalziel, J., Tordon, R., Huang, J., & Holsen, T. M. (2013). Comparisons of mercury sources and atmospheric mercury processes between a coastal and inland site. *Journal of Geophysical Research: Atmospheres*, 118(5), 2434-2443. doi:10.1002/jgrd.50169.

- Cheng, I., Zhang, L., & Xu, X. (2016). Impact of Measurement Uncertainties on Receptor Modeling of Speciated Atmospheric Mercury. *Scientific Reports*, 6(1). doi:10.1038/srep20676.
- Chow, J. C., & Watson, J. G. (2002). Review of PM_{2.5} and PM₁₀ Apportionment for Fossil Fuel Combustion and Other Sources by the Chemical Mass Balance Receptor Model. *Energy & Fuels*, 16(2), 222-260. doi:10.1021/ef0101715.
- Cheng, Z., Wang, S., Fu, X., Watson, J. G., Jiang, J., Fu, Q., . . . Hao, J. (2013). Impact of biomass burning on haze pollution in the Yangtze River Delta, China: A case study in summer 2011. *Atmospheric Chemistry and Physics Discussions*, 13(11), 30687-30720. doi:10.5194/acpd-13-30687-2013.
- Corbitt, E. S., Jacob, D. J., Holmes, C. D., Streets, D. G., & Sunderland, E. M. (2011). Global Source–Receptor Relationships for Mercury Deposition Under Present-Day and 2050 Emissions Scenarios. *Environmental Science & Technology*, 45(24), 10477-10484. doi:10.1021/es202496y.
- Davis, J. C. (2002). *Statistics and data analysis in geology*. New York: J. Wiley.
- Denby, B., Ketzler, M., Ellermann, T., Stojiljkovic, A., Kupiainen, K., Niemi, J., . . . Sundvor, I. (2016). Road salt emissions: A comparison of measurements and modelling using the NORTRIP road dust emission model. *Atmospheric Environment*, 141, 508-522. doi:10.1016/j.atmosenv.2016.07.027.
- Deng, J., Zhang, Y., Qiu, Y., Zhang, H., Du, W., Xu, L., . . . Chen, J. (2018). Source apportionment of PM 2.5 at the Linan regional background site in China with three receptor models. *Atmospheric Research*, 202, 23-32. doi:10.1016/j.atmosres.2017.11.017.
- Dicosty, R. J., Callahan, M. A., & Stanturf, J. A. (2006). Atmospheric Deposition and Re-Emission of Mercury Estimated in a Prescribed Forest-Fire Experiment in Florida, USA. *Water, Air, and Soil Pollution*, 176(1-4), 77-91. doi:10.1007/s11270-006-9149-3.
- Duan, L., Wang, X., Wang, D, Duan, Y., Cheng N. and Xiu G. (2017). Atmospheric mercury speciation in Shanghai, China. *Science of The Total Environment*, 578:, 460-468. Doi: 10.1016/j.scitotenv.2016.10.209.
- Ebinghaus, R., Kock, H.H. , Temme, c., Einax, J.W .. Lowe. A.G., Richter, A., Burrows, A.P., and Schroeder, W.H. (2003). Antarctic springtime depletion of atmospheric mercury. *Environmental Science and Technology* 36. 1238 - 244.
- Eckley, C. S., Blanchard, P., Mclennan, D., Mintz, R., & Sekela, M. (2015). Soil–Air Mercury Flux near a Large Industrial Emission Source before and after Closure (Flin Flon,

- Manitoba, Canada). *Environmental Science & Technology*, 49(16), 9750-9757. doi:10.1021/acs.est.5b01995.
- Eckley, C. S., Parsons, M. T., Mintz, R., Lapalme, M., Mazur, M., Tordon, R., . . . Louis, V. S. (2013). Impact of Closing Canada's Largest Point-Source of Mercury Emissions on Local Atmospheric Mercury Concentrations. *Environmental Science & Technology*, 130904083640001. doi:10.1021/es401352n.
- Environment and Climate Change Canada (2010a). Speciated Mercury data for 2010-2011 [online]: Accessed on December 1st, 2017 from <http://open.canada.ca/data/en/dataset/82ab6e33-e41d-4f45-9dde-72c7886e1b16>.
- Environment and Climate Change Canada (2010b). National Air Pollution Surveillance data for 2010-2011 [online]. Accessed on July 20, 2018, from <http://maps-cartes.ec.gc.ca/rmspa-naps/data.aspx>
- Environment and Climate Change Canada (2010c). Historical weather data for 2010-2011 [online]: Accessed on Accessed on July 20th, 2018, from http://climate.weather.gc.ca/historical_data/search_historic_data_e.html.
- Environment and Climate Change Canada (2011). National Pollution Release Inventory for 2010-2011 [online]. <http://www.ec.gc.ca/inrp-npri/default.asp?lang=En&n=4A577BB9-1> (Accessed December 20, 2018).
- Environment and Climate Change Canada (2016). Network and Studies for Mercury speciation and monitoring: Metadata [Online]: Accessed on July 20th, 2018, from http://donnees.ec.gc.ca/data/air/monitor/monitoring-of-combined-atmospheric-gases-and-particles/speciated-mercury/Networks_Studies-Rseaux_tudes-SMM-Description_EN-FR.pdf.
- Environment and Climate Change Canada (2018). Canadian climate normals [online]: Available from climate.weather.gc.ca/climate_normals/index_e.html.
- Ferrari, C. P., Padova, C., Fain, X., Gauchard, P., Dommergue, A., Aspmo, K., . . . Boutron, C. (2008). Atmospheric mercury depletion event study in Ny-Alesund (Svalbard) in spring 2005. Deposition and transformation of Hg in surface snow during springtime. *Science of The Total Environment*, 397(1-3), 167-177. doi:10.1016/j.scitotenv.2008.01.064.
- Franzin, W. G., Mcfarlane, G. A., & Lutz, A. (1979). Atmospheric fallout in the vicinity of a base metal smelter at Flin Flon, Manitoba, Canada. *Environmental Science & Technology*, 13(12), 1513-1522. doi:10.1021/es60160a014.
- Fraser, W.W., (1998). Review of Clean Environment Commission, Hudson Bay Mining and Smelting, Flin Flon, MB. Order No. 899VO.

- Friedli, H. R., Radke, L. F., Prescott, R., Hobbs, P. V., & Sinha, P. (2003). Mercury emissions from the August 2001 wildfires in Washington State and an agricultural waste fire in Oregon and atmospheric mercury budget estimates. *Global Biogeochemical Cycles*, 17(2). doi:10.1029/2002gb001972.
- Fu, X. W., Feng, X., Dong, Z. Q., Yin, R. S., Wang, J. X., Yang, Z. R., & Zhang, H. (2010). Atmospheric gaseous elemental mercury (GEM) concentrations and mercury depositions at a high-altitude mountain peak in south China. *Atmospheric Chemistry and Physics*, 10(5), 2425-2437. doi:10.5194/acp-10-2425-2010.
- Gallup, D. L. (2018). The behavior of mercury in water, alcohols, monoethylene glycol and triethylene glycol II. Elemental mercury solubility in alcohols, ethers and acetone; gas plant mercury distribution; and speciation in monoethylene glycol solution. *Fluid Phase Equilibria*, 477, 58-61. doi:10.1016/j.fluid.2018.08.014.
- Guo, H., Wang, T., & Louie, P. (2004). Source apportionment of ambient non-methane hydrocarbons in Hong Kong. *Environmental Pollution*, 129(3), 489-498. doi:10.1016/j.envpol.2003.11.006.
- Gustin, M. S. (2011). Exchange of Mercury between the Atmosphere and Terrestrial Ecosystems. *Environmental Chemistry and Toxicology of Mercury*, 423-451. doi:10.1002/9781118146644.ch13.
- Gustin, M. S., Biester, H., & Kim, C. S. (2002). Investigation of the light-enhanced emission of mercury from naturally enriched substrates. *Atmospheric Environment*, 36(20), 3241-3254. doi:10.1016/s1352-2310(02)00329-1.
- Gustin, M. S., Lindberg, S. E., Austin, K., Coolbaugh, M., Vette, A., & Zhang, H. (2000). Assessing the contribution of natural sources to regional atmospheric mercury budgets. *Science of the Total Environment*, 259(1-3), 61-71. doi:10.1016/s0048-9697(00)00556-8.
- Gworek, B., Dmuchowski, W., Baczewska, A. H., Braęoszewska, P., Bemowska-Kařabun, O., & Wrzosek-Jakubowska, J. (2017). Air Contamination by Mercury, Emissions and Transformations—a Review. *Water, Air, & Soil Pollution*, 228(4). doi:10.1007/s11270-017-3311-y.
- Hall, B. (1995). The Gas Phase Oxidation of Elemental Mercury by Ozone. Mercury as a Global Pollutant, 301-315. doi:10.1007/978-94-011-0153-0_34.
- Han, Y., Holsen, T. M., Lai, S., Hopke, P. K., Yi, S., Liu, W., . . . Andolina, C. (2004). Atmospheric gaseous mercury concentrations in New York State: Relationships with meteorological data and other pollutants. *Atmospheric Environment*, 38(37), 6431-6446. doi:10.1016/j.atmosenv.2004.07.031.

- Harrison, R. M., Smith, D., Piou, C., & Castro, L. (1997). Comparative receptor modelling study of airborne particulate pollutants in Birmingham (United Kingdom), Coimbra (Portugal) and Lahore (Pakistan). *Atmospheric Environment*, 31(20), 3309-3321. doi:10.1016/s1352-2310(97)00152-0.
- Heaton, R. W., Rahn, K. A., & Lowenthal, D. H. (1992). Regional apportionment of sulfate and tracer elements in Rhode Island precipitation. *Atmospheric Environment. Part A. General Topics*, 26(8), 1529-1543. doi:10.1016/0960-1686(92)90137-a.
- Hedgecock, I. M., Pirrone, N., Trunfio, G. A., & Sprovieri, F. (2006). Integrated mercury cycling, transport, and air-water exchange (MECAWEx) model. *Journal of Geophysical Research*, 111(D20). doi:10.1029/2006jd007117.
- Ho, W., Tseng, K., Liou, M., Chan, C., & Wang, C. (2018). Application of Positive Matrix Factorization in the Identification of the Sources of PM_{2.5} in Taipei City. *International Journal of Environmental Research and Public Health*, 15(7), 1305. doi:10.3390/ijerph15071305.
- Holmes, C. D., Jacob, D. J., Corbitt, E. S., Mao, J., Yang, X., Talbot, R., & Slemr, F. (2010). Global atmospheric model for mercury including oxidation by bromine atoms. *Atmospheric Chemistry and Physics Discussions*, 10(8), 19845-19900. doi:10.5194/acpd-10-19845-2010.
- Hope E. Ratcliffe, G. Marie Swanson, Law. (1996). Human Exposure To Mercury: A Critical Assessment Of The Evidence Of Adverse Health Effects. *Journal of Toxicology and Environmental Health Part A*, 49(3), 221-270. doi:10.1080/009841096160817.
- Hopke, P. K. (2016). Review of receptor modeling methods for source apportionment. *Journal of the Air & Waste Management Association*, 66(3), 237-259. doi:10.1080/10962247.2016.1140693.
- Hopke, P. K., & Cohen, D. D. (2011). Application of receptor modeling methods. *Atmospheric Pollution Research*, 2(2), 122-125. doi:10.5094/apr.2011.016.
- Horowitz, H. M., Jacob, D. J., Zhang, Y., Dibble, T. S., Slemr, F., Amos, H. M., . . . Sunderland, E. M. (2017). A new mechanism for atmospheric mercury redox chemistry: Implications for the global mercury budget. *Atmospheric Chemistry and Physics Discussions*, 1-33. doi:10.5194/acp-2016-1165.
- Huang, J., Chen, X., Liu, C., Huang, C., & Fang, G. (2013). Ambient Trace Metals Sources in Taichung, Taiwan: Principal Component Analysis. *Aerosol and Air Quality Research*, 13(2), 672-679. doi:10.4209/aaqr.2012.05.0137.

- Huang, J., Choi, H., Hopke, P. K., & Holsen, T. M. (2010). Ambient Mercury Sources in Rochester, NY: Results from Principle Components Analysis (PCA) of Mercury Monitoring Network Data. *Environmental Science & Technology*, 44(22), 8441-8445. doi:10.1021/es102744j.
- Jeong, C., Mcguire, M. L., Herod, D., Dann, T., Dabek-Zlotorzynska, E., Wang, D., . . . Evans, G. (2011). Receptor model based identification of PM_{2.5} sources in Canadian cities. *Atmospheric Pollution Research*, 2(2), 158-171. doi:10.5094/apr.2011.021.
- Jeuris, B., Iannazzo, B., & Pompili, F. (2015). Nonnegative Matrix Factorization based on the Geometry of Positive Numbers. *Pamm*, 15(1), 661-662. doi:10.1002/pamm.201510320.
- Jiang, Y., Zhuang, G., Wang, Q., Liu, T., Huang, K., Fu, J. S., . . . Deng, C. (2011). Characteristics, sources and formation of aerosol oxalate in an Eastern Asia megacity and its implication to haze pollution. *Atmospheric Chemistry and Physics Discussions*, 11(8), 22075-22112. doi:10.5194/acpd-11-22075-2011.
- Joliffe, I. T. (2010). *Principal component analysis*. 2nd Ed. New York: Springer.
- Kamp, J., Skov, H., Jensen, B., & Sørensen, L. L. (2018). Fluxes of gaseous elemental mercury (GEM) in the High Arctic during atmospheric mercury depletion events (AMDEs). *Atmospheric Chemistry and Physics*, 18(9), 6923-6938. doi:10.5194/acp-18-6923-2018.
- Keeler, G. J., Landis, M. S., Norris, G. A., Christianson, E. M., & Dvonch, J. T. (2006). Sources of Mercury Wet Deposition in Eastern Ohio, USA. *Environmental Science & Technology*, 40(19), 5874-5881. doi:10.1021/es060377q.
- Khodeir, M., Shamy, M., Alghamdi, M., Zhong, M., Sun, H., Costa, M., . . . Maciejczyk, P. (2012). Source apportionment and elemental composition of PM_{2.5} and PM₁₀ in Jeddah City, Saudi Arabia. *Atmospheric Pollution Research*, 3(3), 331-340. doi:10.5094/apr.2012.037
- Kim, E. and Hopke, P.K. (2004). Improving Source Identification of Fine Particles in a Rural Northeastern U.S. Area Utilizing Temperature-Resolved Carbon Fractions. *J. Geophys. Res.*, 109, DOI 10.1029/2003JD004199.
- Kim, M., & Zoh, K. (2012). Fate and Transport of Mercury in Environmental Media and Human Exposure. *Journal of Preventive Medicine & Public Health*, 45(6), 335-343. doi:10.3961/jpmph.2012.45.6.335.
- Kristensen, L. J., & Taylor, M. P. (2012). Fields and Forests in Flames: Lead and Mercury Emissions from Wildfire Pyrogenic Activity. *Environmental Health Perspectives*, 120(2). doi:10.1289/ehp.1104672.

- Lando, A. M., & Lo, S. C. (2014). Consumer Understanding of the Benefits and Risks of Fish Consumption During Pregnancy. *American Journal of Lifestyle Medicine*, 8(2), 88-92. doi:10.1177/1559827613514704.
- Laurier, F. J. (2003). Reactive gaseous mercury formation in the North Pacific Oceans marine boundary layer: A potential role of halogen chemistry. *Journal of Geophysical Research*, 108(D17). doi:10.1029/2003jd003625.
- Lee, E., Chan, C. K., & Paatero, P. (1999). Application of positive matrix factorization in source apportionment of particulate pollutants in Hong Kong. *Atmospheric Environment*, 33(19), 3201-3212. doi:10.1016/s1352-2310(99)00113-2.
- Li, Y., Wang, Y., Li, Y., Li, T., Mao, H., Talbot, R., . . . Qie, G. (2017). Characteristics and potential sources of atmospheric particulate mercury in Jinan, China. *Science of the Total Environment*, 574, 1424-1431. doi:10.1016/j.scitotenv.2016.08.069.
- Liang, P., Zhang, C., Yang, Y., & Wang, D. (2014). A simulation study of mercury release fluxes from soils in wet-dry rotation environment. *Journal of Environmental Sciences*, 26(7), 1445-1452. doi:10.1016/j.jes.2014.05.010.
- Liao, Yanyin, "Analysis of potential sources and processes affecting ambient speciated mercury concentrations at Kejimikujik National Park, Nova Scotia" (2016). Electronic Theses and Dissertations. 5840. <https://scholar.uwindsor.ca/etd/5840>.
- Lim, H. E., Shim, J. J., Lee, S. Y., Lee, S. H., Jo, J. Y., In, K. H., . . . Kang, K. H. (1998). Mercury inhalation poisoning and acute lung injury. *The Korean Journal of Internal Medicine*, 13(2), 127-130. doi:10.3904/kjim.1998.13.2.127.
- Lin, C., & Pehkonen, S. O. (1999). The chemistry of atmospheric mercury: A review. *Atmospheric Environment*, 33(13), 2067-2079. doi:10.1016/s1352-2310(98)00387-2.
- Lin, C., Gustin, M. S., Singhasuk, P., Eckley, C., & Miller, M. (2010). Empirical Models for Estimating Mercury Flux from Soils. *Environmental Science & Technology*, 44(22), 8522-8528. doi:10.1021/es1021735.
- Lin, C., Zhu, W., Li, X., Feng, X., Sommar, J., & Shang, L. (2012). Novel Dynamic Flux Chamber for Measuring Air-Surface Exchange of Hg⁰ from Soils. *Environmental Science & Technology*, 46(16), 8910-8920. doi:10.1021/es3012386
- Lindberg, S. E. (1980). Mercury partitioning in a power plant plume and its influence on atmospheric removal mechanisms. *Atmospheric Environment* (1967), 14(2), 227-231. doi: 10.1016/0004-6981(80)90282-6.
- Lindberg, S. E., Brooks, S., Lin, C., Scott, K. J., Landis, M. S., Stevens, R. K., . . . Richter, A. (2002). Dynamic Oxidation of Gaseous Mercury in the Arctic Troposphere at Polar

- Sunrise. *Environmental Science & Technology*, 36(6), 1245-1256. doi:10.1021/es0111941.
- Lindberg, S., Bullock, R., Ebinghaus, R., Engstrom, D., Feng, X., Fitzgerald, W., . . . Seigneur, C. (2007). A Synthesis of Progress and Uncertainties in Attributing the Sources of Mercury in Deposition. *AMBIO: A Journal of the Human Environment*, 36(1), 19-33. doi:10.1579/0044-7447(2007)36[19:asopau]2.0.co;2.
- Liu, W., Hopke, P. K., Han, Y., Yi, S., Holsen, T. M., Cybart, S., . . . Milligan, M. (2003). Application of receptor modeling to atmospheric constituents at Potsdam and Stockton, NY. *Atmospheric Environment*, 37(36), 4997-5007. doi:10.1016/j.atmosenv.2003.08.036.
- Liu, B., Keeler, G. J., Dvonch, J. T., Barres, J. A., Lynam, M. M., Marsik, F. J., & Morgan, J. T. (2010). Urban–rural differences in atmospheric mercury speciation. *Atmospheric Environment*, 44(16), 2013-2023. doi:10.1016/j.atmosenv.2010.02.012.
- Lynam, M. M., & Keeler, G. J. (2006). Source–receptor relationships for atmospheric mercury in urban Detroit, Michigan. *Atmospheric Environment*, 40(17), 3144-3155. doi:10.1016/j.atmosenv.2006.01.026.
- Manitoba Co-operator (2017). Controlled crop residue burning authorizations begin Aug. 1. Available online at <https://www.manitobacooperator.ca/news-opinion/news/local/controlled-crop-residue-burning-authorizations-begin-aug-1/>. [Accessed on August 26th, 2019].
- Maxwell, J. A., Holsen, T. M., & Mondal, S. (2013). Gaseous Elemental Mercury (GEM) Emissions from Snow Surfaces in Northern New York. *PLoS ONE*, 8(7). doi:10.1371/journal.pone.0069342.
- Michael, R., Stuart, A. L., Trotz, M. A., & Akiwumi, F. (2016). Source apportionment of wet-deposited atmospheric mercury in Tampa, Florida. *Atmospheric Research*, 170, 168-175. doi:10.1016/j.atmosres.2015.11.017.
- Miller, S. L., Anderson, M. J., Daly, E. P., & Milford, J. B. (2002). Source apportionment of exposures to volatile organic compounds. I. Evaluation of receptor models using simulated exposure data. *Atmospheric Environment*, 36(22), 3629-3641. doi:10.1016/s1352-2310(02)00279-0.
- Munthe, J. (1992). The aqueous oxidation of elemental mercury by ozone. *Atmospheric Environment. Part A. General Topics*, 26(8), 1461-1468. doi:10.1016/0960-1686(92)90131-4

- National Pollutant Release Inventory (2017). Data Search. Retrieved September 01, 2018, from <https://pollution-waste.canada.ca/national-release-inventory/archives/index.cfm?lang=en>
- Noor, N. M., Yahaya, A., Ramli, N., & Abdullah, M. M. (2015). Filling the Missing Data of Air Pollutant Concentration Using Single Imputation Methods. *Applied Mechanics and Materials*, 754-755, 923-932. doi:10.4028/www.scientific.net/amm.754-755.923.
- Obrist, D., Moosmüller, H., Schürmann, R., Chen, L. A., & Kreidenweis, S. M. (2008). Particulate-Phase and Gaseous Elemental Mercury Emissions During Biomass Combustion: Controlling Factors and Correlation with Particulate Matter Emissions. *Environmental Science & Technology*, 42(3), 721-727. doi:10.1021/es071279n.
- Otten, B. V., Buitrago, P. A., Senior, C. L., & Silcox, G. D. (2011). Gas-Phase Oxidation of Mercury by Bromine and Chlorine in Flue Gas. *Energy & Fuels*, 25(8), 3530-3536. doi:10.1021/ef200840c.
- Paatero, P., & Tapper, U. (1994). Positive matrix factorization: A non-negative factor model with optimal utilization of error estimates of data values. *Environmetrics*, 5(2), 111-126. doi:10.1002/env.3170050203.
- Pacyna, E. G., Pacyna, J. M., Steenhuisen, F., & Wilson, S. (2006). Global anthropogenic mercury emission inventory for 2000. *Atmospheric Environment*, 40(22), 4048-4063. doi:10.1016/j.atmosenv.2006.03.041.
- Pacyna, E.G. and Pacyna, J.M. (2002). Global emission of mercury from anthropogenic sources in 1995. *Air and Soil Pollution*, 137, 149-165.
- Pacyna, J. M., & Pacyna, E. G. (2001). An assessment of global and regional emissions of trace metals to the atmosphere from anthropogenic sources worldwide. *Environmental Reviews*, 9(4), 269-298. doi:10.1139/a01-012.
- Pal, B., & Ariya, P. A. (2004). Studies of ozone initiated reactions of gaseous mercury: Kinetics, product studies, and atmospheric implications. *Physical Chemistry Chemical Physics*, 6(3), 572. doi:10.1039/b311150d.
- Pandey, S. K., Kim, K., & Brown, R. J. (2011). Measurement techniques for mercury species in ambient air. *TrAC Trends in Analytical Chemistry*, 30(6), 899-917. doi:10.1016/j.trac.2011.01.017.
- Petrucci, R.H., Harwood, W.S., Herring, G.E. and Madura J. (2007). *General Chemistry: Principles & Modern Applications*, 9th Edition. New Jersey: Pearson Education, Inc.,

- Pires, J., Sousa, S., Pereira, M., Alvim-Ferraz, M., & Martins, F. (2008). Management of air quality monitoring using principal component and cluster analysis—Part I: SO₂ and PM₁₀. *Atmospheric Environment*, 42(6), 1249-1260. doi:10.1016/j.atmosenv.2007.10.044.
- Pirrone, N., Cinnirella, S., Feng, X., Finkelman, R. B., Friedli, H. R., Leaner, J., . . . Telmer, K. (2010). Global mercury emissions to the atmosphere from anthropogenic and natural sources. *Atmospheric Chemistry and Physics Discussions*, 10(2), 4719-4752. doi:10.5194/acpd-10-4719-2010.
- Pirrone, N., Costa, P., Pacyna, J., & Ferrara, R. (2001). Mercury emissions to the atmosphere from natural and anthropogenic sources in the Mediterranean region. *Atmospheric Environment*, 35(17), 2997-3006. doi:10.1016/s1352-2310(01)00103-0.
- Pitchford, M. L., Poirot, R. L., Schichtel, B. A., & Malm, W. C. (2009). Characterization of the Winter Midwestern Particulate Nitrate Bulge. *Journal of the Air & Waste Management Association*, 59(9), 1061-1069. doi:10.3155/1047-3289.59.9.1061.
- Poissant, L. (1997). Field observations of total gaseous mercury behavior: Interactions with ozone concentration and water vapour mixing ratio in air at a rural site. *Water, Air, & Soil Pollution*, 97(3-4), 341-353. doi:10.1007/bf02407471.
- Poissant, L., Pilote, M., Beauvais, C., Constant, P., & Zhang, H. (2005). A year of continuous measurements of three atmospheric mercury species (GEM, RGM and Hg) in southern Québec, Canada. *Atmospheric Environment*, 39(7), 1275-1287. doi:10.1016/j.atmosenv.2004.11.007.
- Porcella, D. B., Chu, P., & Allan, M. A. (1996). Inventory of North American Hg Emissions to the Atmosphere. *Global and Regional Mercury Cycles: Sources, Fluxes and Mass Balances*, 179-190. doi:10.1007/978-94-009-1780-4_8.
- Rao, S. T., Ku, J., & Rao, K. S. (1991). Analysis of Toxic Air Contaminant Data Containing Concentrations Below the Limit of Detection. *Journal of the Air & Waste Management Association*, 41(4), 442-448. doi:10.1080/10473289.1991.10466856.
- Reff, A., Eberly, S. I., & Bhave, P. V. (2007). Receptor Modeling of Ambient Particulate Matter Data Using Positive Matrix Factorization: Review of Existing Methods. *Journal of the Air & Waste Management Association*, 57(2), 146-154. doi:10.1080/10473289.2007.10465319.
- Reimann, C., Filzmoser, P., & Garrett, R. G. (2002). Factor analysis applied to regional geochemical data: Problems and possibilities. *Applied Geochemistry*, 17(3), 185-206. doi:10.1016/s0883-2927(01)00066-x.

- Ren, X., Luke, W., Kelley, P., Cohen, M., Ngan, F., Artz, R., . . . Huey, L. (2014). Mercury Speciation at a Coastal Site in the Northern Gulf of Mexico: Results from the Grand Bay Intensive Studies in Summer 2010 and Spring 2011. *Atmosphere*, 5(2), 230-251. doi:10.3390/atmos5020230.
- Ross, H.B. and Vermette, S.J. (1995). Precipitation. In: Salbu, B.,Steinnes, E. (Eds.), Trace Elements in Natural Waters. CRCPress, Ann Arbor, MI, pp. 99Ð116.
- Schroeder, W. H. (2005). Gaseous mercury emissions from natural sources in Canadian landscapes. *Journal of Geophysical Research*, 110(D18). doi:10.1029/2004jd005699.
- Schroeder, W.H., &Munthe, J. (1998). Atmospheric mercury—An overview. *Atmospheric Environment*,32(5), 809-822. doi:10.1016/s1352-2310(97)00293-8.
- Selin, N. E., & Jacob, D. J. (2008). Seasonal and spatial patterns of mercury wet deposition in the United States: Constraints on the contribution from North American anthropogenic sources. *Atmospheric Environment*, 42(21), 5193-5204. doi:10.1016/j.atmosenv.2008.02.069.
- Shannon, J.D., and E.C. Voldner (1994) Modelling Atmospheric Concentrations and Deposition of Mercury to the Great Lakes. Presented at the DOE/FDA/EPA Workshop on Methylmercury and Human Health, Bethesda, MD March 22-23 1994.
- Simone, F. D., Cinnirella, S., Gencarelli, C. N., Carbone, F., Hedgecock, I. M., & Pirrone, N. (2016). Particulate-Phase Mercury Emissions during Biomass Burning and Impact on Resulting Deposition: A Modelling Assessment. *Atmospheric Chemistry and Physics Discussions*, 1-22. doi:10.5194/acp-2016-685.
- Slemr, F., Brunke, E., Ebinghaus, R., Temme, C., Munthe, J., Wängberg, I., . . . Berg, T. (2003). Worldwide trend of atmospheric mercury since 1977. *Geophysical Research Letters*, 30(10). doi:10.1029/2003gl016954.
- Sommar, J., Gårdfeldt, K., Strömberg, D., & Feng, X. (2001). A kinetic study of the gas-phase reaction between the hydroxyl radical and atomic mercury. *Atmospheric Environment*, 35(17), 3049-3054. doi:10.1016/s1352-2310(01)00108-x.
- Song, S., Selin, N. E., Soerensen, A. L., Angot, H., Artz, R., Brooks, S., . . . Zhang, Q. (2015). Top-down constraints on atmospheric mercury emissions and implications for global biogeochemical cycling. *Atmospheric Chemistry and Physics*,15(12), 7103-7125. doi:10.5194/acp-.
- Song, Y., Xie, S., Zhang, Y., Zeng, L., Salmon, L. G., & Zheng, M. (2006). Source apportionment of PM_{2.5} in Beijing using principal component analysis/absolute principal

- component scores and UNMIX. *Science of the Total Environment*, 372(1), 278-286. doi:10.1016/j.scitotenv.2006.08.041.
- Squizzato, S., Masiol, M., Rich, D. Q., & Hopke, P. K. (2018). A long-term source apportionment of PM_{2.5} in New York State during 2005–2016. *Atmospheric Environment*, 192, 35-47. doi:10.1016/j.atmosenv.2018.08.044.
- Statistics Canada. (2018). Population and dwelling count amendments, 2016 Census. Retrieved October 28, 2018, from <https://www12.statcan.gc.ca/census-recensement/2016/dp-pd/corr/index-eng.cfm>.
- Tabachnick, B. G., & Fidell, L. S. (2007). Using multivariate statistics. Boston: Pearson Education.
- Tao, Z., Liu, Y., Zhou, M., & Chai, X. (2017). Exchange pattern of gaseous elemental mercury in landfill: Mercury deposition under vegetation coverage and interactive effects of multiple meteorological conditions. *Environmental Science and Pollution Research*, 24(34), 26586-26593. doi:10.1007/s11356-017-0275-9.
- Tauler R., Peré-Trepat E., Lacorte S., Barceló D. (2004). Chemometrics Modeling of Environmental Data. Department of Environmental Chemistry, Institute of Chemical and Environmental Research IIQAB-CSIC, Spain.
- Temme, C., Blanchard, P., Steffen, A., Banic, C., Beauchamp, S., Poissant, L., . . . Wiens, B. (2007). Trend, seasonal and multivariate analysis study of total gaseous mercury data from the Canadian atmospheric mercury measurement network (CAMNet). *Atmospheric Environment*, 41(26), 5423-5441. doi:10.1016/j.atmosenv.2007.02.021.
- Tewalt, S. J., Bragg, L. J., & Finkelman, R. B. (2001). Mercury in U.S. coal; abundance, distribution, and modes of occurrence. *Fact Sheet*. doi:10.3133/fs09501.
- Thurston, G. D., & Spengler, J. D. (1985). A quantitative assessment of source contributions to inhalable particulate matter pollution in metropolitan Boston. *Atmospheric Environment* (1967), 19(1), 9-25. doi:10.1016/0004-6981(85)90132-5.
- Thurston, G. D., Ito, K., & Lall, R. (2011). A source apportionment of U.S. fine particulate matter air pollution. *Atmospheric Environment*, 45(24), 3924-3936. doi:10.1016/j.atmosenv.2011.04.070.
- United National Environmental Programme. Mercury (2013). Time to Act; Kirby, A., Rucevska, I., Yemelin, V., Cooke, C., Simonett, O., Novikov, V., Hughes, G., Eds.; UNEP: Nairobi, Kenya; p 44.
- United Nations Environmental Program (2008). The Global Atmospheric Mercury Assessment: Sources, Emissions and Transport. UNEP-Chemicals, Geneva.

- United States Environmental Protection Agency (2014). Fundamentals and User Guide for Positive Matrix Factorization PMF5.0. U.S. Environmental Protection Agency National Exposure Research Laboratory Research Triangle Park, NC27711.
- United States Environmental Protection Agency National Emission Inventory (2007). <http://www.epa.gov/ttnchie1/net/2008inventory.html> (Accessed December 20, 2018).
- Viana, M., Kuhlbusch, T., Querol, X., Alastuey, A., Harrison, R., Hopke, P.,... Hitzenberger, R. (2008). Source apportionment of particulate matter in Europe: A review of methods and results. *Journal of Aerosol Science*, 39(10), 827-849. doi:10.1016/j.jaerosci.2008.05.007.
- Watson, J. G., Chow, J. C., & Fujita, E. M. (2001). Review of volatile organic compound source apportionment by chemical mass balance. *Atmospheric Environment*, 35(9), 1567-1584. doi:10.1016/s1352-2310(00)00461-1.
- Weiss-Penzias, P. S., Gay, D. A., Brigham, M. E., Parsons, M. T., Gustin, M. S., & Schure, A. T. (2016). Trends in mercury wet deposition and mercury air concentrations across the U.S. and Canada. *Science of the Total Environment*, 568, 546-556. doi:10.1016/j.scitotenv.2016.01.061.
- Wright, L. P., Zhang, L., Cheng, I., Aherne, J., & Wentworth, G. R. (2018). Impacts and Effects Indicators of Atmospheric Deposition of Major Pollutants to Various Ecosystems - A Review. *Aerosol and Air Quality Research*, 18(8), 1953-1992. doi:10.4209/aaqr.2018.03.0107.
- Wright, L. P., Zhang, L., & Marsik, F. J. (2016). Overview of mercury dry deposition, litter fall, and through fall studies. *Atmospheric Chemistry and Physics Discussions*, 1-46.
- Wu, C., Cao, Y., He, C., Dong, Z., & Pan, W. (2010). Study of elemental mercury re-emission through a lab-scale simulated scrubber. *Fuel*, 89(8), 2072-2080. doi:10.1016/j.fuel.2009.11.045.
- Xiong, Y., Zhou, J., Schauer, J. J., Yu, W., & Hu, Y. (2017). Seasonal and spatial differences in source contributions to PM_{2.5} in Wuhan, China. *Science of the Total Environment*, 577, 155-165. doi:10.1016/j.scitotenv.2016.10.150.
- Xu, X., Liao, Y., Cheng, I., & Zhang, L. (2017). Potential sources and processes affecting speciated atmospheric mercury at Kejimikujik National Park, Canada: Comparison of receptor models and data treatment methods. *Atmospheric Chemistry and Physics*, 17(2), 1381-1400. doi:10.5194/acp-17-1381-2017.

- Yao, L., Yang, L., Yuan, Q., Yan, C., Dong, C., Meng, C., . . . Wang, W. (2016). Sources apportionment of PM 2.5 in a background site in the North China Plain. *Science of The Total Environment*, 541, 590-598. doi:10.1016/j.scitotenv.2015.09.123.
- Zhang, L., Blanchard, P., Gay, D. A., Prestbo, E. M., Risch, M. R., Johnson, D., . . . Dalziel, J. (2012). Estimation of speciated and total mercury dry deposition at monitoring locations in Eastern and Central North America. *Atmospheric Chemistry and Physics Discussions*, 12(1), 2783-2815. doi:10.5194/acpd-12-2783-2012.
- Zhang, R., Cao, J., Tang, Y., Arimoto, R., Shen, Z., Wu, F., . . . Li, G. (2014). Elemental profiles and signatures of fugitive dusts from Chinese deserts. *Science of The Total Environment*, 472, 1121-1129. doi:10.1016/j.scitotenv.2013.11.011.
- Zhang, L., Wang, S. X., Wang, L., & Hao, J. M. (2013). Atmospheric mercury concentration and chemical speciation at a rural site in Beijing, China: Implications of mercury emission sources. *Atmospheric Chemistry and Physics*, 13(20), 10505-10516. doi:10.5194/acp-13-10505-2013.
- Zhao, Y., Mann, M. D., Olson, E. S., Pavlish, J. H., & Dunham, G. E. (2006). Effects of Sulfur Dioxide and Nitric Oxide on Mercury Oxidation and Reduction under Homogeneous Conditions. *Journal of the Air & Waste Management Association*, 56(5), 628-635. doi:10.1080/10473289.2006.10464483.
- Zhou, Y., Huang, X. H., Bian, Q., Griffith, S. M., Louie, P. K., & Yu, J. Z. (2015). Sources and atmospheric processes impacting oxalate at a suburban coastal site in Hong Kong: Insights inferred from 1 year hourly measurements. *Journal of Geophysical Research: Atmospheres*, 120(18), 9772-9788. doi:10.1002/2015jd023531.
- Zhou, H., Zhou, C., Lynam, M. M., Dvonch, J. T., Barres, J. A., Hopke, P. K., . . . Holsen, T. M. (2017). Atmospheric Mercury Temporal Trends in the Northeastern United States from 1992 to 2014: Are Measured Concentrations Responding to Decreasing Regional Emissions? *Environmental Science & Technology Letters*, 4(3), 91-97. doi: 10.1021/acs.estlett.6b00452.
- Zhu, W., Li, Z., Li, P., Yu, B., Lin, C., Sommar, J., & Feng, X. (2018). Re-emission of legacy mercury from soil adjacent to closed point sources of Hg emission. *Environmental Pollution*, 242, 718-727. doi:10.1016/j.envpol.2018.07.002.
- Zong, Z., Wang, X., Tian, C., Chen, Y., Fu, S., Qu, L., . . . Zhang, G. (2018). PMF and PSCF based source apportionment of PM 2.5 at a regional background site in North China. *Atmospheric Research*, 203, 207-215. doi:10.1016/j.atmosres.2017.12.013.

APPENDICES

APPENDICES

Appendix A: Elsevier Licence

Jul 20, 2019

This Agreement between Mr. Morounfolu Adeyeye ("You") and Elsevier ("Elsevier") consists of your license details and the terms and conditions provided by Elsevier and Copyright Clearance Center.

License Number 4633251088850

License date Jul 20, 2019

Licensed Content Publisher Elsevier

Licensed Content Publication Journal of Aerosol Science

Licensed Content Title Source apportionment of particulate matter in Europe: A review of methods and results

Licensed Content Author M. Viana, T.A.J. Kuhlbusch, X. Querol, A. Alastuey, R.M. Harrison, P.K. Hopke, W. Winiwarter, M. Vallius, S. Szidat, A.S.H. Prévôt, C. Hueglin, H. Bloemen, P. Wählin, R. Vecchi, A.I. Miranda, A. Kasper-Giebl, W. Maenhaut, R. Hitzenberger

Licensed Content Date Oct 1, 2008

Licensed Content Volume 39

Licensed Content Issue 10

Licensed Content Pages 23

Start Page 827

End Page 849

Type of Use reuse in a thesis/dissertation

Intended publisher of new work other

Portion figures/tables/illustrations

Number of figures/tables /illustrations 1

Format both print and electronic

Are you the author of this Elsevier article? No

Will you be translating? No

Original figure numbers Figure 1

Title of your thesis/dissertation Source Apportionment of Ambient Mercury at Flin Flon, Manitoba

Expected completion date Jul 2019

Estimated size (number of pages) 145

Publisher Tax ID GB 494 6272 12

Total 0.00 CAD

Appendix B: Point sources of Hg and other air pollutants

Table B1: Point sources of Hg and other pollutants in Manitoba in 2010

Facility	Location (^a Lat, Long)	^b Distance between coordinates (km)	Direction	Hg	PM _{2.5}	SO ₂	NO ₂	NH ₃	Zn
Hudson Bay Mining and Smelting Co., Limited – HBMS Metallurgical Complex	Flin Flon (54.7710, -101.8840)	111	-	283	1.2	58,234			62
Gerdau AmeriSteel - Gerdau AmeriSteel Manitoba	Selkirk (50.1302, -96.9013)	615	Southeast	20	11	69	117		1.5
Vale Canada Limited - Thompson Operations	Thompson (55.7138, -97.8561)	276	Northeast	0.006	183	134,617			
Crowflight Minerals Incorporated - Bucko Lake Mine	Wabowden (54.8779, -98.6562)	209	Northeast		3.9				0.001
1126774 Ontario - New Britannia Mine	Snow Lake (54.8864, -100.0228)	119	Northeast		0.480				
Manitoba Hydro - Brandon Generating Station	Brandon (49.8449, -99.8896)	562	Southeast		4.9	105	138		
Manitoba Hydro - Grand Rapids Generating Station	Grand Rapids (53.1605, -99.2859)	245	Southeast		1.0				
Manitoba Hydro - Lac Brochet	Lac Brochet (58.3900, -97.2200)	429	North		0.900		60		
Manitoba Hydro - Brochet	Brochet (57.5300, -101.4100)	347	North		0.690		46		
Manitoba Hydro - Tadoule Lake	Tadoule Lake (58.7157, -98.4898)	485	Northeast		0.590		39		
Manitoba Hydro - Kelsey Generating Station	Kelsey (56.0382, -96.5435)	366	Northeast		0.570				
Manitoba Hydro- Jenpeg generating Station	Jenpeg (54.5444, -98.0261)	248	East		0.320				
Graymont Western Canada Inc. - Faulkner Plant	Faulkner (51.4135, -98.7650)	426	Southeast	1.9	47		293		
Husky Oil Operations Limited - Minnedosa Ethanol Plant	Minnedosa (50.2543, -99.8498)	520	Southeast		3.4		69		

Koch Fertilizer Canada, Ulc - Koch Fertilizer Canada, Ulc	Brandon (49.8309, -99.9078)	565	Southeast		5.3		556	1,519	
Canexus Chemicals Canada Limited Partnership - Brandon	Brandon (49.8265, -99.8293)	562	Southeast		2.7	0.011	43		
Erco Worldwide, A Division Of Superior Plus Lp - Hargrave Plant	Virden (49.8537, -100.9258)	544	Southeast		0.611		0.969		
Viterra Inc. - Brandon	Brandon (49.9786, -101.1241)	564	Southeast		1.4			6.5	
Richardson Pioneer Ltd. - Shoal Lake	Shoal Lake (50.4369, -100.5906)	488	Southeast		0.968			0.165	
Richardson Pioneer Ltd. - Brandon	Brandon (49.8472, -100.1191)	562	Southeast		0.783				
Richardson Pioneer Ltd. - Dauphin	Dauphin (51.1501, -100.0494)	420	Southeast		0.474				
Viterra Inc. - BinscarthHtp	Binscarth (50.6261,-101.2878)	461	South		0.172				
Agrium Inc. - Bloom Terminal	Portage La Prairie (49.9733, -98.3302)	586	Southeast		0.300			0.020	
Cargill Limited - Cargill Aghorizons, Dauphin, Mb	Dauphin (51.1416,-100.0361)	420	Southeast		0.349				
Cargill Limited - Cargill Aghorizons, Nesbitt, Mb	Nesbitt (49.5931, -99.9284)	590	Southeast		0.446				
Cargill Limited - Cargill Aghorizons, Oakner, Mb	Hamiota (50.0884, -100.5879)	517	Southeast		0.672				
Cargill Limited - Cargill Aghorizons, Swan River, Mb	Swan River (52.0696, -101.2722)	299	Southeast		as				
Maple Leaf Agri-Farms Inc. - Souris Feedmill	Souris (49.6212, -100.2582)	583	Southeast		0.506				
Mccain Foods Canada Ltd. - Mccain Foods (Canada) - Portage La Prairie	Portage La Prairie (49.9885, -98.2698)	585	Southeast		0.533		28		
Mccain Foods Canada Ltd. - Carberry Factory	Carberry (49.8694, -99.3686)	571	Southeast		0.435		23		

Simplot Canada (Ii) Ltd. - Portage La Prairie	Portage La Prairie (49.9721, -98.3943)	577	Southeast		1.6	80			
Enerplus Corporation - Kirkella Oil Battery 07-10	^c NA (49.9785,-101.3577)	550	Southeast		0.603	32			
Viterra Inc. - Souris East (Au)	Souris (49.6211, -100.2575)	582	Southeast		1.3				
Richardson Pioneer Ltd. - Dundonald	Westbourne (50.1297, -98.5811)	562	Southeast		0.310			0.081	
Maple Leaf Consumer Foods Inc. - Maple Leaf Foods – Brandon	Brandon (49.8321, -99.8549)	566	Southeast		3.2			6.0	
Maple Leaf Consumer Foods Inc. - Consumer Foods - Winnipeg	Winnipeg (49.8806, -97.0741)	583	Southeast		0.345			1.9	
Tolko Industries Ltd. - Manitoba Kraft Papers Division	The Pas (53.8610, -101.2133)	112	Southeast		691	272	258	127	
Eog Resources Canada Inc. - Waskada Oil Battery 15-09	^c NA (49.1128, -100.7658)	112	Southeast		11	30			
Louisiana-Pacific Canada Ltd. - Lp Swan Valley Osb	Minitonas (52.0858, -101.0380)	304	Southeast		10		58		
Viterra Inc. - Portage La Prairie Division (Can-Oat)	Portage La Prairie (49.9664, -98.3530)	586	Southeast		1.8				
Diageo Canada Inc. - Gimli Plant	Gimli (50.6550, -97.0026)	563	Southeast		1.5		59		
Lehigh Hanson Materials Ltd. - Glacier Quarry	RM of Rockwood (50N, 96W)	591	Southeast		1.1				

Note:

- ^aThe geographic coordinates (latitude and longitude) of each facility was obtained from the facility information on NPRI
- ^bThe distances of each point source facility to the monitoring station were calculated using distance calculator with coordinate <https://gps-coordinates.org/distance-between-coordinates.php>

Table B2: Point sources of Hg and other pollutants in Manitoba in 2011

Facility	Location (^a Lat, Long)	^b Distance between coordinates (km)	Direction	Hg (kg)	PM _{2.5} (tonnes)	SO ₂ (tonnes)	NO ₂ (tonnes)	NH ₃ (tonnes)	Zn (tonnes)
Hudson Bay Mining and Smelting Co., Limited – HBMS Metallurgical Complex	Flin Flon (54.7683, -101.8774)	111	-	0	0.989	72			
Gerdau AmeriSteel - Gerdau AmeriSteel Manitoba	Selkirk (50.1302, -96.9013)	615	Southeast	21	12	73	122		1.5
Vale Canada Limited - Thompson Operations	Thompson (55.7138, -97.8561)	276	Northeast	0.007	413	125,397			
Graymont Western Canada Inc. - Faulkner Plant	Faulkner (51.4135, -98.7650)	426	Southeast		60		287		
Sangold Corporation - Mill & Mine Site	Bissett (51.0218, -95.6795)	587	Southeast		0.412				
Manitoba Hydro - Brandon Generating Station	Brandon (49.8449, -99.8896)	562	Southeast		5.4	109	170		
Richardson Pioneer Ltd. - Grand Plains	Grandview (51.1546, -100.4920)	407	Southeast					0.125	
Manitoba Hydro - Lac Brochet	Lac Brochet (58.3900, -97.2200)	429	North		0.750		50		
Manitoba Hydro - Brochet	Brochet (57.5300, -101.4100)	347	North		0.680		46		
Manitoba Hydro - Tadoule Lake	Tadoule Lake (58.7157, -98.4898)	485	Northeast		0.700		47		
Manitoba Hydro - Kelsey Generating Station	Kelsey (56.0382, -96.5435)	366	Northeast		0.600				
Manitoba Hydro- Jenpeg generating Station	Jenpeg (54.5444, -98.0261)	248	East		0.500				
Viterra Inc. - Southlakes Elevator (Stonewall - Au)	Stonewall (49.8953, -97.1389)	600	Southeast		7.6				
Richardson Pioneer Ltd. - Shoal Lake	Shoal Lake (50.4369, -100.5906)	488	Southeast		0.752			0.124	
Viterra Inc. - BinscarthHtp	Binscarth (50.6261, -101.2878)	461	South		0.152			0.358	
Louis Dreyfus Canada Ltd - Louis Dreyfus	Viriden	544	South		0.522				

Canada Ltd.- Virden	(49.8961,-101.0239)								
Snow Lake Mine - New Britannia Mine	Snow Lake (54.8864,-100.0228)	119	Northeast		0.480				
Richardson Pioneer Ltd. - Minnedosa	Minnedosa (50.2469,-99.8399)	520	Southeast		0.392				
Richardson Pioneer Ltd. – Swan River Valley	Swan River (52.1170,-101.2670)	299	Southeast		0.384			0.161	
Richardson Pioneer Ltd. - Brandon	Brandon (49.8472, -100.1191)	562	Southeast		0.524				
Husky Oil Operations Limited - Minnedosa Ethanol Plant	Minnedosa (50.2543, -99.8498)	520	Southeast		4.1		66		
Canexus Chemicals Canada Limited Partnership - Canexus Chemicals Lp	Brandon (49.8265, -99.8293)	562	Southeast		2.6	0.011	62		
Graymont Western Canada Inc. - Faulkner Plant	Faulkner (51.4135, -98.7650)	426	Southeast		60		287		
Tolko Industries Ltd. - Manitoba Kraft Papers Division	The Pas (53.8610, -101.2133)	112	Southeast		653	264	250	120	
Bunge Canada Holdings I Ulc - Bunge Canada - Harrowby Plant	Harrowby (50.7555, -101.4522)	446	South		14	0.167	19		
Adm Agri-Industries - Adm Agri-Industries - Adm Milling Co. - Winnipeg	Winnipeg (49.9033,-97.1156)	574	Southeast		4.0				
Viterra Inc. - Portage La Prairie Division (Can-Oat)	Portage La Prairie (49.9664, -98.3530)	586	Southeast		1.7				
Cargill Limited - Cargill Aghorizons, Oakner, Mb	Hamiota (50.0884, -100.5879)	517	Southeast		0.790				
Cargill Limited - Cargill Aghorizons, Swan River, Mb	Swan River (52.0696, -101.2722)	299	Southeast		0.741				
Cargill Limited - Cargill Aghorizons, Dauphin, Mb	Dauphin (51.1416,-100.0361)	420	Southeast		0.330				
Viterra Inc. –Brandon facility (WESTCO) Viterra	Brandon (49.8276,-99.8941)	564	Southeast					6.7	
Simplot Canada (Ii) Ltd. - Portage La Prairie	Portage La Prairie (49.9721, -98.3943)	577	Southeast		1.7	83			
Maple Leaf Agri-Farms Inc. - Souris Feedmill	Souris (49.6212, -100.2582)	583	Southeast		0.556				

Mccain Foods Canada Ltd. - Carberry Factory	Carberry (49.8694, -99.3686)	571	Southeast		0.430		23			
Louisiana-Pacific Canada Ltd. - Lp Swan Valley Osb	Minitonas (52.0858, -101.0380)	304	Southeast		9.3		72			
Enbridge Pipelines Inc. - Cromer Terminal	Cromer (49.7333, -101.0810)	559	South		5.7					
Koch Fertilizer Canada, Ulc - Koch Fertilizer Canada, Ulc	Brandon (49.8309, -99.9078)	565	Southeast		6.2	51	764	1,730		
Lafarge North America - Lafarge Canada Inc., Greater Winnipeg, Stonewall Quarry	Stonewall (50.1546, -97.2709)	600	Southeast		6.2					
Maple Leaf Consumer Foods Inc. - Maple Leaf Foods – Brandon	Brandon (49.8321, -99.8549)	566	Southeast		3.3		20	6.0		
Diageo Canada Inc. - Gimli Plant	Gimli (50.6550, -97.0026)	563	Southeast		1.5		49			
Viterra Inc. - Brandon	Brandon (49.9786, -101.1241)	564	Southeast		0.297			0.752		
Viterra Inc. - Souris East (Au)	Souris (49.6211, -100.2575)	582	Southeast		0.731					
Richardson Pioneer Ltd. - Dundonald	Westbourne (50.1297, -98.5811)	562	Southeast					0.028		
Richardson Pioneer Ltd. - Grand Plains	Grandview (51.1546,-100.4920)	407	Southeast					0.125		
Lehigh Hanson Materials Ltd. - Glacier Quarry	RM of Rockwood (50N, 96W)	591	Southeast		0.655					
Erco Worldwide, A Division Of Superior Plus Lp - Hargrave	Virden (49.8537, -100.9258)	544	Southeast		0.588		1.0			
Enerplus Corporation - Kirkella Oil Battery 07-10	^c NA (49.9785,-101.3577)	550	Southeast		0.489	26				
Transcanada Pipelines Ltd. - Station 30 – Rapid city	Rapid city (50.0755,-99.9988)	531	Southeast				23			
Total					21	1,386	126,075	2,094	1866	1.5

Note:

- ^aThe geographic coordinates (latitude and longitude) of each facility was obtained from the facility information on NPRI
- ^bThe distances of each point source facility to the monitoring station were calculated using distance calculator with coordinate <https://gps-coordinates.org/distance-between-coordinates.php>

Table B3: Point sources of Hg and other pollutants reported in Saskatchewan in 2010

Facility	Location (^a Lat, Long)	^b Distance between coordinates (km)	Direction	Hg (kg)	PM _{2.5} (tonnes)	SO ₂ (tonnes)	NO ₂ (tonnes)	NH ₃ (tonnes)	Zn (tonnes)
Saskatchewan Power Corporation - Boundary Dam Power Station	Estevan (49.0961,-103.0305)	635	Southwest	255	97	43,585	17,873		
Saskatchewan Power Corporation - Poplar River Power Station	Coronach (49.0472,-105.4883)	681	Southwest	240	147	43,141	15,962		
Saskatchewan Power Corporation - Shand Power Station	Estevan (49.0879,-102.8640)	632	Southwest	105	18	9,819	4,339		
Transalta Generation Partnership - Meridian Cogeneration Plant	Lloydminster (53.2593,-109.9512)	543	Southwest				736		
Nal Resources Management - Nottingham Gas Plant 07-17-005-32-W1	Nottingham (49.3837,-102.2809)	559	Southwest			4,064	189		
Arc Resources - Lougheed Sour Gas Plant 11-12	n/a (49.4601,-103.9032)	526	Southwest			2,317			
Husky Oil Operations Limited - Lloydminster Upgrader	Lloydminster (53.2630,-109.9489)	548	Southwest			1,926	622		
Cenovus Energy Inc. - Weyburn Oil Battery	N/A (49.4711,-103.7061)	542	Southwest			1,493	33		
Canadian Natural Resources Limited - North Tangleflags In-Situ Oilsands Facility	N/A (53.5051,-109.5716)	532	Southwest			672	107		
BP Canada Energy Company - Glen Ewen Gas Plant	Estevan (49.2055,-102.0425)	532	Southwest			597			
Canadian Natural Resources Limited - Senlac	N/A (52.4037,-109.7189)	521	Southwest			415			
Nal Resources Management - Weyburn Unit 04-11-007-13-W2	Weyburn (49.5401,-103.6734)	532	Southwest			382			
Enerplus Corporation - Colgate Oil Battery 04-24	n/a (49.3936,-103.9093)	534	Southwest			298			
Petrobank Energy And Resources Ltd. - Kerrobert Project	Kerrobert (51.8261,-109.2780)	523	Southwest			149	112		
Rife Resources Ltd. - Lashburn 1-24	Lashburn	563	Southwest				539		

	(53.1469,-109.6715)								
Nexen Inc. - Hatton 01-16	Medicine Hat (50.0786, -109.9043)	543	Southwest		0.470		301		
Canadian Natural Resources Limited - Horsham Medicine Hat Syst	n/a (50.3108, -109.9244)	547	Southwest		1.1		270		
Transgas Limited - Hatton	Maple Creek (49.8994,-109.4758)	532	Southwest				1,000		
Transcanada Pipelines Ltd. - Station 2 - Burstall	Na (50.6784, -109.9780)	530	Southwest		3.5		302		
Foothills Pipe Lines Ltd. - Monchy	Na (49.0036, -107.5467)	572	Southwest		1.7		288		
Transgas Limited - Success	Swift Current (50.1461, -108.0266)	529	Southwest				440		
Cameco - Key Lake Operation	Saskatoon (57.2122,-105.6788)	564	Southwest			145	114		0.003
Cameco - Mcarthur River	Saskatoon (57.7622, -105.0500)	534	Southwest		79		276	41	
Doepker Industries Ltd. - Head Office / Main Plant	Annahaem (52.3209,-104.8186)	549	Southwest	0.093		0.005	22		15
Doepker Industries Ltd. - Moose Jaw Branch - Caribou St.	Moose Jaw (50.3968,-105.5909)	540	Southwest	0.063		0.003	117		8.8
Consumers' Co-Operative Refineries Limited - Co-Op Refinery Complex	Regina (50.4843,-104.5794)	510	Southwest	25		1,511	1,199	14	
Moose Jaw Refinery Partnership - Moose Jaw Refinery	Moose Jaw (50.3884,-105.5196)	536	Southwest			417			
Prairie Mines & Royalty Ltd - Beinfait Mine - Char Plant	Estevan (49.1418,-103.0019)	523	Southwest			671	221		
Meadow Lake Mechanical Pulp - Meadow Lake Mechanical Pulp	Meadow Lake (54.1569,-108.2857)	557	Southwest			6.3	169		
Yara Belle Plaine Inc. - Yara Belle Plaine Inc.	Belle Plaine (50.4333, -105.1833)	514	Southwest				496	677	
City Of Saskatoon - Wastewater Treatment Plant	Saskatoon (52.1827,-106.6060)	534	Southwest				521	69	
Mosaic Canada Ulc - Mosaic Potash Belle Plaine	Belle Plaine (50.4287,-105.1984)	542	Southwest				1,200		

BP Canada Energy Company - Steelman Gas Plant	Estevan (49.3164,-102.6244)	532	Southwest			4,421			
EvrzInc Na Canada - EvrazInc Na Canada - Regina Facilities	Regina (50.5176,-104.6301)	515	Southwest	121		197	314		4.7
Total				746	251	47,477	47,788	801	29

Note: ^aThe geographic coordinates (latitude and longitude) of each facility was obtained from the facility information page on NPRI

^bThe straight line distance and direction between each facility and the monitoring location (Flin Flon) were calculated by typing the location of the facility into an online distance calculator available on https://distancecalculator.globefeed.com/Canada_Distance_Calculator.asp?state=03

Table B4: Point sources of Hg and other pollutants in Saskatchewan in 2011

Facility	Location (*Lat, Long)	^b Distance between coordinates	Direction	Hg (kg)	PM _{2.5} (tonnes)	SO ₂ (tonnes)	NO ₂ (tonnes)	NH ₃ (tonnes)	Zn (tonnes)
Saskatchewan Power Corporation - Boundary Dam Power Station	Estevan (49.0961,-103.0305)	635	Southwest	245	66	42,662	16,354		
Saskatchewan Power Corporation - Poplar River Power Station	Coronach (49.0472,-105.4883)	681	Southwest	208	151	39,006	14,369		
Saskatchewan Power Corporation - Queen Elizabeth Power Station	Saskatoon (52.0944, -106.7050)	437	Southwest				381		
Atco Power Canada Ltd. - Cory Cogeneration Station	Saskatoon (52.0919, -106.8475)	444	Southwest				329		
Transalta Generation Partnership - Meridian Cogeneration Plant	Lloydminster (53.2593,-109.9512)	554	Southwest				736		
BP Canada Energy Company - Steelman Gas Plant	Estevan (49.3164,-102.6244)	608	Southwest			4,421			
Nal Resources Management - Nottingham Gas Plant 07-17-005-32-W1	Nottingham (49.3837,-102.2809)	599	Southwest			4,064	189		
Arc Resources - Lougheed Sour Gas Plant 11-12	n/a (49.4601,-103.9032)	606	Southwest			2,317			
Husky Oil Operations Limited - Lloydminster Upgrader	Lloydminster (53.2630,-109.9489)	554	Southwest			1,926	622		
Cenovus Energy Inc. - Weyburn Oil Battery	N/A (49.4711,-103.7061)	602	Southwest			1,493	33		
Canadian Natural Resources Limited - North Tangleflags In-Situ Oilsands Facility	N/A (53.5051,-109.5716)	521	Southwest			672	107		
BP Canada Energy Company - Glen Ewen Gas Plant	Estevan (49.2055,-102.0425)	619	Southwest			597			
Atco Midstream Ltd. - Kisbey	Kisbey (49.6446,-102.7034)	572	Southwest			522	26		
Canadian Natural Resources Limited - Senlac	N/A (52.4037,-109.7189)	581	Southwest			415			
Nal Resources Management - Weyburn Unit 04-11-007-13-W2	Weyburn (49.5401,-103.6734)	594	Southwest			382			
Enerplus Corporation - Colgate Oil Battery 04-24	n/a (49.3936,-103.9093)	613	Southwest			298			
Petrobank Energy And Resources	Kerrobert	591	Southwest			149	112		

Ltd. - Kerrobert Project	(51.8261,-109.2780)								
Enerplus Corporation - Heward Oil Battery 13-14	n/a (49.7392,-103.1326)	566	Southwest			130			
Enerplus Corporation - Weyburn Oil Battery 01-22	n/a (49.4819,-103.8020)	602	Southwest			128			
Husky Oil Operations Limited - Bolney Thermal	Lloydminster (53.5270, -109.3568)	507	Southwest				254		
Pengrowth Energy Corporation - Cactus Lake - North (16-19-36-28 W3)	Na (52.1121, -109.9903)	614	Southwest				216		
Rife Resources Ltd. - Lashburn 1-24	Lashburn (53.1469,-109.6715)	542	Southwest				539		
EvrazInc Na Canada - EvrazInc Na Canada - Regina Facilities	Regina (50.5176,-104.6301)	508	Southwest	108	53	176	964		4.7
Cameco - Mcarthur River	Saskatoon (57.7622, -105.0500)	386	Southwest		79		276	41	
Transgas Limited - Coleville	Coleville (51.7114, -109.2455)	597	Southwest				230		
Transgas Limited - Beacon Hill	Pierceland (54.3415, -109.7805)	513	Southwest				210		
Consumers' Co-Operative Refineries Limited - Co-Op Refinery Complex	Regina (50.4843,-104.5794)	510	Southwest	24	82	1,511	1,199	14	
Prairie Mines & Royalty Ltd - Beinfait Mine - Char Plant	Estevan (49.1418,-103.0019)	630	Southwest			671	221		
Cameco - Key Lake Operation	Saskatoon (57.2122,-105.6788)	360	Southwest			145	114		0.003
Meadow Lake Mechanical Pulp - Meadow Lake Mechanical Pulp	Meadow Lake (54.1569,-108.2857)	420	Southwest			6.3	169		
Mosaic Canada Ulc - Mosaic Potash Belle Plaine	Belle Plaine (50.4287,-105.1984)	532	Southwest				1,200		
City Of Saskatoon - Wastewater Treatment Plant	Saskatoon (52.1827,-106.6060)	425	Southwest				521	69	
Yara Belle Plaine Inc. - Yara Belle Plaine Inc.	Belle Plaine (50.4333, -105.1833)	531	Southwest				496	677	
Total				585	270	102,146	40,191	801	29

Note:

^aThe geographic coordinates (latitude and longitude) of each facility was obtained from the facility information page on NPRI

^bThe straight line distance and directions of the facilities with no reported located were calculated by supplying the name of the facility on the online distance calculator available on https://distancecalculator.globefeed.com/Canada_Distance_Calculator.asp?state=03

Appendix C: List of outputs from Principal Component Analysis (PCA)

Table C: List of PCA outputs categorized as ‘used’ and ‘unused’

Output	Definition	Used/Not used
Correlation matrix	Matrix of correlation coefficients between variables	Not used
KMO and Bartlett’s test	Test of suitability of the dataset for analysis in PCA	Used
Communalities	Proportion of variance in variable measurements accounted for	Used
Total variance explained	The cumulative percentage of variance explained by all components	Used
Scree plot	The line used to select the number of components to retain	Not used
Eigenvalue	Determines the magnitude of directions of new feature space	Used
Factor loadings	Correlation coefficient between variable and component	Used
Component matrix	Estimates of correlation between each variable and the estimated component before rotation	Not used
Rotated component matrix	Estimates of correlations between each of the variables and the estimated components after rotation	Used
Principal component scores	The transformed variable values corresponding to a particular data point	Not used

Appendix D: Correlations between air pollutants

Table D1: Correlations between variables before imputation (Absolute value significant in bold)

	GEM	GOM	PBM	PM _{2.5}	Al	Si	K	Fe	Zn	SO ₄ ²⁻	NO ₃ ⁻	Ca ²⁺	Cl ⁻	Na ⁺	NH ₄ ⁺	Mg ²⁺	K ⁺	Oxalate	SO ₂	Temp	RH	Preci	WS	
GEM		0.58	0.47	0.49	0.03	0.01	0.13	0.12	0.05	0.36	0.17	0.01	0.21	0.04	0.33	0.16	0.02	0.20	0.13	0.52	0.37	0.20	0.27	
GOM			0.61	0.62	0.32	0.29	0.45	0.20	0.11	0.03	0.43	0.23	0.27	0.42	0.01	0.64	0.69	0.69	0.06	0.48	0.48	0.03	0.12	
PBM				0.26	0.26	0.26	0.38	0.15	0.03	0.11	0.83	0.63	0.62	0.85	0.10	0.79	0.80	0.49	0.09	0.16	0.36	0.02	0.09	
PM _{2.5}					0.26	0.21	0.49	0.35	0.26	0.74	0.32	0.45	0.40	0.36	0.72	0.50	0.38	0.68	0.19	0.11	0.27	0.19	0.04	
Al						0.87	0.81	0.67	0.07	0.08	0.40	0.35	0.27	0.46	0.12	0.63	0.44	0.60	0.09	0.29	0.07	0.16	0.15	
Si							0.84	0.82	0.05	0.05	0.23	0.39	0.17	0.22	0.05	0.46	0.23	0.41	0.01	0.12	0.02	0.15	0.35	
K								0.62	0.08	0.04	0.62	0.36	0.25	0.53	0.01	0.68	0.65	0.53	0.09	0.10	0.10	0.19	0.27	
Fe									0.26	0.18	0.04	0.38	0.13	0.01	0.16	0.21	0.05	0.35	0.20	0.00	0.10	0.18	0.23	
Zn										0.40	0.05	0.57	0.50	0.03	0.31	0.03	0.14	0.01	0.23	0.22	0.11	0.11	0.32	
SO ₄ ²⁻											0.05	0.01	0.16	0.11	0.99	0.18	0.17	0.61	0.70	0.08	0.15	0.14	0.36	
NO ₃ ⁻												0.31	0.53	0.03	0.03	0.80	0.83	0.42	0.25	0.54	0.21	0.22	0.12	
Ca ²⁺													0.42	0.21	0.03	0.29	0.15	0.19	0.03	0.18	0.03	0.20	0.26	
Cl ⁻														0.72	0.11	0.68	0.19	0.31	0.06	0.37	0.10	0.18	0.08	
Na ⁺															0.13	0.91	0.65	0.49	0.14	0.50	0.14	0.19	0.22	
NH ₄ ⁺																0.20	0.23	0.66	0.64	0.07	0.15	0.15	0.31	
Mg ²⁺																	0.65	0.65	0.01	0.39	0.22	0.23	0.13	
K ⁺																			0.61	0.10	0.38	0.27	0.20	0.04
Oxalate																			0.20	0.07	0.30	0.28	0.04	
SO ₂																				0.08	0.06	0.28	0.16	
Temp																					0.43	0.25	0.01	
RH																							0.14	0.10
Precip																								0.01
WS																								

Table D2: Correlation between variables in the input data set after imputation (N = 81)

	GEM	GOM	PBM	PM _{2.5}	Al	Br	Fe	K	Si	Zn	NH ₄ ⁺	Ca ²⁺	Cl ⁻	Mg ²⁺	NO ₃ ⁻	Oxal	K ⁺	Na ⁺	SO ₄ ²⁻	SO ₂	Temp	RH	WS
GOM	0.62																						
PBM	0.46	0.58																					
PM _{2.5}	0.02	0.17	0.05																				
Al	0.04	0.22	0.12	0.57																			
Br	0.03	0.17	0.22	0.25*	0.33*																		
Fe	0.05	0.11	0.06	0.71	0.76	0.08																	
K	0.18	0.14	0.30*	0.56	0.91	0.40	0.68																
Si	0.04	0.19	0.11	0.57	0.97	0.30	0.82	0.92															
Zn	-0.03	-0.09	-0.07	0.60	-0.06	0.06	0.27	-0.04	-0.04														
NH ₄ ⁺	-0.10	-0.04	-0.17	0.48	-0.00	-0.08	0.19	-0.10	-0.02	0.35													
Ca ²⁺	0.42	0.54	0.97	0.09	0.09	0.26*	0.07	0.27*	0.10	0.04	-0.20												
Cl ⁻	0.40	0.53	0.94	0.15	0.12	0.24*	0.10	0.29*	0.11	0.10	-0.11	0.96											
Mg ²⁺	0.43	0.58	0.98	0.12	0.20	0.22	0.13	0.37	0.20	-0.08	-0.14	0.95	0.95										
NO ₃ ⁻	0.44	0.56	0.98	0.06	0.14	0.24*	0.08	0.33	0.15	-0.06	-0.26*	0.97	0.95	0.98									
Oxal	0.41	0.59	0.93	0.19	0.20	0.19	0.18	0.34	0.20	-0.06	0.09	0.89	0.91	0.95	0.90								
K ⁺	0.44	0.59	0.98	0.08	0.18	0.22*	0.11	0.37	0.19	-0.13	-0.17	0.95	0.94	0.99	0.98	0.95							
Na ⁺	0.43	0.56	0.97	0.08	0.16	0.24*	0.08	0.35	0.16	-0.08	-0.21	0.96	0.96	0.99	0.99	0.91	0.98						
SO ₄ ²⁻	-0.14	-0.10	-0.26	0.49	-0.02	-0.09	0.18	-0.13	-0.03	0.41	0.99	-0.28*	-0.17	-0.22	-0.34	-0.01	-0.27 ^b	-0.28*					
SO ₂	-0.20	-0.06	-0.08	0.50	0.02	-0.16	0.21	-0.06	0.03	0.34	0.69	-0.05	0.03	-0.03	-0.11	0.08	-0.07	-0.07	0.70				
Temp	0.51	0.67	0.29*	0.01	0.06	-0.25*	0.11	0.09	0.08	-0.16	0.16	0.23*	0.23*	0.29*	0.23*	0.37	0.29*	0.24*	0.11	0.07			
RH	-0.16	-0.54	-0.33*	-0.43	-0.48	-0.22	-0.50	-0.50	-0.50	-0.20	-0.12	-0.31*	-0.37	-0.38	-0.32	-0.41	-0.36	-0.35	-0.09	-0.15	-0.33*		
WS	-0.34	-0.20	-0.12	-0.12	-0.30*	-0.15	-0.19	-0.30*	-0.28*	0.12	0.24*	-0.13	-0.09	-0.10	-0.14	-0.05	-0.15	-0.15	0.26*	0.23*	0.10	0.06	
Precip	-0.09	-0.15	-0.13	-0.23*	-0.17	0.80	-0.25*	-0.17	-0.19	-0.14	0.02	-0.15	-0.18	-0.15	-0.15	-0.16	-0.16	-0.14	0.03	-0.07	0.01	0.14	0.11

Numbers in bold are significant at p<0.01

Number asterisked are significant at p-value <0.05

Appendix E: Calculated values of Q and IM&IS from scaled residuals

Table E1: Table of Q values

Number of factors	Qrobust	Qtrue
3	7037.09	11351.3
4	5337.95	7835.88
5	3098.69	3634.36
6	2185.2	2390.44
7	1577.53	1708.03
8	1190.19	1294.45
9	951.81	1010.5

Table E2: Table of IM and IS values

Number of factors	IM	IS
3	4.180	4.980
4	4.139	4.866
5	0.644	2.346
6	0.436	1.819
7	0.207	1.608
8	0.147	1.373
9	0.107	1.318

Appendix F: Time series graphs of air pollutants

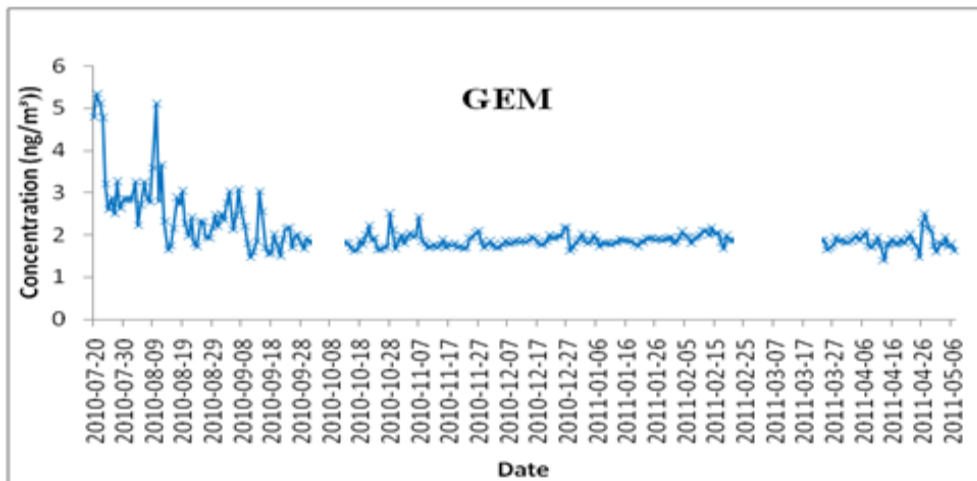


Figure F1: Time series plot of GEM with date from July 2010 – May 2011

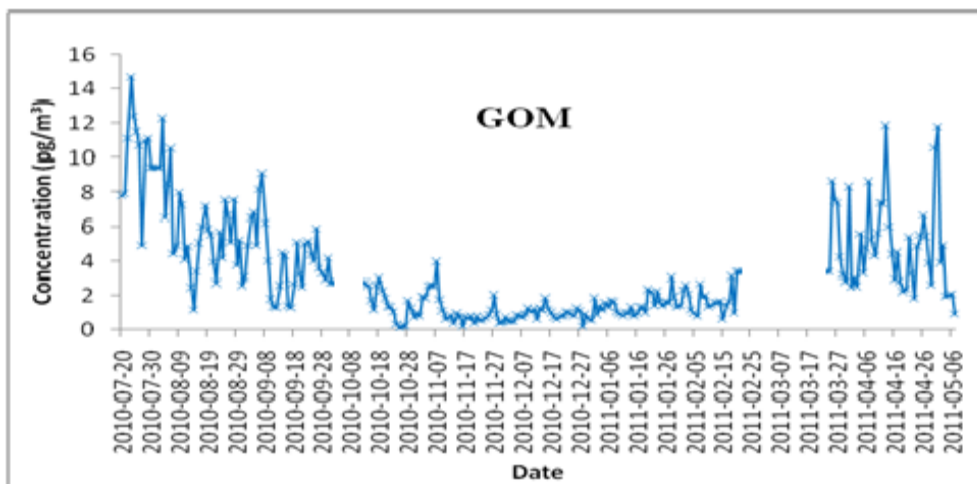


Figure F2: Time series plot of GOM with date from July 2010 – May 2011

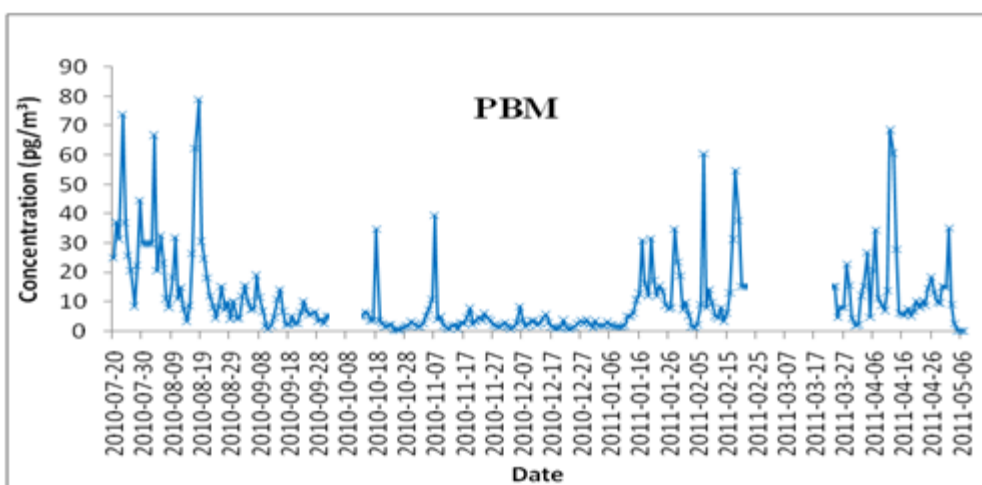


Figure F3: Time series plot of PBM with date from July 2010 – May 2011

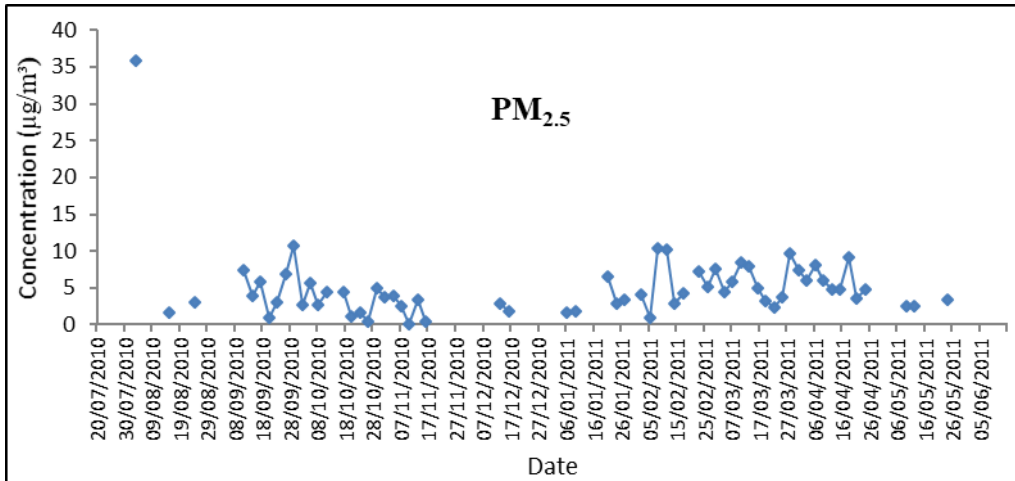


Figure F4: Time series plot of PM_{2.5} mass with date from July 2010 – May 2011

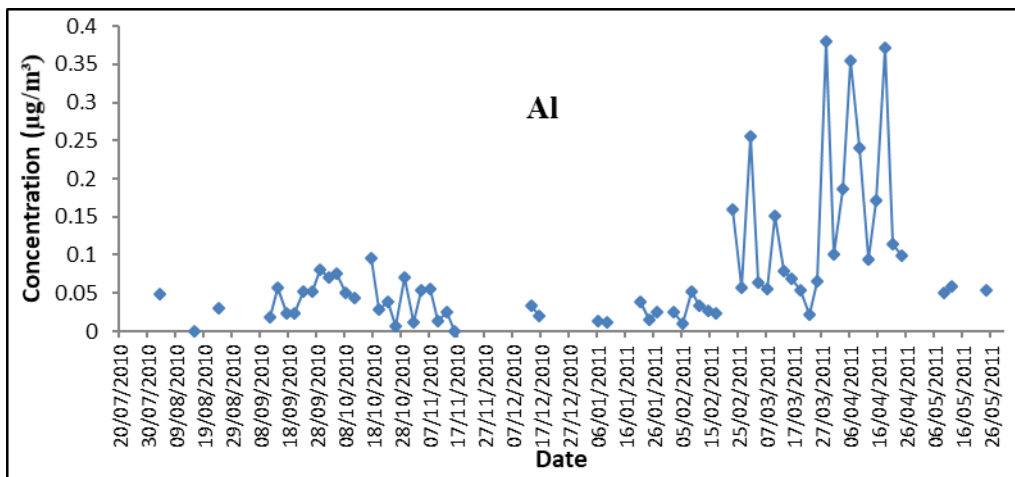


Figure F5: Time series plot of Al with date from July 2010 – May 2011

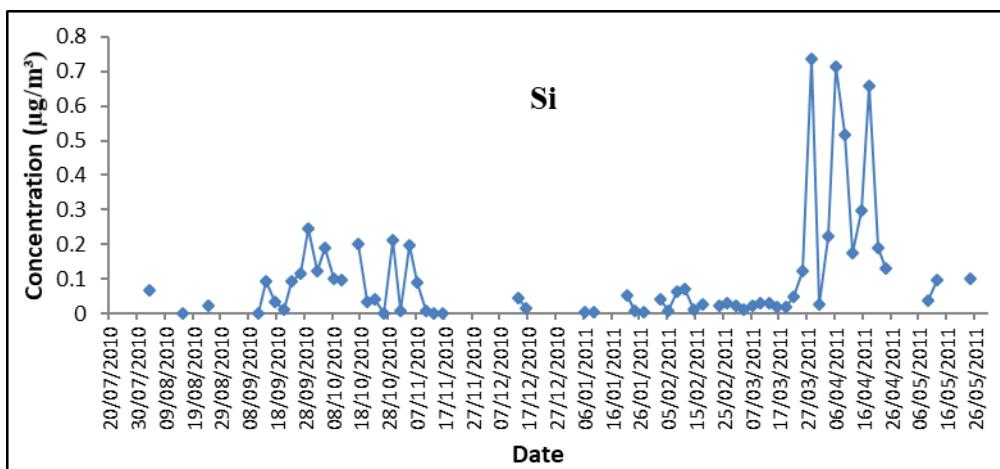


Figure F6: Time series plot of Si with date from July 2010 – May 2011

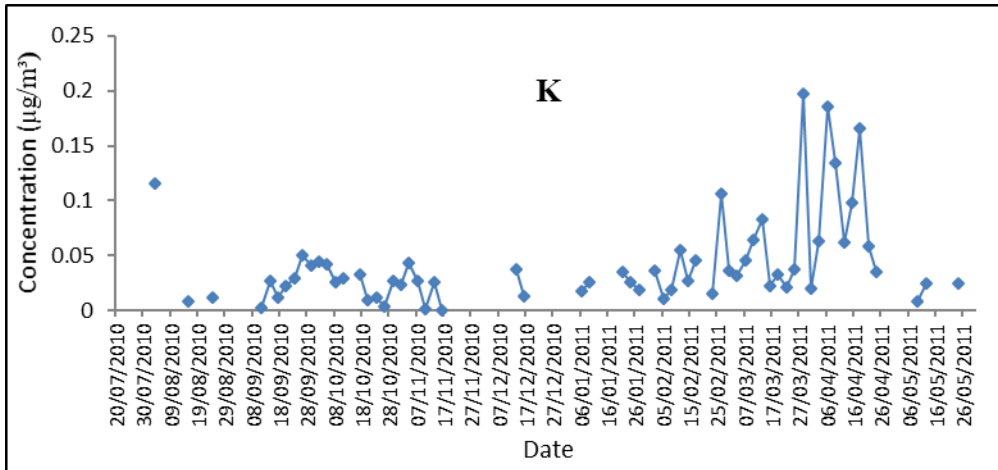


Figure F7: Time series plot of K with date from July 2010 – May 2011

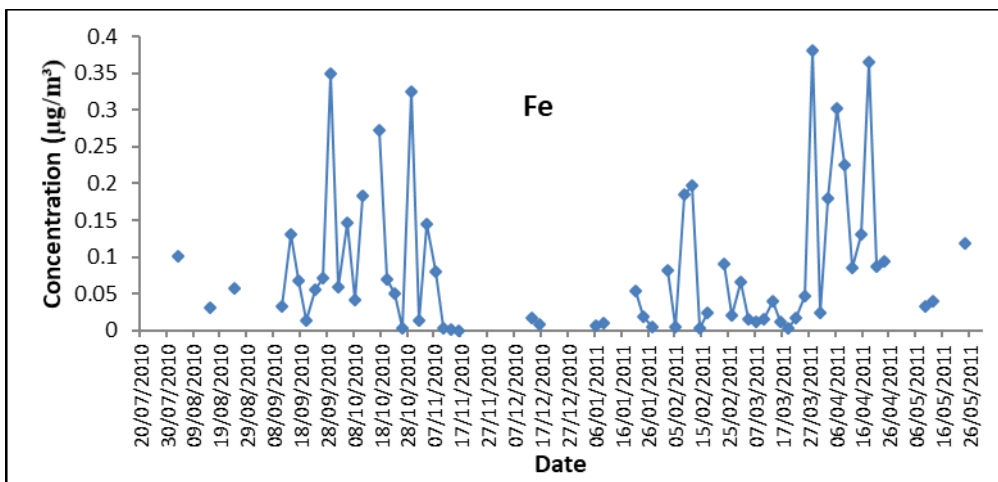


Figure F8: Time series plot of Fe with date from July 2010 – May 2011

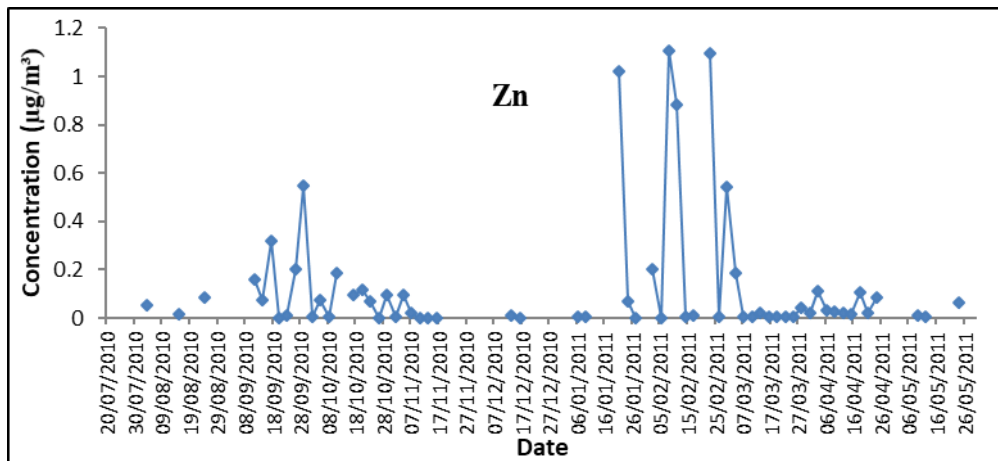


Figure F9: Time series plot of Zn with date from July 2010 – May 2011

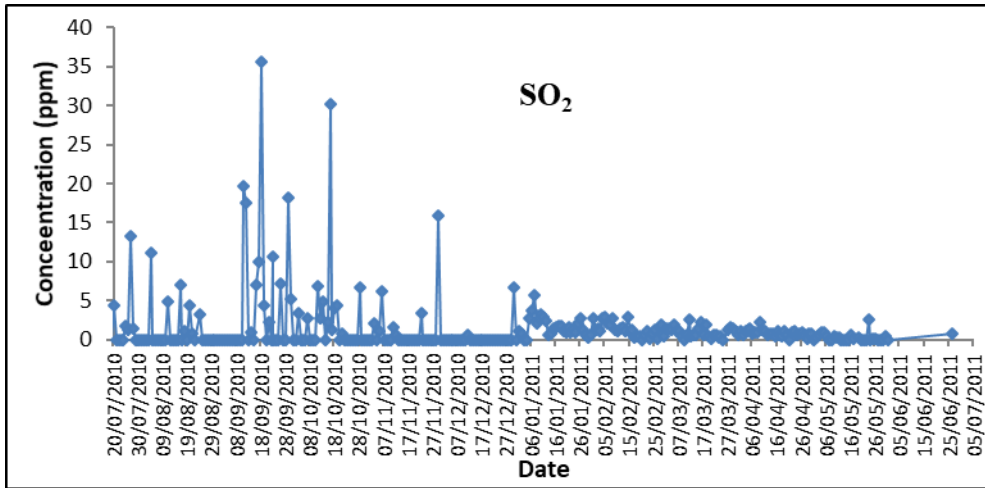


Figure F10: Time series plot of SO₂ with date from July 2010 – May 2011

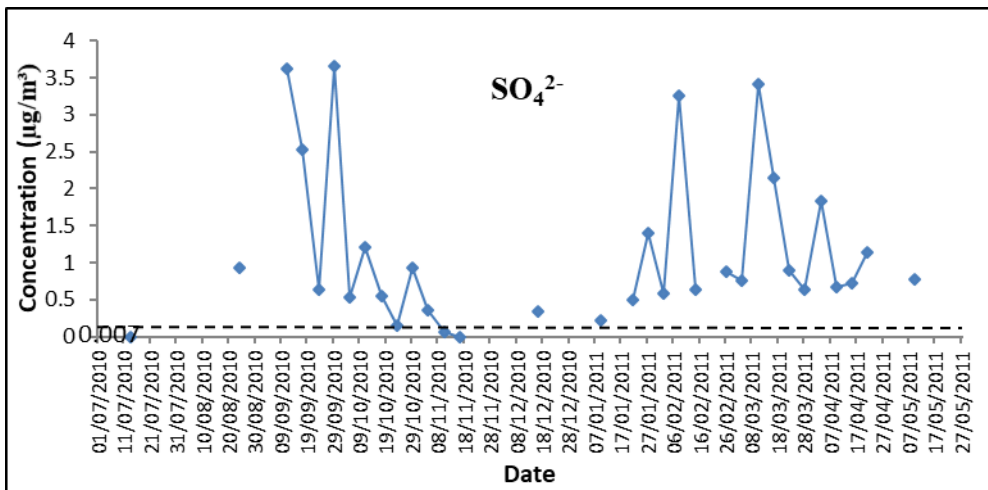


Figure F11: Time series plot of SO₄²⁻ with date from July 2010 – May 2011

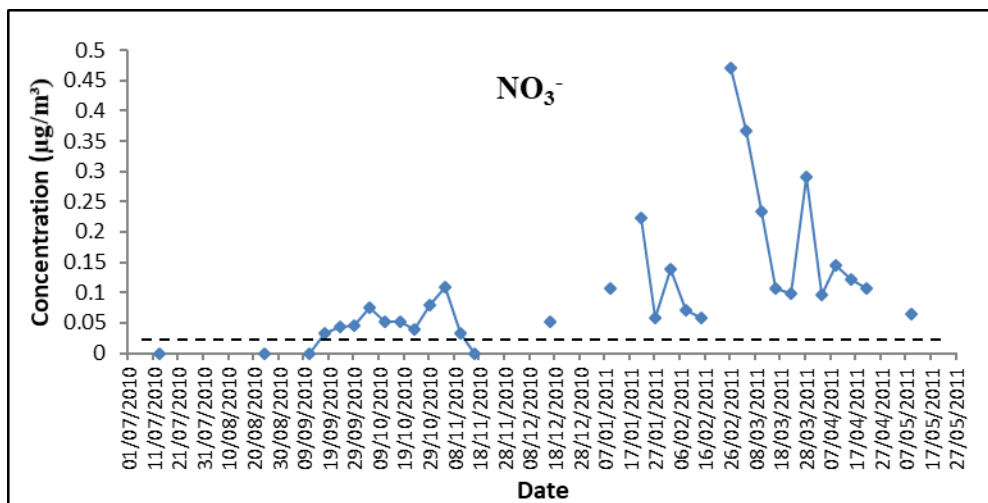


Figure F12: Time series plot of NO₃⁻ with date from July 2010 – May 2011

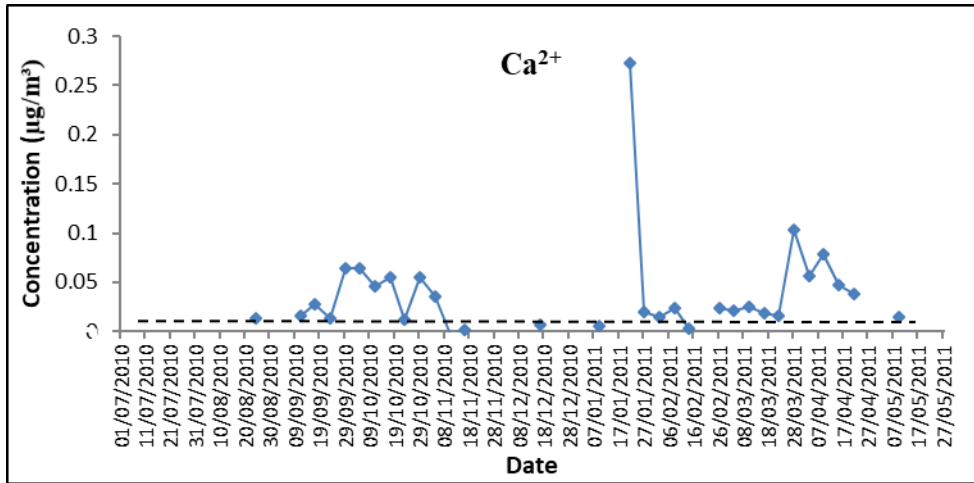


Figure F13: Time series plot of Ca²⁺ with date from July 2010 – May 2011

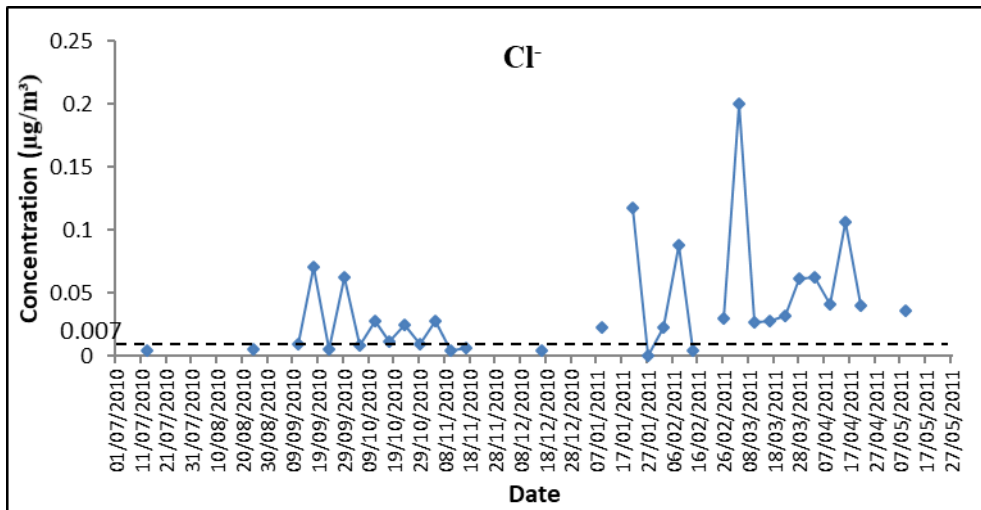


Figure F14: Time series plot of Cl⁻ with date from July 2010 – May 2011

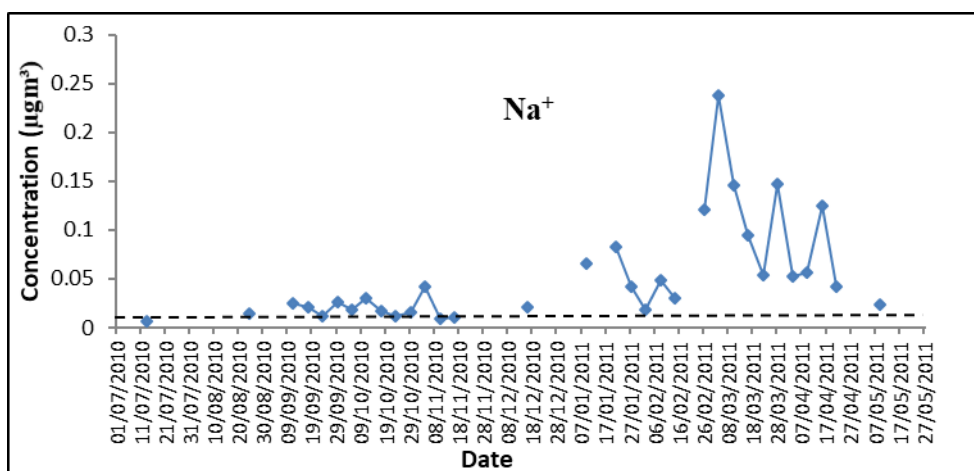


Figure F15: Time series plot of Na⁺ with date from July 2010 – May 2011

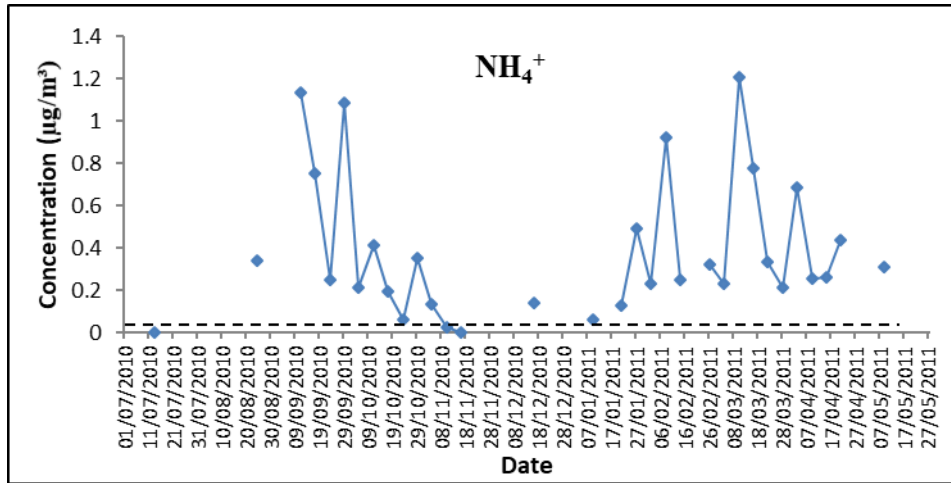


Figure F16: Time series plot of NH₄⁺ with date from July 2010 – May 2011

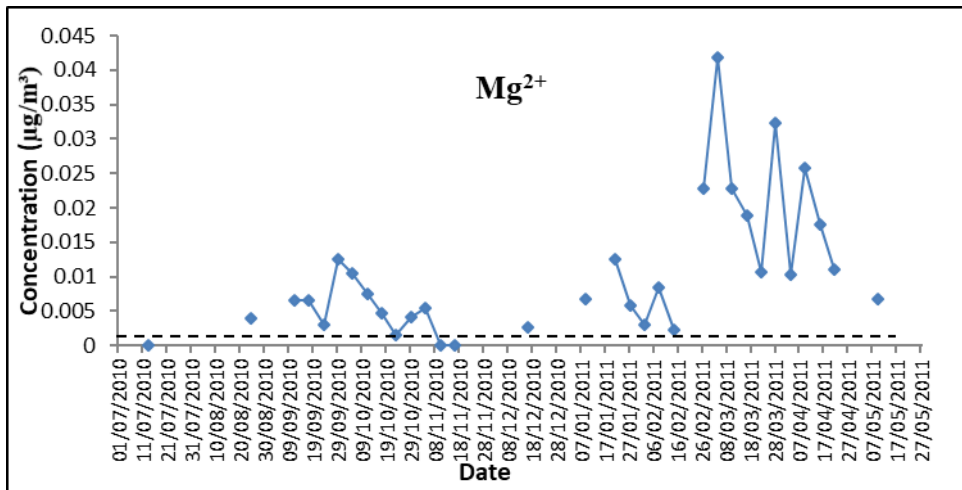


Figure F17: Time series plot of Mg²⁺ with date from July 2010 – May 2011

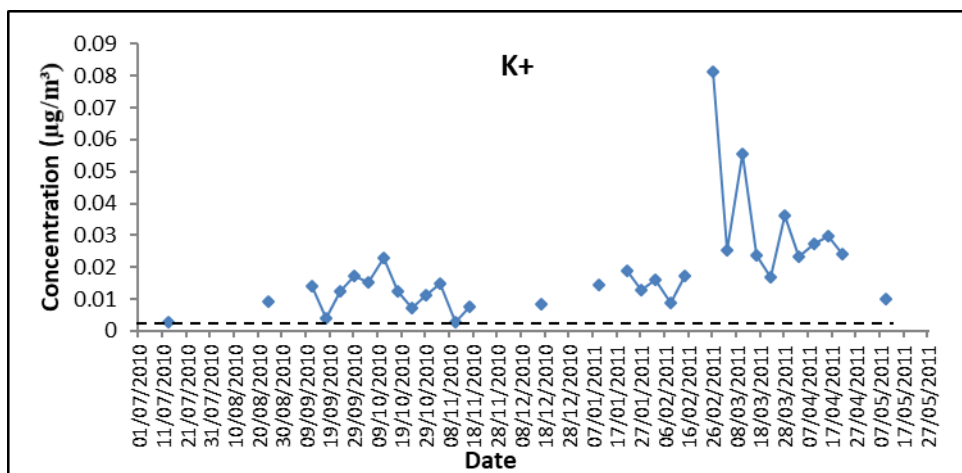


Figure F18: Time series plot of K⁺ with date from July 2010 – May 2011

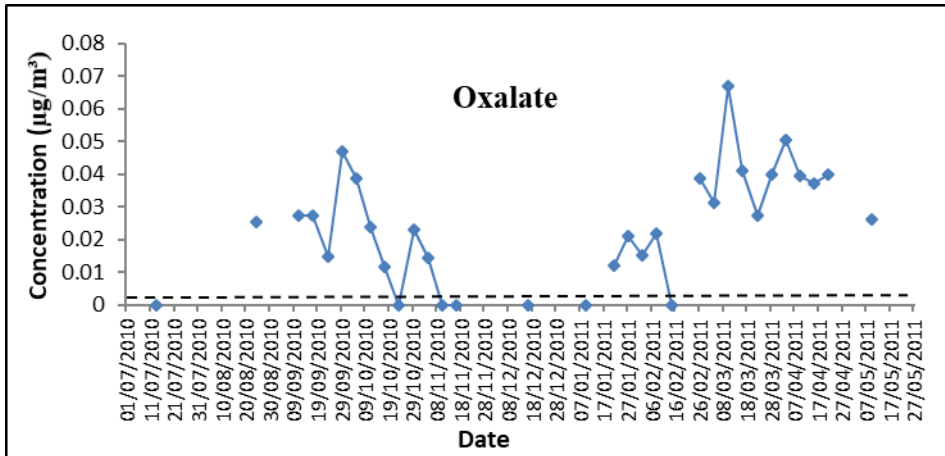


Figure F19: Time series plot of Oxalate with date from July 2010 – May 2011

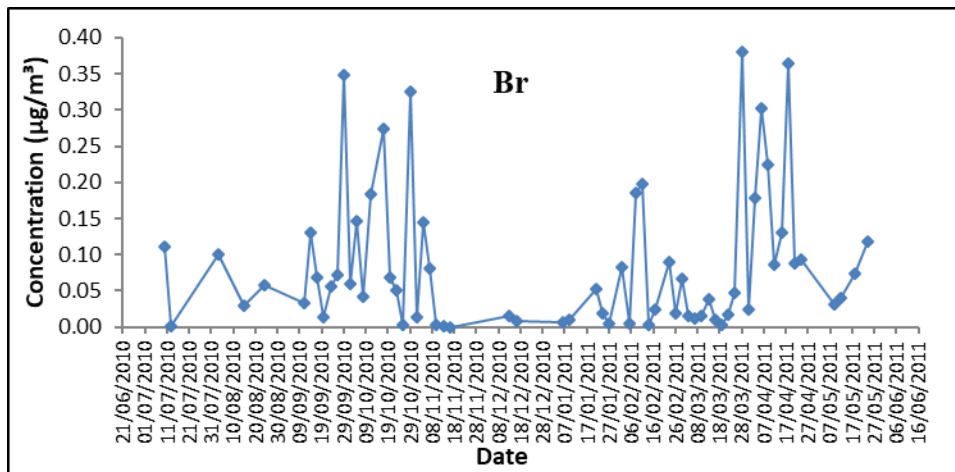


Figure F20: Time series plot of Br with date from July 2010 – May 2011

Appendix G: PMF Outputs

Table G1: Base run summary table for 5-factors

Run #	Q(Robust)	Q(True)	Converged	# Steps	Q(true)/Qexp
1	3099.09	3634.46	Yes	666	3.259605408
2	3098.82	3634.35	Yes	1071	3.259506702
3	3098.96	3634.22	Yes	972	3.259390116
4	3098.69	3634.36	Yes	1370	3.259515762
5	3098.95	3634.41	Yes	1121	3.259560585
6	3098.75	3634.23	Yes	968	3.259399176
7	3098.81	3634.37	Yes	1228	3.259524584
8	3098.97	3634.36	Yes	1189	3.259515762
9	3098.95	3634.3	Yes	1160	3.25946188
10	3098.85	3634.24	Yes	995	3.259407997
11	3098.86	3634.35	Yes	973	3.259506702
12	3098.95	3634.39	Yes	1144	3.259542704
13	3098.86	3634.26	Yes	723	3.259426117
14	3098.98	3634.28	Yes	982	3.259443998
15	3098.96	3634.3	Yes	1153	3.25946188
16	3099	3634.36	Yes	809	3.259515762
17	3098.96	3634.37	Yes	1013	3.259524584
18	3098.93	3634.34	Yes	836	3.259497643
19	3098.83	3634.21	Yes	1045	3.259381056
20	3098.96	3634.3	Yes	887	3.25946188

Table G2: Factor Profiles for 5-factor solution (% of species sum)

	F1	F2	F3	F4	F5
GEM	5	3	75	1	15
GOM	9	0	58	1	31
PBM	4	6	9	1	81
SO ₂	9	2	1	87	0
PM	28	23	37	7	6
Al	77	2	16	2	3
Br	11	0	67	0	22
Fe	54	36	6	0	5
K	71	0	24	0	5
Si	90	6	0	1	3
Zn	0	86	11	3	0
NH ₄ ⁺	0	0	85	12	3
Ca ²⁺	6	7	0	2	85
Cl ⁻	4	12	14	2	69
Mg ²⁺	8	4	13	4	71
NO ₃ ⁻	8	6	10	0	76
Oxalate	8	1	38	6	47
K ⁺	10	0	35	3	52
Na ⁺	5	4	16	2	73
SO ₄ ²⁻	0	1	86	13	0
Factor name	Crustal/soil dust	Industrial	secondary aerosol and re-emission+bromine source	Coal combustion	Road salt + biomass burning

Table G3:Regression diagnostics for 5-factors

Species	Intercept	Slope	SE	r ²	KS Test	
					Stat	P Value
GEM	0.001	0.398	0.001	0.146	0.163	0.027
GOM	0.000	0.336	0.000	0.379	0.139	0.088
PBM	0.000	0.915	0.000	0.981	0.191	0.005
SO ₂	-0.116	1.112	0.463	0.987	0.333	0.000
PM	0.054	0.942	0.994	0.803	0.178	0.012
Al	0.002	0.940	0.012	0.970	0.211	0.001
Br	0.001	0.178	0.000	0.147	0.282	0.000
Fe	0.015	0.746	0.032	0.788	0.217	0.001
K	0.000	0.914	0.012	0.886	0.163	0.027
Si	0.002	0.951	0.017	0.985	0.149	0.055
Zn	0.044	0.492	0.068	0.658	0.346	0.000
NH ₄ ⁺	0.062	0.797	0.033	0.954	0.123	0.171
Ca ²⁺	0.002	0.901	0.019	0.957	0.255	0.000
Cl ⁻	-0.002	0.992	0.014	0.932	0.161	0.030
Mg ²⁺	0.000	0.914	0.002	0.980	0.202	0.003
NO ₃ ⁻	-0.005	1.016	0.022	0.978	0.283	0.000
Oxalate	0.003	0.861	0.005	0.943	0.175	0.014
K ⁺	-0.001	1.003	0.003	0.960	0.193	0.005
Na ⁺	-0.002	0.999	0.013	0.965	0.257	0.000
SO ₄ ²⁻	0.202	0.763	0.113	0.950	0.135	0.106

Table G4: Base run summary for 6-factor solution

Run #	Q(Robust)	Q(True)	Converged	# Steps	Q(true)/Qexp
1	2185.34	2390.34	Yes	2235	2.357337236
2	2185.32	2390.37	Yes	1760	2.3573668
3	2185.45	2390.41	Yes	1103	2.357406378
4	2185.34	2390.27	Yes	1170	2.357268333
5	2185.28	2390.21	Yes	950	2.357208967
6	2185.3	2390.33	Yes	1768	2.357327461
7	2185.33	2390.35	Yes	1577	2.35734725
8	2185.36	2390.36	Yes	2235	2.357357025
9	2185.34	2390.36	Yes	1972	2.357357025
10	2185.32	2390.35	Yes	1367	2.35734725
11	2185.35	2390.35	Yes	1676	2.35734725
12	2185.32	2390.36	Yes	1791	2.357357025
13	2185.34	2390.34	Yes	1409	2.357337236
14	2185.33	2390.29	Yes	980	2.357287884
15	2185.31	2390.27	Yes	1140	2.357268333
16	2185.36	2390.36	Yes	1768	2.357357025
17	2185.2	2390.44	Yes	1983	2.357435942
18	2185.28	2390.23	Yes	1010	2.357228756
19	2185.34	2390.31	Yes	1288	2.357307673
20	2185.3	2390.36	Yes	2281	2.357357025

Table G5: Factor Profiles for 6-factor solution (% of species sum)

	F1	F2	F3	F4	F5	F6
GEM	41	5	0	5	49	0
GOM	36	0	3	20	41	0
PBM	10	3	0	75	13	0
SO ₂	5	1	0	0	5	88
PM	18	22	21	2	29	8
Al	13	4	66	1	16	0
Br	13	0	0	0	87	0
Fe	6	31	52	5	4	2
K	6	0	49	0	44	0
Si	6	7	79	1	7	0
Zn	0	79	4	2	4	11
NH ₄ ⁺	78	11	0	3	0	7
Ca ²⁺	8	4	3	84	0	1
Cl ⁻	5	7	0	57	28	3
Mg ²⁺	13	3	3	67	11	2
NO ₃ ⁻	0	1	2	63	32	1
Oxalate	39	5	6	47	0	2
K ⁺	21	0	5	41	31	1
Na ⁺	7	0	0	59	31	2
SO ₄ ²⁻	79	12	0	0	0	9
Factor name	Secondary aerosol and re-emission	Industrial	Crustal/soil dust	Road salt+ biomass burning	Bromine source	Coal combustion

Table G6: Regression diagnostics for 6-factors

Species	Intercept	Slope	SE	r ²	KS Test	
					Stat	P Value
GEM	0.001	0.521	0.000	0.285	0.130	0.132
GOM	0.000	0.349	0.000	0.440	0.134	0.109
PBM	0.000	0.942	0.000	0.981	0.177	0.013
SO ₂	-0.027	1.029	0.211	0.997	0.340	0.000
PM	0.176	0.927	0.868	0.838	0.161	0.030
Al	0.002	0.941	0.012	0.971	0.203	0.002
Br	0.001	0.276	0.000	0.270	0.283	0.000
Fe	0.011	0.814	0.032	0.823	0.206	0.002
K	0.004	0.846	0.007	0.945	0.137	0.097
Si	-0.001	0.995	0.013	0.992	0.142	0.076
Zn	0.039	0.552	0.067	0.715	0.306	0.000
NH ₄ ⁺	0.013	0.960	0.017	0.992	0.107	0.313
Ca ²⁺	-0.001	0.981	0.023	0.946	0.220	0.001
Cl ⁻	0.000	0.960	0.013	0.938	0.157	0.038
Mg ²⁺	0.000	0.960	0.002	0.980	0.223	0.001
NO ₃ ⁻	-0.001	0.998	0.016	0.988	0.211	0.001
Oxalate	0.001	0.942	0.004	0.958	0.174	0.014
K ⁺	0.000	0.972	0.003	0.971	0.121	0.187
Na ⁺	0.001	0.950	0.010	0.978	0.162	0.029
SO ₄ ²⁻	0.092	0.895	0.077	0.982	0.130	0.130

Table G7: Base run summary for 7-factor solution

Run #	Q(Robust)	Q(True)	Converged	# Steps	Q(true)/Qexp
1	1577.53	1708.04	Yes	2288	1.870799541
2	1577.57	1708.03	Yes	2537	1.870788574
3	1577.61	1708.03	Yes	2065	1.870788574
4	1775.22	1916.98	Yes	1669	2.099649429
5	1577.58	1708	Yes	3168	1.870755792
6	1775.08	1916.94	Yes	1616	2.099605799
7	1775.12	1916.95	Yes	2025	2.099616766
8	1577.53	1708.03	Yes	2592	1.870788574
9	1577.58	1708.01	Yes	1614	1.870766759
10	1577.54	1708.07	Yes	3013	1.870832443
11	1774.27	1918.12	Yes	1090	2.100898027
12	1577.57	1708.03	Yes	2155	1.870788574
13	1775.15	1916.93	Yes	1737	2.099594831
14	1775.09	1916.92	Yes	1794	2.099583864
15	1577.55	1708.03	Yes	2431	1.870788574
16	1577.61	1708.05	Yes	1347	1.870810509
17	1577.57	1708.01	Yes	2846	1.870766759
18	1577.61	1708.01	Yes	1804	1.870766759
19	1577.55	1708.04	Yes	1705	1.870799541
20	1775.05	1916.88	Yes	1663	2.099539995

Table G8: Factor Profiles for 7-factor solution (% of species sum)

	F1	F2	F3	F4	F5	F6	F7
GEM	2	0	1	0	51	2	43
GOM	0	4	17	0	42	0	37
PBM	4	1	75	0	8	3	9
SO ₂	1	0	0	88	4	0	6
PM	13	21	1	8	22	11	25
Al	2	66	0	1	7	12	11
Br	11	14	7	0	45	0	23
Fe	4	35	0	3	1	52	5
K	3	58	0	0	25	3	12
Si	1	74	0	1	0	24	0
Zn	68	1	2	8	2	13	6
NH ₄ ⁺	5	0	3	8	0	1	83
Ca ²⁺	0	0	81	2	0	14	3
Cl ⁻	11	3	57	2	18	0	8
Mg ²⁺	2	5	68	3	6	4	12
NO ₃ ⁻	4	3	60	1	28	4	0
Oxalate	0	4	46	3	1	7	38
K ⁺	0	5	39	2	29	3	22
Na ⁺	4	4	61	2	19	0	10
SO ₄ ²⁻	6	0	0	9	0	0	84
Factor name	Zn source	Crustal/soil dust	Road salt+ biomass burning	Coal combustion	Bromine source	Iron source	secondary aerosol and re-emission

Table G9:Regression diagnostics for 7-factors

Species	Intercept	Slope	SE	r ²	KS Test	
					Stat	P Value
GEM	0.001	0.650	0.000	0.532	0.133	0.113
GOM	0.000	0.353	0.000	0.479	0.138	0.090
PBM	0.000	0.952	0.000	0.983	0.191	0.005
SO ₂	-0.037	1.036	0.145	0.998	0.330	0.000
PM	0.268	0.909	0.854	0.837	0.143	0.074
Al	0.001	0.965	0.012	0.970	0.180	0.010
Br	0.001	0.221	0.000	0.216	0.258	0.000
Fe	0.003	0.955	0.007	0.992	0.171	0.017
K	0.001	0.942	0.009	0.927	0.194	0.005
Si	0.000	0.984	0.011	0.994	0.168	0.021
Zn	0.003	0.961	0.031	0.973	0.235	0.000
NH ₄ ⁺	0.002	0.994	0.013	0.995	0.131	0.123
Ca ²⁺	0.000	0.964	0.023	0.944	0.200	0.003
Cl ⁻	0.000	0.988	0.011	0.957	0.169	0.019
Mg ²⁺	0.000	0.978	0.002	0.983	0.239	0.000
NO ₃ ⁻	0.002	0.976	0.014	0.990	0.156	0.038
Oxalate	0.001	0.950	0.004	0.960	0.222	0.001
K ⁺	0.001	0.951	0.002	0.977	0.137	0.094
Na ⁺	0.000	0.977	0.009	0.979	0.212	0.001
SO ₄ ²⁻	0.048	0.946	0.052	0.993	0.162	0.029

Appendix H: PCA Outputs

Table H1: Varimax rotated factor loadings with data set (5 factors)

	PC1	PC2	PC3	PC4	PC5	Commu
GEM	0.31	0.00	-0.10	0.88	0.01	0.88
GOM	0.48	0.17	-0.02	0.71	-0.04	0.77
PBM	0.97	0.04	-0.09	0.16	0.02	0.98
PM _{2.5}	0.05	0.62	0.53	0.07	0.49	0.91
Al	0.07	0.97	-0.04	0.01	-0.01	0.96
Br	0.19	0.28	-0.27	-0.06	0.56	0.51
Fe	0.02	0.84	0.24	0.04	0.12	0.78
K	0.24	0.92	-0.13	0.10	0.07	0.93
Si	0.07	0.99	-0.03	0.00	-0.01	0.98
Zn	-0.06	-0.04	0.42	0.02	0.81	0.84
NH ₄ ⁺	-0.11	0.01	0.93	0.04	0.03	0.89
Ca ²⁺	0.96	0.02	-0.10	0.12	0.13	0.97
Cl ⁻	0.96	0.04	0.00	0.11	0.15	0.96
Mg ²⁺	0.98	0.13	-0.05	0.13	-0.02	0.99
NO ₃ ⁻	0.97	0.07	-0.16	0.12	0.05	0.99
Oxalate	0.94	0.13	0.14	0.16	-0.07	0.95
K ⁺	0.97	0.12	-0.10	0.14	-0.04	0.99
Na ⁺	0.97	0.09	-0.12	0.12	0.02	0.98
SO ₄ ²⁻	-0.20	0.00	0.93	0.01	0.08	0.91
SO ₂	0.04	0.05	0.85	-0.18	0.02	0.77
Eigenvalue	7.9	4.0	3.2	1.5	1.3	
% Var. Exp	39.7	20.1	15.9	7.4	6.5	
Commu (%)	39.7	60.0	75.7	83.1	89.5	
Factor name	Road salt + Biomass burning	Crustal/ soil dust	Coal combustion + agriculture	Long-range transport of Hg	Industrial	
Extraction Method: Principal Component Analysis.						
Rotation Method: Varimax with Kaiser Normalization.						
a. Rotation converged in 5 iterations.						

Table H2: Varimax rotated factor loadings with data set (6 factors)

	PC1	PC2	PC3	PC4	PC5	PC6	Commu
GEM	0.32	0.01	-0.12	0.87	0.06	-0.07	0.88
GOM	0.48	0.15	0.03	0.73	-0.11	0.09	0.80
PBM	0.97	0.04	-0.08	0.16	-0.02	0.05	0.98
PM _{2.5}	0.06	0.63	0.47	0.05	0.52	0.12	0.92
Al	0.06	0.96	-0.01	0.02	-0.10	0.14	0.96
Br	0.17	0.21	-0.09	0.00	0.06	0.95	0.97
Fe	0.04	0.87	0.15	0.01	0.26	-0.17	0.88
K	0.23	0.90	-0.09	0.11	-0.05	0.20	0.93
Si	0.07	0.98	-0.02	0.00	-0.06	0.07	0.98
Zn	-0.03	0.01	0.27	-0.02	0.94	0.04	0.97
NH ₄ ⁺	-0.12	0.00	0.97	0.05	0.06	0.02	0.95
Ca ²⁺	0.96	0.02	-0.12	0.11	0.10	0.07	0.97
Cl ⁻	0.97	0.04	-0.02	0.10	0.13	0.06	0.96
Mg ²⁺	0.98	0.13	-0.04	0.13	-0.05	0.03	0.99
NO ₃ ⁻	0.97	0.07	-0.16	0.12	0.01	0.05	0.99
Oxalate	0.94	0.13	0.17	0.17	-0.10	0.02	0.96
K ⁺	0.97	0.11	-0.08	0.14	-0.09	0.04	0.99
Na ⁺	0.97	0.09	-0.11	0.12	-0.03	0.06	0.98
SO ₄ ²⁻	-0.20	-0.01	0.95	0.01	0.13	0.01	0.96
SO ₂	0.05	0.07	0.82	-0.19	0.16	-0.16	0.77
Eigenvalue	8.8	4.1	2.9	1.1	1.0	0.9	
% Var. Exp	43.9	20.7	14.2	5.6	5.1	4.4	
Commu (%)	43.9	64.6	78.9	84.4	89.5	93.9	
Factor name	Road salt + biomass burning	Crustal/soil dust	Coal combustion + agriculture	Long-range transport of Hg	Industrial	Bromine source	
Extraction Method: Principal Component Analysis.							
Rotation Method: Varimax with Kaiser Normalization.							
a. Rotation converged in 6 iterations.							

Table H3: Varimax rotated factor loadings with meteorological factors (6 factors)

	PC1	PC2	PC3	PC4	PC5	PC6	Commu
GEM	0.32	-0.02	-0.17	0.76	0.29	-0.03	0.80
GOM	0.48	0.19	-0.03	0.75	0.05	0.06	0.83
PBM	0.97	0.05	-0.09	0.16	0.01	0.01	0.98
PM _{2.5}	0.07	0.63	0.56	-0.02	0.43	-0.06	0.90
Al	0.05	0.97	-0.06	0.02	-0.01	0.05	0.95
Br	0.23	0.30	-0.11	-0.17	0.38	0.67	0.77
Fe	0.01	0.84	0.21	0.02	0.11	-0.23	0.82
K	0.23	0.91	-0.13	0.06	0.05	0.09	0.91
Si	0.05	0.98	-0.06	0.01	-0.02	-0.01	0.97
Zn	0.00	0.00	0.53	-0.15	0.65	-0.13	0.75
NH ₄ ⁺	-0.14	0.02	0.92	0.10	-0.01	0.06	0.87
Ca ²⁺	0.97	0.03	-0.08	0.10	0.10	-0.01	0.96
Cl ⁻	0.97	0.05	0.02	0.08	0.11	-0.03	0.96
Mg ²⁺	0.97	0.14	-0.05	0.14	-0.04	-0.01	0.99
NO ₃ ⁻	0.97	0.08	-0.16	0.10	0.04	-0.01	0.99
Oxalate	0.93	0.15	0.13	0.20	-0.09	-0.01	0.95
K ⁺	0.96	0.12	-0.11	0.15	-0.04	0.00	0.98
Na ⁺	0.97	0.10	-0.11	0.12	0.02	0.01	0.98
SO ₄ ²⁻	-0.21	0.01	0.92	0.06	0.03	0.05	0.91
SO ₂	0.02	0.07	0.83	-0.09	-0.04	-0.13	0.71
Temp	0.18	0.06	0.16	0.82	-0.36	-0.11	0.88
RH	-0.31	-0.55	-0.22	-0.29	-0.05	-0.06	0.54
WS	0.00	-0.26	0.43	-0.25	-0.52	0.02	0.58
Precip	-0.15	-0.21	0.02	0.03	-0.25	0.76	0.71
Eigenvalue	8.1	4.5	3.4	2.2	1.4	1.1	
% var. exp	33.7	18.6	14.2	9.1	5.6	4.8	
Cummu	33.7	52.3	66.6	75.7	81.3	86.1	
Factor name	Road salt + biomass burning	Crustal/s oil dust	Coal combustion + agriculture	Re-emission	Industrial source+ dispersion	Bromine source	
Extraction Method: Principal Component Analysis.							
Rotation Method: Varimax with Kaiser Normalization.							
a. Rotation converged in 7 iterations.							

Table H4: Varimax rotated factor loadings with meteorological factors (7 factors)

	PC1	PC2	PC3	PC4	PC5	PC6	PC7	Comm
GEM	0.34	-0.05	-0.10	0.65	0.07	0.50	-0.02	0.81
GOM	0.47	0.17	-0.07	0.76	0.07	0.11	0.06	0.86
PBM	0.97	0.04	-0.08	0.15	-0.01	0.04	0.02	0.98
PM _{2.5}	0.06	0.62	0.50	-0.01	0.49	0.11	-0.02	0.90
Al	0.06	0.97	-0.01	0.01	-0.08	0.10	0.05	0.96
Br	0.22	0.29	-0.16	-0.17	0.30	0.13	0.70	0.78
Fe	0.02	0.84	0.19	0.05	0.16	0.03	-0.21	0.82
K	0.24	0.91	-0.10	0.06	-0.01	0.11	0.11	0.92
Si	0.06	0.98	-0.02	0.01	-0.06	0.06	0.00	0.98
Zn	-0.04	0.00	0.32	-0.08	0.88	-0.04	-0.07	0.89
NH ₄ ⁺	-0.12	0.01	0.95	0.09	0.08	-0.05	0.05	0.93
Ca ²⁺	0.97	0.03	-0.10	0.09	0.10	0.05	0.01	0.96
Cl ⁻	0.96	0.05	-0.01	0.09	0.14	0.01	-0.01	0.96
Mg ²⁺	0.97	0.13	-0.05	0.14	-0.04	0.01	0.00	0.99
NO ₃ ⁻	0.97	0.08	-0.16	0.10	0.01	0.05	0.00	0.99
Oxalate	0.93	0.14	0.15	0.20	-0.07	-0.02	-0.01	0.96
K ⁺	0.97	0.12	-0.08	0.14	-0.07	0.05	0.00	0.99
Na ⁺	0.97	0.09	-0.10	0.10	-0.01	0.05	0.02	0.98
SO ₄ ²⁻	-0.20	0.00	0.94	0.05	0.13	-0.06	0.04	0.95
SO ₂	0.03	0.07	0.83	-0.08	0.10	-0.14	-0.14	0.75
Temp	0.17	0.04	0.14	0.88	-0.22	-0.14	-0.13	0.90
RH	-0.27	-0.55	-0.05	-0.43	-0.31	0.24	-0.08	0.72
WS	-0.05	-0.23	0.19	-0.01	0.03	-0.87	0.01	0.86
Precip	-0.15	-0.21	0.06	0.04	-0.29	-0.11	0.73	0.71
Eigenvalue	8.1	4.4	3.1	2.1	1.5	1.2	1.1	
% var. exp	33.8	18.4	12.7	8.9	6.1	5.1	4.8	
Cummu	33.7	52.1	64.9	73.8	79.9	84.9	89.7	
Factor name	Road salt+ biomass burning	Crustal/soil dust	Coal combustion + agriculture	Re- emission	Industrial source	Dispersion	Bromine source	
Extraction Method: Principal Component Analysis.								
Rotation Method: Varimax with Kaiser Normalization.								
a. Rotation converged in 6 iterations.								

VITA AUCTORIS

NAME: Morounfolu Adeyeye

PLACE OF BIRTH: Ile-Ife, Nigeria

YEAR OF BIRTH: 1984

EDUCATION: Moremi High School, Ile-Ife, Nigeria
1996 - 2002

Obafemi Awolowo University, Ile-Ife, Nigeria
2003-2009 B.Sc. (Chemical Engineering)

Obafemi Awolowo University, Ile-Ife, Nigeria
2012-2014, M.Sc. (Chemical Engineering)

University of Windsor, Ontario, Canada
2017-2019 M.A.Sc. (Environmental Engineering)